ELISABETH VERWÜSTER

Modeling the Impact of Imperfections on Prototypical Self-Assembled Monolayers

DISSERTATION

zur Erlangung des akademischen Grades

Doktorin der technischen Wissenschaften

eingereicht an der

Technischen Universität Graz

Betreuer

Ao.Univ.-Prof. Dipl.Ing. Dr.techn. Egbert Zojer

Institut für Festkörperphysik

Graz, Juli 2017

EIDESSTATTLICHE ERKLÄRUNG

Ich erkläre an Eides statt, dass ich die vorliegende Arbeit selbstständig verfasst, andere als die angegebenen Quellen/Hilfsmittel nicht benutzt, und die den benutzten Quellen wörtlich und inhaltlich entnommenen Stellen als solche kenntlich gemacht habe. Das in TUGRAZonline hochgeladene Textdokument ist mit der vorliegenden Dissertation identisch.

Datum

Unterschrift

Acknowledgements

I sincerely thank the following institutions and people, who made the completion of my thesis possible:

Austrian Academy of Sciences, Austrian Science Fund: for financially supporting the research project

ZID (TU Graz): for providing the computational resources on the d-cluster

Vienna Scientific Cluster (VSC): for the computational resources on the vsc3 cluster and its administration

Egbert: for providing the resources and patience throughout my thesis and for enabling yet another chemist to explore the colorful world of solid state physics

Oliver: for breaking the glass ceiling showing physicists what chemists are able to do and his persistence

EgbertInnen: for a great time in a densely packed office

Abstract

In the context of novel electronic devices, the need for more versatile materials grows exponentially. Especially the field of organic electronics gains ever more interest as recent research shows promising results. Interfaces between metallic substrates and organic layers represent a highly versatile playground for extensive fundamental research of the physical aspects at play, as well as for applications in organic electronic devices. Investigating such metal/organic interfaces is, thus, of paramount importance to gain fundamental insight into the interwoven structural and electronic properties. Investigating such interfaces poses a significant challenge, as two fundamentally different materials are combined, forming a system of considerable complexity. In this thesis, metal/organic interfaces are investigated by means of first-principle calculations based on density-functional theory (DFT).

The main focus of this theses lies on examining the impact of imperfections in self-assembled monolayers (SAMs) on their electronic and structural properties. Reliably modeling such interfaces not only demands state-of-the-art computational methods that include the multitude of interactions that occur, but also the consideration of possible imperfections of such system. In this context, one prototypical biphenylthiole-based SAM on Au(111) is perturbed by specific imperfections that impact the system structure and, subsequently, its electronic properties.

As examples for such imperfections, adatoms are introduced at the metal/organic interface in different configurations. The resulting impact on structural and electronic properties strongly depends on the final adatom-configuration, of which the most stable motif adopts a dimer-structure. Such dimeric adatom-configurations are well known to occur in SAMs of short alkylthioles on Au(111), whereas information on adatom-induced interfaces of densely packed arylthioles is scarce. Modeling monomeric (R-S-Au_{ad}) as well as dimeric/polymeric (RS-Au_{ad}-RS-Au_{ad}, Au_{ad}-RS-Au_{ad}) adatom-configurations for a biphenylthiole-based SAM reveals a strongly motif-dependent impact on the electronic properties. While monomeric configurations result in strong changes for, e.g., the work-function modification and the density of states compared to an unreconstructed system, the overall impact of dimeric-/polymeric-adatom configurations is surprisingly small. This finding suggests a considerable probability of a yet undetected existence of dimer-/polymer-motifs in a multitude of high-density SAMs on a Au(111) substrates.

As the type of SAM investigated in this work is rather prone to exhibit monolayers of low-quality and polymorphism, also the impact of backbone-configuration and molecular arrangement on the surface on the driving forces behind SAM-formation was investigated. The imperfection in this case, is the deviation of the monolayer-motif from its typically reported arrangement. Exploring the potential

energy surface via systematically varied starting geometries, revealed six possible monolayer-motifs. These polymorphs act as suitable test-set to understand the physical effects at play, that stabilize certain polymorph over others. This was achieved by modeling a hypothetical SAM-formation process. It was found that, although covalently bound, such monolayers would not adsorb on the surface without van-der-Waals interactions. However, the main force determining the motif-conformation arises from electrostatic interactions within the monolayer. Tuning the molecular conformation in SAMs, enabling the growth of highly ordered films can, thus, be achieved by modifying the intra-molecular charge distributions.

During the fabrication of such biphenylthiole-based SAMs, the molecules are deposited onto the substrate in a controlled manner. Throughout this deposition, various different monolayer motifs varying in their surface coverage have been reported. This difference in coverage poses the last imperfection investigated in this work. To model varying surface coverages, differently sized unit cells were calculated, investigating the non-trivial dependence between coverage and resulting work-function modification. A strong change in work-function modification ($\Delta\Phi$) was observed, displaying even a shift in sign for $\Delta\Phi$ for a donor-substituted SAM at half coverage. These observations are a direct consequence of the molecular tilt angle that increases with decreasing coverage. The occurring Pauli-Pushback effect that grows in magnitude with increasing tilt plays a crucial role for the resulting work-function modification. The densely packed SAM consisting of covalently bound upright-standing molecules progressively resembles a physisorbed monolayer with decreasing coverage.

Kurzfassung

Die wachsende Nachfrage an modernen elektronischen Bauteile, im Speziellen im Bereich der organischen Elektronik, begründet die steigenden Erfordernisse für vielseitig einsetzbare Materialien. Grenzflächen zwischen Metallen und organischen Molekülen stellen diesbezüglich eine leistungsfähige Materialklasse dar. Der Einsatz organischer Moleküle ermöglicht aufgrund moderner Synthesewege ein zielgerichtetes Design der erwünschten Funktionalitäten.
Um eine erfolgreiche Anwendung dieser Materialien zu gewährleisten, bedarf es eines grundlegenden Verständnisses der physikalischen Prozesse und Effekte an diesen Grenzflächen. Kenntnis über die eng miteinander verknüpften strukturellen und elektronischen Eigenschaften metall-organischer Grenzflächen ermöglicht nicht nur ein effizientes Design dieser Materialien sondern auch die Entwicklung neuer Anwendungsmöglichkeiten. Die Erforschung der grundlegenden Eigenschaften dieser komplexen Systeme mittels computerbasierter Methoden, stellt jedoch eine große Herausforderung dar. In dieser Arbeit werden metall-organische Grenzflächen mittels atomistischer Simulationen basierend auf der Dichtefunktionaltheorie studiert. Der Hauptfokus richtet sich dabei auf den Einfluss von strukturellen Anordnungen dieser Grenzflächen, die der nicht der üblichen Form entsprechen, auf deren strukturelle und elektronische Eigenschaften. Um eine realitätsnahe Modellierung solch organischer Monolagen auf metallischen Substraten zu erzielen, ist es wichtig solch strukturelle Abweichungen miteinzubeziehen. In der vorliegenden Dissertation wird ein prototypisches metall-organisches System, bestehend aus Biphenylthiolen auf Au(111), durch spezifische strukturelle Veränderungen gestört und deren Auswirkungen untersucht.

Dabei werden u.a. zusätzliche Metallatome (Adatome) in das System eingebracht, die zur Ausbildung unterschiedlicher Adatom-Thiol Komplexe führen. Die stabilste Konfiguration stellt ein Adatom-Dimer (RS-Au_{Ad}-SR) dar, welches für kurzkettige alkylthiolbasierte Systeme geringer Oberflächenbedeckung auf Au(111) bereits bekannt ist. Für Monolagen bestehend aus größeren dicht gepackten Arylthiolen ist dessen Auftreten jedoch wenig erforscht. Bei den untersuchten Adatom-Komplexen handelt sich um sowohl monomere als auch polymere Konfigurationen. Die resultierenden elektronischen Eigenschaften hängen stark von der vorliegenden Konfiguration ab, wobei sich große Unterschiede zwischen den monomeren und polymeren Strukturen beobachten lassen. Ein Vergleich mit dem perfekten ungestörten System zeigt, dass die monomeren Adatom-Komplexe eine stark abweichende Austrittsarbeitsänderung zeigen und die Verteilung der berechneten Zustandsdichten auf Fermi-Level Pinning schließen lässt. Die elektronischen Eigenschaften der um vieles stabileren polymeren Konfigurationen sind hingegen kaum von denen des ungestörten Systems zu unterscheiden. Letzteres lässt auf eine hohe Wahrscheinlichkeit deren unbemerkter Vorkommnis in realen Proben schließen.

Eine weitere mögliche Abweichung von der Idealstruktur solch prototypischer metall-organischer Systeme, zeigt sich in den verschiedenen Anordnungsmöglichkeiten der Moleküle in der Monolage (Motiv). Da die hier untersuchten Systeme zu Polymorphismus tendieren, wird die Auswirkung unterschiedlicher Monolagenmotive auf den Bildungsprozess der Grenzfläche untersucht. Hierfür wird die Potentialoberfläche einer Biphenylthiolmonolage auf Au(111) sondiert, um mögliche Monolagenmotive zu generieren. Dabei lassen sich sechs verschiedene Motive identifiziert. Diese eignen sich als Testset um die grundlegenden physikalischen Effekte zu verstehen, die die Stabilität gewisser Motive begünstigen. Die im Rahmen der Dissertation durchgeführten Forschungen zeigen, dass starke elektrostatische Wechselwirkungen zur Ausbildung spezifischer Monolagenmotive führen, die Stabilität des Gesamtsystems jedoch aufgrund van-der-Waals Wechselwirkungen gegeben ist.

Währen der Herstellung der hier untersuchten Grenzflächen werden die organischen Moleküle kontrolliert auf das metallische Substrat aufgebracht. Dabei tritt eine Vielzahl an unterschiedlichen Monolagenmotiven aufgrund der wachsenden Bedeckung des Gold-Substrates auf. Die Bedeckung der Oberfläche stellt die letzte Abweichung von der Idealstruktur dar, die im Rahmen dieser Doktorarbeit behandelt wird. Die Untersuchung der elektronischen Eigenschaften des metall-organischen Systems in Abhängigkeit der Oberflächenbedeckung ergibt einen nicht-trivialen Zusammenhang zwischen der Bedeckung und der resultierenden Austrittsarbeitsänderung. Im Falle eines donorsubstituierten Systems führt diese Abhängigkeit sogar zu einem Vorzeichenwechsel der Austrittsarbeitsänderung bei halber Bedeckung. Der ungewöhnliche Zusammenhang zwischen der Bedeckung, des Kippwinkels und der Austrittsarbeitsänderung konnte mit dem Auftreten des Pauli-Pushback Effektes erklärt werden. Insgesamt zeigt sich, dass bei abnehmender Oberflächenbedeckung die dicht gepackte Monolage aus kovalent gebundenen Molekülen zunehmend den Charakter einer physisorbierten Monolage annimmt.

Structure of this Thesis

The following work is a so-called partly-cumulative Ph.D. thesis. It contains two published peer-reviewed scientific articles to which the author of this thesis has extensively contributed during the scientific work of the Ph.D. studies. These papers deal with the impact of i) coverage and ii) monolayer-motifs on the structural and electronic properties of self-assembled monolayers on Au(111). Additionally a chapter discussing the impact of adatoms on self-assembled monolayers is presented. According to the structure suggested for such a thesis by the *Doctoral School of Physics* at the Graz University of Technology, it consists of an introductory chapter, a results and publication chapter concluded by a summary. The general introduction contains the used computational methods as well as an overview of the scientific background bringing the presented results into context. The results and publications section contains two published articles in their original form and one chapter containing unpublished work.

It is deeply rooted in the nature of a scientific publication that authors and coauthors contribute to the underlying scientific content. Prior to each publication, detailed information on the contribution of each author is given.

List of enclosed Publications

Paper I

Electronic Properties of Biphenylthiolates on Au(111): The Impact of Coverage Revisited

Verwüster E.; Hofmann O.T.; Egger D.A.; Zojer E.
J. Phys. Chem. C., vol. 119, no. 14, pp. 7817-7825, 2015

published under Ref.[1]

Paper II

Exploring the Driving Forces behind the Structural Assembly of Biphenylthiolates on Au(111)

Verwüster E.; Wruss E.; Zojer E.; Hofmann O.T.
J. Chem. Phys., vol. 147, no. 2, p. 024706, 2017

published under Ref.[2]

Contents

I Introduction

1 Computational Approach

Computationally investigating many-body inorganic/organic systems at the nanoscale level demands a quantum mechanical approach to describe the electronic structure of such complex systems. However, calculating the properties of a many-body system, e.g. molecules in the gas phase or large scale solid state materials, in an exact manner is impossible, raising the need for reasonable approximations. In theoretical chemistry and solid state physics, the standard computational method at the moment is density functional theory (DFT). The popularity of DFT is based on the fact that it combines a conceptionally exact description of the electronic structure with approximations that reduce computational effort, allowing a description of many-body systems at reasonable costs.
In this work, molecules in the gas phase, free standing monolayers, bulk metal systems as well as combined metal/organic systems are investigated. For that a flexible tool such as DFT is a suitable fit.
The appeal of DFT originates from a thought on how to simplify the traditional wave-function based description of a many-body system by substituting the "strange complicated beast of a wave function"[3] by one observable, the electron density $n(r)$. This substitution of expressing a system with N electrons in its ground-state by the ground-state density $n_0(r)$ instead of the ground-state wave-function Ψ_0, simplifies the problem from considering $3N$ variables to only one scalar function of 3 spatial coordinates.
In the following, a short description of DFT will be presented based on references.[3–6]

1.1 Density Functional Theory

For calculating the ground state energy E_0 of a given many-body system with N electrons at positions r_i and M nuclei at positions R_I, one needs to solve the stationary Schrödinger equation 1,

$$\hat{H}\Psi(r_1,\ldots,r_N,R_1,\ldots,R_M) = E\Psi(r_1,\ldots,r_N,R_1,\ldots,R_M) \tag{1}$$

for a many-electron wave function Ψ using the Hamiltonian $\hat{H}$:

$$\hat{H} = \frac{\hbar^2}{2m_e}\sum_{i=1}^{N}\nabla_i^2 - \frac{\hbar^2}{2M_I}\sum_{I=1}^{M}\nabla_I^2 - \sum_{i=1}^{N}\sum_{I=1}^{M}\frac{Z_I e^2}{|r_i - R_I|} + \frac{1}{2}\sum_{i=1}^{N}\sum_{\substack{j=1\\ j\neq i}}\frac{e^2}{|r_i - r_j|} + \frac{1}{2}\sum_{I=1}^{M}\sum_{\substack{J=1\\ J\neq I}}\frac{Z_I Z_J e^2}{|R_I - R_J|} \tag{2}$$

The first term in 2 describes the kinetic energy of the electrons, the second term the kinetic energy of the nuclei, the third term the attractive interaction between electrons and nuclei, the fourth and fifth terms the Coulomb repulsion between electrons, respectively, nuclei.
A convenient approximation to simplify this Hamiltonian is the Born-Oppenheimer approximation.[7] As the nuclei have a much higher mass than the electrons, thus

move a lot slower, one solves the Schrödinger equation for fixed positions of the nuclei. Electronic and nuclei movement can now be separated, resulting in the elimination of part two (kinetic energy of the nuclei) of equation 2. As the position of the nuclei is kept fixed, also their electrostatic interactions with each other (last term in the Hamiltonian, Coulomb repulsion of the nuclei) describe a constant potential, which then is merely an energy offset.

Applying the BO-approximation reduces the Hamiltonian to the following expression,

$$\hat{H} = \hat{T} + \hat{V}_{int} + \hat{V}_{ext} \tag{3}$$

where $\hat{T}$ is the kinetic energy of the electrons, $\hat{V}_{int}$ the electronic Coulomb repulsion and $\hat{V}_{ext}$, the external potential created by the nuclei acting on the electrons. Albeit reducing the complexity of the Hamiltonian, solving the Schrödinger equation still poses a highly complex problem as the many-body wave function still depends on $3N$ variables for the N electrons in the system.

At this point the idea behind density functional theory enormously simplifies subsequent calculations. Instead of using the complex multi dependent many-body wave function describing a system, Ψ is substituted by the electron density $n(r)$. In the following the Hohenberg-Kohn Theorems[6] will be discussed, justifying this substitution of Ψ by $n_0(r)$.

Hohenberg-Kohn Theorems:

Theorem I[6] demonstrates the correlation between the ground-state wave function and the ground-state electron density, $n_0(r)$, proving that all ground-state properties of the system are completely determined by $n_0(r)$.
This ground-state electron density can be expressed by the ground-state wave function as the square of the absolute value of Ψ_0, which gives an electron probability density:

$$n_0(r) = \langle \Psi_0 | \sum_{i=1}^{N} \delta(r - r_i) | \Psi_0 \rangle \tag{4}$$

Since Ψ_0 determines $n_0(r)$ and the ground-state energy of the system E_0, a connection between electron density and energy becomes evident. Thus, there is *only one* ground-state energy and wave-function associated with $n_0(r)$ of a system.

Theorem II[6] states that E_0 can be obtained variationally. As the energy is a functional of the electron density, valid for any external potential $\hat{V}_{ext}$, the expression for the total energy needs to be rewritten as a functional of $n(r)$:

$$E[n(r)] = T[n(r)] + \int dr V_{ext}(r) n(r) + U[n(r)] \tag{5}$$

The first term gives the kinetic energy of an auxiliary non-interacting system, assuming that it has the same ground-state electron density as a system of interacting electrons, thereby greatly simplifying this many-body problem.[5] A fictitious set of N non-interacting electrons is introduced, replacing the interacting many-body system with an artificial non-interacting one.

$$T[n(r)] = \frac{1}{2} \sum_i \int |\nabla \psi_i|^2 \tag{6}$$

The many-body wave function can thus be described by a Slater-Determinant of non-interacting one-particle wave functions,ψ_i which in turn are used to construct the auxiliary electron density,

$$n(r) = \sum_{i=1}^{N} |\psi_i(r)|^2 \tag{7}$$

The second term of equation 5 describes the interaction of the electron density with the external potential, V_{ext}, created by the nuclei and the last term denotes all electron-electron interactions, $U[n(r)]$.

$$U[n(r)] = E_{Hartree}[n(r)] + E_{XC}[n(r)] \tag{8}$$

This electron-electron interaction consists of the classical electrostatic Coulomb repulsion (Hartree-Interaction) with $E_{Hartree}[n(r)]$ being

$$E_{Hartree}[n(r)] = \frac{1}{2} \int dr \frac{n(r')}{r - r'} \tag{9}$$

and the quantum mechanical exchange-correlation interaction, $E_{XC}[n(r)]$, containing all missing many-body effects that are otherwise not included. The exact form of this functional, $E_{XC}[n(r)]$ is and will probably remain unknown, but in principle, equation 5 describes the ground-state energy of an interacting system, exactly!

The Hohenberg-Kohn theorems prove that it is possible to replace the complicated expression of the wave-function with one observable, the electron density, a quantity only depending on 3 instead of $3N$ variables and thereby greatly simplifying computational effort. Although the whole interacting system is described by an auxiliary system of non-interacting electrons, the description done by DFT is still exact, with only one approximation stemming from the choice in the exchange-correlation functional, $E_{XC}[n(r)]$.

Minimizing the total energy functional, $E[n_0(r)]$, in equation 5 one obtains the ground-state electron density and corresponding ground-state energy,

$$E_0 = E[n_0(r)] \tag{10}$$

The minimization is done variationally. Using the expression for the non-interacting electron density by single-particle Kohn-Sham wave functions 11, one can substitute $n(r)$ by these KS single-particle wave functions, to vary the energy functional in terms of $\psi_r(r)$. This yields a set of self-consistent non-interacting single-particle Kohn-Sham equations,

$$(-\frac{1}{2}\nabla^2 + V_{KS}(r))\psi_r(r) = e_i\psi_i(r) \tag{11}$$

including the effective KS-potential $V_{KS}(r)$

$$V_{KS}(r) = V_{ext}(r) + V_{Hartree}(r) + V_{XC}(r) \tag{12}$$

The solution to the self-consistent KS-equations give single electron KS-wave functions ψ_i with energies $\in_i$ and is done iteratively. This means that as a first step a "trial-density" is estimated, with which the V_{KS} can be constructed according to equation 12. With V_{KS} at hand one can subsequently solve the KS-equations, from which the single-particle wave functions can be obtained. With these KS-wave functions, a new electron density can be built, which will then be compared to the "old" electron density. This procedure is carried out until the difference between the "old" and "new" electron densities lie below a set convergence criteria. This procedure would give an exact solution if the expression for the exchange correlation functional, $E_{XC}[n(r)]$ would be exact. However, as it remains unknown, the accuracy of approximating this exchange-correlation functional determines the quality of the whole calculation.

Exchange-Correlation Functionals:

The most simple approximation is the Local Density Approximation (LDA),[8]

$$E_{xc}^{LDA}[n(r)] = \int d^3r \in_{xc}^{hom} (n(r))n(r) \tag{13}$$

where $\in_{xc}^{hom}$ describes the exchange-correlation energy of one electron in a homogeneous electron gas with density $n(r)$. The LDA approximation is derived from the ideal uniform electron gas, however, as most systems are more complex and exhibit a heterogeneous distribution of electron density E_{xc}^{LDA} would not be suitable for, e.g., molecules in the gas phase or an organic monolayer on a metal substrate.
Including the generalized gradient of the electron density greatly improves this approximation. This is done in the Generalized Gradient Approach (GGA),[8]

$$E_{xc}^{GGA}[n(r)] = \int d^3r \in_x (n(r), \nabla)n(r) \tag{14}$$

The functional applied throughout this work is the so called PBE (Perdew-Burke-Ernzerhof)[8,9] functional, the most widely used form of the GGA approach. Further developments beyond GGA functionals include second and higher derivatives of the electron density (meta-GGA functionals),[10] as well as a part-inclusion of exact exchange from the Hartree-Fock Theory (Hybrid Functionals).[11] With increased accuracy also the computational effort rises, thus, one hast to find a balance between the needed accuracy and computational cost when computationally investigating complex systems, such as organic self-assembled monolayers on metal substrates.

Van der Waals Forces:

Van der Waals (vdW) interactions are distance-dependent non-local attractive interactions between atoms and/or molecules, arising from interacting multipoles. Such dipoles or multipoles originate from charge density fluctuations that are either induced or of permanent character. As vdW-forces are distance dependent with $1/R^6$ (R = Distance) they belong to the shortest-range non-bonding chemical/physical forces and are, thus, easily perturbed. However, they play a crucial role if polarizable entities such as long alkyl-chains or conjugated π-systems are present. This is the case when large π-systems either stack into certain arrangements or adsorb on metal surfaces.
Including vdW-forces in the computational modeling procedure used in this work, is done as additional correctional term outside of the self-consistent routine. Meaning, that after calculating the electronic structure of the system at hand, a vdW-correction energy is added, typically lowering the total energy. In this work, vdW-interactions are accounted for by applying the DFT+vdW$^{\text{surf}}$ scheme,[12] developed to accurately determine the structure and stability of organic molecules on surfaces.[12,13]

$$E_{vdW} = -\frac{1}{2}\sum_{a,b} f_{damp}(R_{ab}, R_a^0, R_b^0) C_6^{ab} R_{ab}^{-6} \tag{15}$$

Here, the vdW-correction to the total energy is given by a sum of $C_6^{ab} R_{ab}^{-6}$ terms, with R_{ab}^{-6} being the distance between atoms a and b and the vdW coefficient C_6^{ab}. The C_6^{ab} vdW-coefficients are determined including the many-body collective response (screening) of the substrate electrons via the Lifshitz-Zaremba-Kohn theory,[14,15] which is of key importance to accurately model organic molecules on metal substrates.

1.2 Computational Details

For calculating the electronic structure of the investigated systems, the program VASP (Vienna ab initio simulation package)[16] was used, which is a band-structure code employing periodic boundary conditions in all 3 spatial directions. As the metal/organic systems in this work are only periodic in two dimensions (x,y), they are separated by a large vacuum gap in the z-direction.[17]
Thereby an infinite slab is created in x- and y-directions represented by one repeated unit cell. To electrostatically decouple the repeated slabs in z-direction, in addition to a large vacuum gap, a potential discontinuity is introduced that compensates for the difference in potential on the lower and upper end of the slab,[18] see Figure 1.

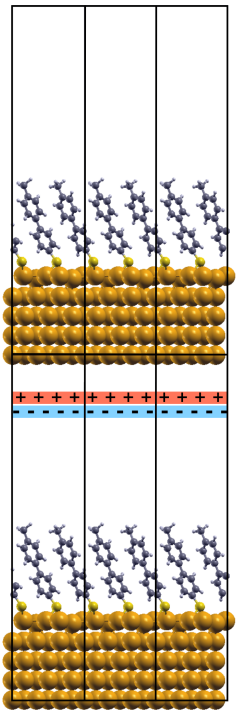

Figure 1: Schematic sketch of the repeated slab approach where one unit cell (indicated by a black box) is infinitely repeated in every spatial direction. To quantum-mechanically and electrostatically decouple the individual 2D SAM-layers in z-direction a large vacuum gap and an artificial dipole layer (blue and red bars) is introduced. This dipole layer is generated self-consistently during the calculation and placed in the top region of the unit cell.

As mentioned earlier, the PBE functional is used to describe exchange and correlation energies. To describe the core and valence electrons projector-augmented wave (PAW) -potentials are used and are available in a "soft" , "normal" or "hard" variety, depending on the required accuracy, with the latter being the most precise. VASP uses a plane-wave basis set, for which the cut-off energy can be individually set, in conjunction with the (PAW)[19] formalism. For a more efficient calculation, the system is described in reciprocal space, where reciprocal space is sampled by an automatic Monkhorst-Pack k-point grid.[20]
The individual settings for the performed calculations, such as the convergence criteria for the total energy, k-point grid and forces in the geometry optimization process are given in each section separately.

Geometry Optimization:

Geometry optimization of the metal/organic systems is performed using the program GADGET[21] which employs a standard conjugate-gradient method. One drawback of this conjugate-gradient approach is the inability to overcome high potential barriers. Thus, one has to start with a reasonable initial guess for the starting geometry. VASP and GADGET work in conjunction, alternating the relaxation of the electronic- and geometric-structure of the system. GADGET relaxes the atomic positions until the forces lie below a previously set convergence criteria and subsequently invokes VASP to relax the according electronic structure until the SCF-procedure converges. These steps are repeated until both convergence criteria are met.
Besides modeling metal/organic systems, also molecules in the gas phase were calculated. The geometry in the gas phase was obtained via pre-optimization with Gaussian09[22] using the PBE functional and the 6-311*+G basis set. Subsequently the molecule was placed in a 40Åx 40Åx 40Åunit cell to obtain a consistent energy within VASP.

Describing the substrate atoms:

To improve computational performance during the geometry optimization, GADGET separates the molecular- and metallic- part of the system when generating the internal coordinates. The metal is typically represented by a five-layered slab. To accurately model the metal/organic interface, the first two layers (closest to the organic layer) are allowed to move during the relaxation process, while the lower rows are kept fixed. It has to be mentioned at this point that the lattice constant of each substrate is optimized beforehand. This way, the atoms that are kept fixed during the relaxation simply remain in their optimized lattice positions. As these metal atoms are part of the substrate, thus not as flexible as the atoms in the organic layer, they are described in a more rigid manner using the so called

inverse-power distance coordinates, especially designed to optimize atomic clusters.[23]

To mark which atoms should be considered as part of the monolayer, respectively, as part of the substrate when using GADGET, a SUBST-tag is implemented into the GADGET-Input file. The default value for this SUBST-tag is 6, which corresponds to the number of next nearest neighbors in one layer of an fcc-lattice, which is the structure of, e.g., gold. However, in case of covalently bound molecules on the metal surface, the close proximity of the docking-group can lead to an increased substrate detection. Not only the metal atoms but also the docking-group atom, e.g., sulfur, can be detected as part of the substrate. This leads to a more rigid treatment of the docking-group atom during the optimization process. The increased substrate-detection subsequently results in either divergence of the calculation or non-reliable local minimum structures. Consequently the SUBST-tag value has to be reevaluated for each new geometry, especially for covalently bound molecules.

Specifically in the case of introducing adatoms into the metal/organic interface, a correct substrate detection is of crucial importance. Placing adatoms into the system raises the question whether they should be described as part of the substrate, thus in a more rigid manner, or as part of the monolayer, where atoms are allowed to move more easily. Testing the effects of both variations in adatom-treatment reveals to be challenging. The difficulty in this case is to find the proper value for the SUBST-tag for GADGET to detect the correct amount of substrate atoms.

Achieving the wanted separation of the metallic and molecular part takes multiple trials before a reliable geometry optimization is performed. The SUBST-tag has to be set to a specific value and the calculation started. GADGET determines the internal coordinates depending on the initial geometry and parameters in the input-file and lists the number of atoms detected as part of the substrate, respectively, the monolayer in an output file. Thus, one has to start the calculation, wait until the first GADGET-output is written and check this list of substrate-/monolayer- atoms. If the detection produces an unwanted separation, the calculation has to be canceled and resubmitted with a different value for SUBST. This procedure has to be repeated until a value for SUBST is found that results in the correct detection.

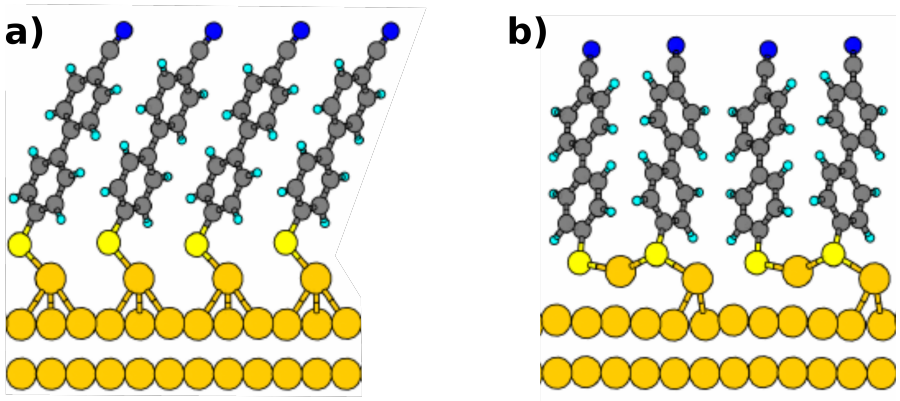

Figure 2: Impact of substrate recognition on the final geometry of a -CN substituted biphenylthiole SAM on Au(111) with adatoms being detected as a) part of the substrate or b) part of the monolayer

The resulting converged geometries for a system in which both adatom-treatments (adatom as part of the substrate and as part of the monolayer) were successfully employed is shown in Figure 2. The two final geometries strongly differ in their interfacial architecture and according total energy. The system with adatoms treated as part of the monolayer is significantly lower in total energy (by 0.5 eV) than the identical system with adatoms treated as part of the substrate. As literature agrees upon the thioles and adatoms at the surface to form mobile thiolate (RS-Au_{ad}) moieties,[24–27] the more flexible treatment was chosen to describe the gold adatoms at the interface.

Getting GADGET to detect adatoms close to the substrate surface as part of the monolayer, is however not simply achieved by increasing the SUBST-tag value. An increased SUBST-tag would demand a higher connectivity-factor for atoms to be recognized as part of the substrate. Therefore, the thiole docking-group, which is only connected to the backbone and the slab at a specific docking site, might not fulfill this increased connectivity-factor. Unfortunately, as shown in Figure 3, increasing SUBST can lead to the detection of arbitrary atoms in the unit cell as part of the substrate.

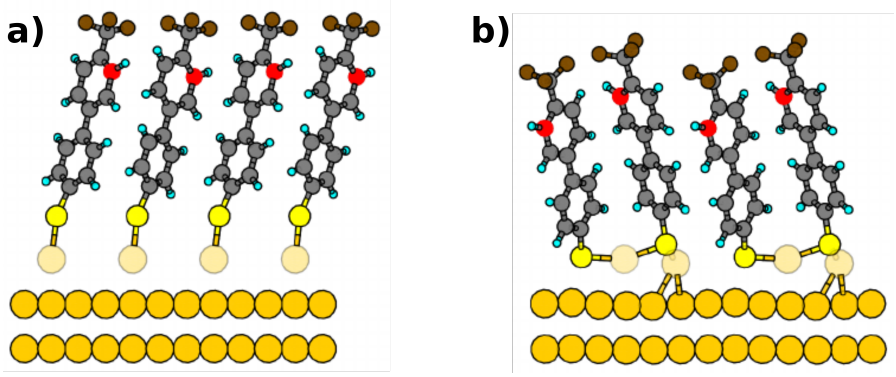

Figure 3: Impact of false substrate recognition on the geometry of a -CF_3 substituted biphenylthiole SAM on Au(111). The staring geometry is depicted in panel a), the resulting geometry in panel b). The red carbon atoms are detected as part of the substrate, whereas the transparent gold-adatoms are detected as part of the molecule

To solve this problem, a proper initial starting geometry has to be generated where the monolayer is placed slightly farther from the substrate surface. Nevertheless, several trial calculations finding a suitable value for SUBST are inevitable.

The systems investigated in Chapter I are biphenylthiole-based SAMs with adatoms at the metal/organic interface. With the help of Tomáš Bučko from the Comenius University in Bratislava, Slovakia, modifying the used GADGET code, it was able to specifically assign each atom as part of the substrate or monolayer, eliminating the previously described difficulties. The manual assignment of each atom was achieved by an additional Input-file (FRAGMENTS) containing a list of atoms for each fragment in the unit cell. The used system in this work is separated into three fragments, where the first fragment constitutes the substrate and the other two the two molecules per unit cell. All atoms are numbered in the file containing the coordinates, thus, one has to simply list the according atomic numbers per fragment.

Vibrational Analysis:

In Publication II, a vibrational analysis was performed on the investigated systems, which is typically done to assure that the optimized geometry is a true local minimum geometry. A geometry that gut stuck in a transition point would lead to imaginary frequencies, of which the according forces signify the relaxation path to the true local minimum. The term local minimum is chosen on purpose, due to the structural flexibility of the calculated systems, meaning that the possibility of finding THE global minimum configuration is limited.

As FT-IR (Fourier Transform Infrared) spectroscopy experiments are frequently used to provide insight into the structure of SAMs, performing such a vibrational analysis additionally enables the comparison between experimentally and computationally obtained data.[28–37]

During such a vibrational analysis, the Hesse matrix is determined, which is a matrix of the second derivatives of the energy with respect to the atomic positions and the vibrational frequencies. This can be done either numerically using finite differences, where each atom is displaced in all three spatial directions, mapping the occurring forces to construct the Hessian, or analytically. In the latter case, the Hessian is determined using density functional perturbation theory (DF-PT).[38–41] This is the computationally more efficient method, thus, also the method used in this work. Besides an increased efficiency when choosing the analytical approach, also the born effective charges can be calculated specifically when using the VASP code.[42] This enables the calculation of the vibrational spectrum of the system, allowing a comparison between experimental and calculated data.
The vibrational analysis employing density-functional perturbation-theory (DF-PT) was performed including vdW-corrections, which was kindly implemented into the used VASP version by Tomáš Bučko from the Comenius University in Bratislava, Slovakia.

2 Self-Assembled Monolayers

When organic molecules spontaneously assemble on a substrate to form a more or less ordered layer, one typically speaks of a self-assembled monolayer. Such monolayers can be formed by flat-lying molecules that physisorb onto the substrate,[43] see Figure 4a or by covalently bound molecules typically arranging in an upright-standing fashion,[44,45] see Figure 4b. The latter represents the type of SAMs investigated throughout this work that constitute of upright-standing organic molecules on a metal (gold) substrate.

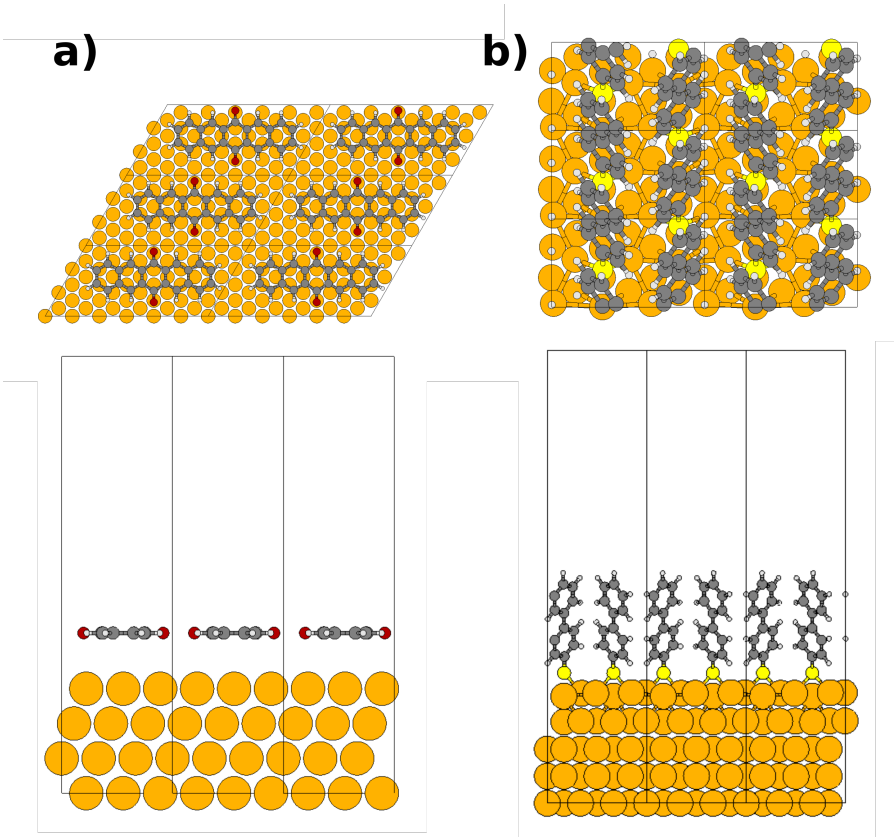

Figure 4: Schematic representation of two prototypical SAMs in top and side view. A (3,4,9,10-perylene-tetracarboxylic-dianhydride) PTCDA-SAM on Au(111) is shown in panel a) representative for flat lying molecules adsorbed on the substrate. For covalently bound monolayers a biphenylthiole-SAM on Au(111) is shown in panel b)

The general interest in such systems originates from i) their ease in preparation either from solution[45,46] or the gas-phase,[47,48] ii) their versatile use in, e.g., organic electronic devices[49] as semiconductor materials[50] or surface coatings[51,52] and iii) the study of physical aspects at play at such substrate/monolayer interfaces.[53–55] The study of such metal/organic interfaces can be conceptionally split into the research of electronic- and structural-properties. However, both properties are strongly related.[30,47,56–62] The main focus of the work presented here, lies on the investigation of structural properties and their subsequent impact on electronic properties of the SAM.

2.1 Fabrication and Investigation

SAM Fabrication:

The growing interest in employing SAMs in a broad spectrum of applications started due to their cheap and easy fabrication. During the fabrication process the organic molecules are deposited onto the (metal) substrate in a controlled environment to ensure the formation of a homogeneously ordered film of high quality. Within the production techniques the molecules are either in solution or evaporated in a vacuum chamber.[45,47,48,63–66] In the following, a general overview of the production steps will be given with a focus on organothiole-SAMs on Au(111) (biphenylthiole-based SAMs in particular), as such systems are investigated throughout this work.

For the substrate, using metal single crystals would be desirable as they offer to choose the crystallographic orientation.[47,67] However, the more affordable possibility is to use evaporated metal on mica.[45] Throughout this work the closed packed Au(111) orientation is used as substrate, which can be characterized by the well-known $22 \times \sqrt{3}$ reconstruction.[68] The electron distribution in Au(111) is smooth, resulting in a small surface potential corrugation, which enables a higher mobility of the adsorbate on the surface. The clean Au surface

Preparation from solution, is the most common method of fabrication. The simplicity of this technique was one factor that greatly promoted the overall use of self-assembled monolayers. Here, the clean (metal) substrate is dipped in a solution containing the molecules that assemble onto the substrate for a certain amount of time. This procedure is followed by drying of the solvent and rinsing.[45,46]
During the preparation from solution a certain delay of the onset in growth can be observed due to the "removal" of the contaminants on the surface by the actual adsorbates.[69–72] The first adsorption step results in 80-90% coverage within minutes. After this first step the growth proceeds much more slowly. The fastest step is the chemisorption of the molecules onto the surface, in case of organothioles on Au(111) forming thiolates (R-S-Au). During the second step, the molecular backbones arrange in a certain packing motif which happens more slowly.[69,71,72] The last and slowest step is the reorientation of the tail-groups, if present. However, very bulky tail-groups might already impact the molecular reorientation in step two, thereby governing the whole motif formation.[73]

In case of SAM fabrication in the gas-phase, the metal substrate has to be cleaned before any molecules are deposited. This is done by annealing and ion-sputtering in a UHV (ultra high vacuum) chamber. The molecules can subsequently be dosed onto the substrate with a controllable flux, while temperature and pressure in the chamber can be adjusted. For biphenylthiole-based SAMs prepared from the gas-phase, typically a phase with the molecules lying-down on the substrate is found,[47] with the domain size significantly varying with substrate temperature (180Å^2 at 279K, 1000Å^2 at 387K).[47] The standing-up phase is very difficult to form, as shown by Tao et.al.[62] and Sabatani et.al.[48] for a 4-mercatpto-biphenyl SAM on Au(111).

In either case of preparation, when such an organothiole (R-S-H) is deposited onto e.g. Au(111), the thiole (S-H) bond gets substituted by a covalent thiolate (R-S-Au) bond, with molecular hydrogen leaving the SAM as H_2.[74,75] This adsorption-mechanism, in particular the fate of the hydrogen atom, is however disputed in literature.[45,76,77]

SAM Investigation:

To experimentally investigate a SAM, a multitude of different thin-film characterization methods are available differing in nature and energy scale. One may roughly differentiate between microscopy-based-, diffraction-based-, and spectroscopy-based techniques. The observables of interest are of electronic as well as of structural nature. For the latter, the overall order and structure of the SAM, e.g., the molecules arrangement on the surface as well as the molecular structure such as the tilt- or twist angle are of interest. Concerning the electronic properties, core-level binding energies, charge transport levels or the work-function modification are investigated. In the following, a short overview over the most commonly used techniques is given.

Scanning-tunneling microscopy (STM)[78] as well as atomic-force microscopy (AFM)[79] belong to the microcopy-based techniques. These techniques are able to directly image the *local* structure of the SAM-surface. Applying these techniques provides information about the arrangement of the molecules on the surface, thus, also about structural defects.

Low-energy electron diffraction (LEED),[80,81] and grazing-incidence X-ray diffraction (GIXD)[82,83] are diffraction-based techniques that provide more versatile information compared to the previously described microscopic methods. Additionally, they probe the whole reciprocal lattice of the 2D sample, in contrast to the local information gathered by STM or AFM.
A LEED experiment is based on the scattering of low-energy electrons on a two dimensional system (e.g. SAM on a metal) which is of great use deducing the symmetry of the surface structure, thus, the quality of the monolayer.
In contrast to the former two methods, GIXD has the best resolution. Depending on the measurement mode, GIXD can provide information about e.g. the layer thickness and tilt of the molecules (rodscans mode along the surface normal),[84] or roughness and electron-density profile along the surface normal (X-ray reflectivity mode).[85,86]

Concerning spectroscopy-based techniques, the most frequently used methods are Infrared spectroscopy (IR),[35,87,88] high-resolution electron energy loss spectroscopy (HREELS),[80] near-edge X-ray absorption fine structure spectroscopy (NEXAFS),[89] UV photoemission spectroscopy (UPS),[90,91] inverse-photoemission spectroscopy (IPES)[92] and X-ray photoelectron spectroscopy (XPS).[88] While IR and NEXAFS,

working in different energy ranges, give information about the structure e.g. the tilt angle of the molecules, the entire valence electronic structure can be studied by employing XPS and UPS.[93,94]
XPS is an element specific measurement technique which can be used to determine atomic binding energies (difference of the kinetic energy of the ejected photoelectrons and the energy of the X-ray incident beam). Since atomic binding energies are very sensitive to their chemical environment, XPS can be used to investigate which chemical compounds are present in a sample, e.g., the configuration of the docking-group.
To measure the work-function modification induced by the SAM compared to the pristine substrate, the combination of UPS and Kelvin probe techniques is applied.[95,96] Here, $\Delta\Phi$ is measured as the cutoff of the secondary electrons. The kinetic energy of the secondary electrons is determined by the energy difference between the vacuum energy right at the substrate (i.e. E_{vac}) and the vacuum level right at the detector.[97]

2.2 Electronic Properties

Elucidating the electronic structure of a metal/organic interface is of paramount importance for understanding and exploiting the physical aspects at play. Within the electronic quantities of such interfaces, one of the main observable of interest is the work-function of the underlying metal substrate, Φ.

The work-function, Φ, of a metal is defined as the minimum energy (at 0 K) it takes to remove one electron from the metal bulk into the vacuum at infinite distance. The energy of this electron at the vacuum level is then described by E_{vac}^{∞}. Thus, Φ equals the energy difference between the Fermi-energy of the metal (the chemical potential) and the vacuum level. Typically, measured values for Φ are lower than the according theoretical value. This difference can be rationalized when taking a closer look at the interface. While calculating the work-function of a metal, the conditions are "perfect" meaning that one operates at 0 K and no contaminations are adsorbed on the surface. In reality measurements are undertaken at finite temperatures and contaminations can hardly be avoided.

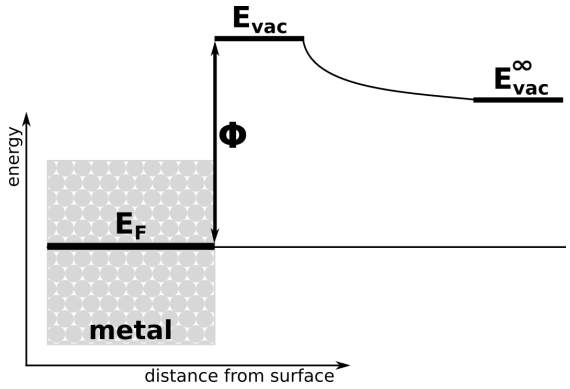

Figure 5: Schematic representation of the vacuum level right at the substrate surface, E_{vac}, and at infinite distance from it, E_{vac}^{∞}. The work-function Φ is presented as the energy difference between the Fermi-energy E_F and E_{vac}

At finite temperatures, following the Fermi-Dirac distribution, the electrons "spill out" of the metal,[98] creating a dipole layer at the surface. This leads to an additional energy barrier for the extracted electron to overcome (positive energy contribution).[97] The work-function is therefore more realistically defined as the difference of the chemical potential (E_F) and the energy of an electron at the substrate surface E_{vac},[99]

$$\Phi = E_{vac} - E_F \tag{16}$$

As this dipole layer that creates an energy barrier is confined at a finite interface, also its lateral extent is finite. Hence, E_{vac} changes with the distance from the metal surface,[97,99] schematically represented in Figure 5. Following Equation 16,

the two main factors that determine the work-function of a metal can be defined as i) the chemical potential (E_F), which is an intrinsic property of the material and ii) the surface dipole (causing the difference between E^{∞}_{vac} and E_{vac}).
The vacuum energy, E_{vac}, can additionally be altered by extrinsic factors such as molecules adsorbing on the surface. As a consequence, the work-function of the material can be intentionally modified by adsorbing a layer of organic molecules.

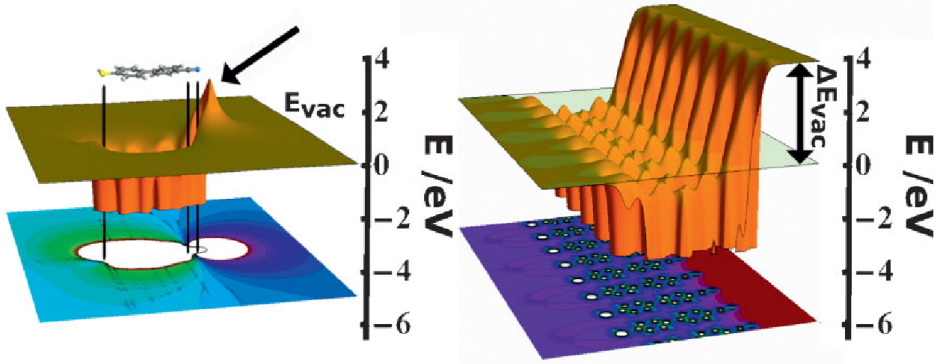

Figure 6: Both plots show the effect of a -CN substituted biphenylthiole (BPTCN, left), respectively an array of BPTCNs (right), on the electrostatic potential. Additionally the corresponding contour plots are projected onto the surface below the potential plots. The plot on the left shows the electrostatic potential of an isolated BPTCN, where a clear "bump" in energy is visible around the dipolar tail-group, while otherwise the potential drops off very quickly to a uniform vacuum level. On the right hand side however, a row of assembled BPTCNs arranged in a free standing monolayer is shown. Due to collective electrostatic effects this array of dipoles forms a step in the electrostatic potential, thus, splitting the vacuum level into two regions. Reproduced with permission from ref[17](©2010 WILEY-VCH Verlag GmbH & Co. KGaA, Weinheim).

The contribution of such a monolayer to the change of E_{vac} strongly depends on how the molecule impacts the surrounding electrostatic potential. If this molecule is substituted with a dipolar group, as depicted in Figure 6 (left panel), a locally confined effect on the electrostatic potential occurs. If such molecules assemble on the surface, a 2D-array of dipoles is created. This array of dipoles leads to a step in the electrostatic potential, ΔE_{vac}, originating from collective electrostatic effects, as depicted in Figure 6 (right panel).
Combining such a dipolar monolayer with a metal substrate, thus leads to a modification of the metal work-function, $\Delta\Phi$, as schematically sketched in Figure 7a. This modification can amount to both positive and negative values, (with drastic changes up to, e.g., 1.4eV,[100]) depending on the adsorbates electronic properties, see Figure 7b.

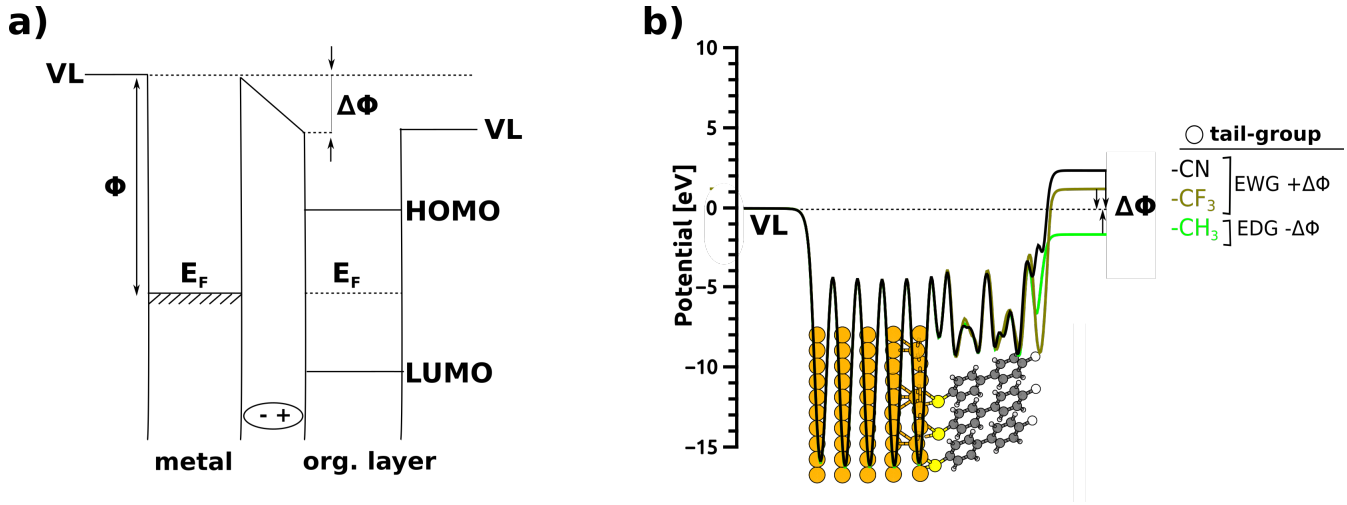

Figure 7: a) Sketch of the interfacial energy diagram upon combining the metal and an organic layer. Two entities with initially different work-functions, thus Fermi-levels, are brought together inducing charge redistributions at the metal/organic interface until the Fermi-levels are aligned. The resulting dipole layer (indicated as ellipsoid) gives rise to a potential step that splits the vacuum into two regions, two different vacuum-levels. Panel b) depicts the plane-averaged electron potential energy showing the effect of electron-accepting (-CN, -CF_3) and donating (-CH_3) substituents on the resulting potential step

The total modification of the work-function, $\Delta\Phi$, conceptionally originates from two sources.[17,101–103] i) The potential step created by collective electrostatic effects of the dipolar monolayer, (ΔE_{vac}), and ii) the bond-dipole, BD, situated at the metal/organic interface.

$$\Delta\Phi = \Delta E_{vac} + BD \tag{17}$$

BD arises from charge rearrangements at the interface upon bond-formation between the adsorbate and the substrate (for covalently bound monolayers). The Pauli-Pushback ("cushion") effect[49,99,104–108] that occurs upon adsorbing such a monolayer on a metal surface can additionally alter this bond-dipole. A more detailed investigation of the latter can be found in Publication II.

By designing the molecules that constitute the monolayer, the electrostatics at the interface can be manipulated to specifically tune the work-function of the underlying metal substrate.[99,109–114] or to e.g. enhance charge-injection properties[115] in organic electronic devices.

Exploiting this possibility to specifically tune the organic layer demands a detailed understanding of the interwoven electronic-/structural-properties. In the following, a brief overview of the structural characteristics of a SAM and how such structure-tuning is employed in various applications will be given.

2.3 Structural Properties - Tuning - Applications

The building blocks in case of a monolayer formed by upright-standing molecules are composed of a docking-group that has a strong affinity towards the substrate, a backbone of usually either alkyl-chains or a conjugated system varying in length and not necessarily but often a tail-group with a certain functionality. As such SAMs constitute of organic molecules, a vast playground in modifying their structure and related properties is readily available via organic chemistry. This opened a broad field of tailoring the organic monolayer to fit specific needs modifying the characteristics of the SAM.

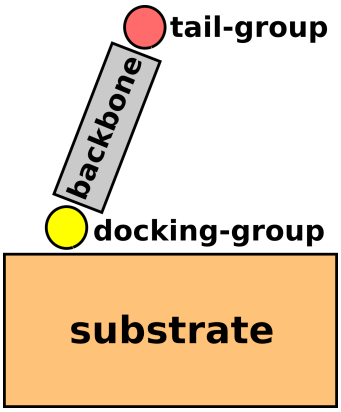

Figure 8: Sketch of the building blocks that constitute an upright-standing SAM, including the naming convention for each part, the docking-group, tail-group and backbone

Such tailoring often relies on the intimate relation between structural and electronic properties of the adsorbate[30,47,56–62] and can be achieved, e.g., via variations of the adsorbate backbone,[116–118] by substitution of additional functional groups[51,109] or by utilizing specific docking groups.[119]

The choice for anchoring the molecules to the substrate is strongly system-specific. In any case a strong interaction via physi- or chemisorption between monolayer and substrate is desired. For flat-lying molecules, a large π-system is favorable to maximize van der Waals attraction, enabling the monolayer to physisorb onto the inorganic substrate. For a SAM of upright-standing molecules, the interaction at the interface is often of covalent character. In case of Au(111) as substrate-material, which is used in this work, a strong binding can be achieved by a thiole (R-S-H) docking-group.[66] Moreover, also iso-cyano[17] (R-NC), thioacetate- (R-S-CO-CH_3)[120] or pyridine[17] docking goups on Au(111) have been employed successfully. Introducing selenoles (R-Se-H) as docking-group gained increasing interest over the last few years, as monolayers of higher quality can be obtained.[121–125]

Substituting the molecular backbone with a functional tail-group is a versatile handle enabling to adjust, e.g., surface properties, structural properties and electronic properties of a SAM. Adding a hydrophobic or hydrophilic tail-group can change the surface-wettability properties allowing for applications as specific coat-

ings, e.g. corrosion protection,[51,52] which was the first application for organic monolayers. Utilizing more complex tail-groups, SAMs can also be found in the field of bio-sensing.[126,127] The preparation of surfaces employing an organic monolayer is also used to initiate a certain growth of the following layer, where the SAM acts as directing substrate.[128–130] Controlling the arrangement of the monolayer can be achieved by utilizing, e.g., azobenzene[73] as tail-group, which "over-powers" the lattice structure given by the Au(111) substrate.
Besides modifications of the SAM-surface properties, also electronic properties of the underlying metal substrate can be tailored. Introducing dipolar groups into the monolayer allows the localization of electronic states,[131,132] as well as tuning of the work-function[99,109–114] to, e.g., enhance device performance in organic electronic devices such as organic thin-film transistors (OT-FT).[133,134]

Concerning the backbone, the most frequently used variations are aliphatic- or aromatic- hydro-carbon chains of varying length. While alykl thioles are known to form well-ordered films, thio-aromatic monolayers more often exhibit polymorphism and low-quality monolayers.[30,47,120,135–138] Utilizing backbone modifications, in terms of, e.g., changing the backbone conjugation, enables adjusting the conductivity,[118,132] or tuning charge-carrier injection in OT-FTs.[115] Alternatively, one can introduce dipolar units into the molecular backbones with the consequence that the electronic properties can be optimized independent of the SAM-ambient interface.[139–141]

Providing the molecule that constitutes the monolayer with a functionality, either via tail-group substitution or embedding functional groups into the backbone, enables the specific tailoring of structural and electronic properties of the SAM. Therefore, investigation and understanding of the physical effects at play is of paramount importance for improving the use of SAMs in modern organic electronic devices.

2.4 Systems of Interest

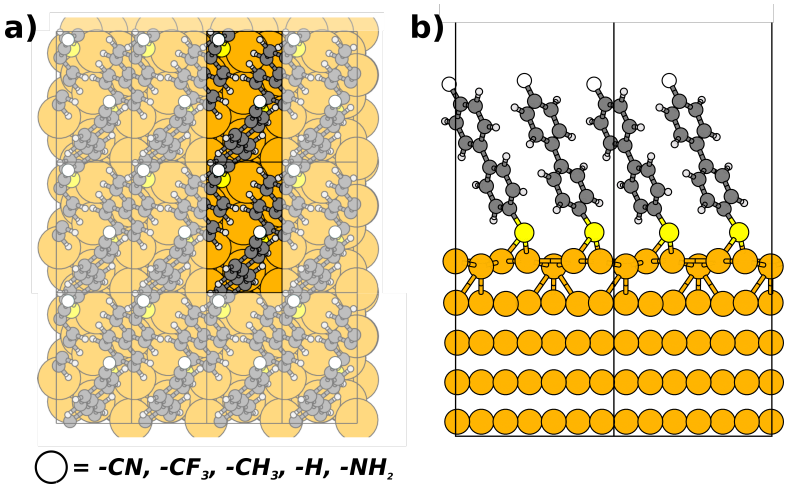

Figure 9: a) Top-view of a schematic biphenylthiole-SAM on Au(111) with the molecules arranged in herringbone-fashion. Two $3 \times \sqrt{3}$ unit-cells are highlighted, each occupied by two biphenylthioles. b) Side-view of two unit-cells

The systems investigated throughout this work are based on a prototypical biphenylthiole-SAM on Au(111), depicted in Figure 9, which is frequently used to study metal/organic interfaces.[1,17,28,30,47,67,114,142–146] Figure 10 presents the biphenylthiole-derivatives used to build the investigated SAMs. The plain biphenylthiole-SAM is used in Publication I, while SAMs build by the substituted derivatives are investigated in Publication II and Chapter I. The substituted tail-groups are either of electron-donating (-CH_3, methyl) or withdrawing (-CF_3, trifluoro-methyl, -CN, cyano) character, altering the electronic properties of the SAM. Typically a $3 \times \sqrt{3}$ unit cell is observed for such biphenylthiole-based SAMs on Au(111), with two molecules per unit-cell occupying the fcc-hollow site shifted to a bridge position.[147,148]

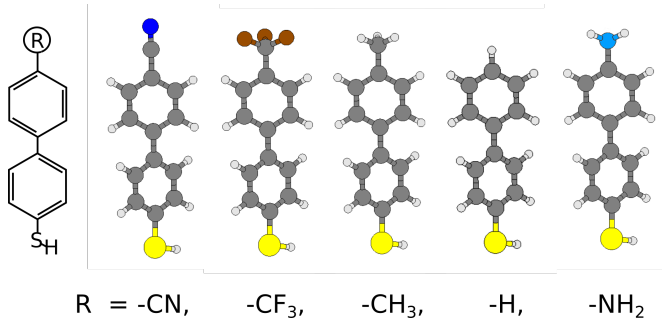

Figure 10: Isolated saturated biphenylthiole-variations that are used as building blocks for the self-assembled monolayers investigated in this thesis. From left to right; schematic sketch of the conjugated biphenyl-backbone, the cyano-substituted-, trifluoro-substituted-, methyl-substituted, unsubstituted and amino-terminated biphenylthiole

Such biphenylthiole-based SAMs are, however, prone to exhibit polymorphism and low-quality monolayers.[30,47,120,135–138] The difficulty in obtaining high-quality monolayers for, e.g., biphenylthioles origins from strong intermolecular interactions, creating additional energetic barriers impeding molecule-reorganization on the surface to form ordered films.[47]

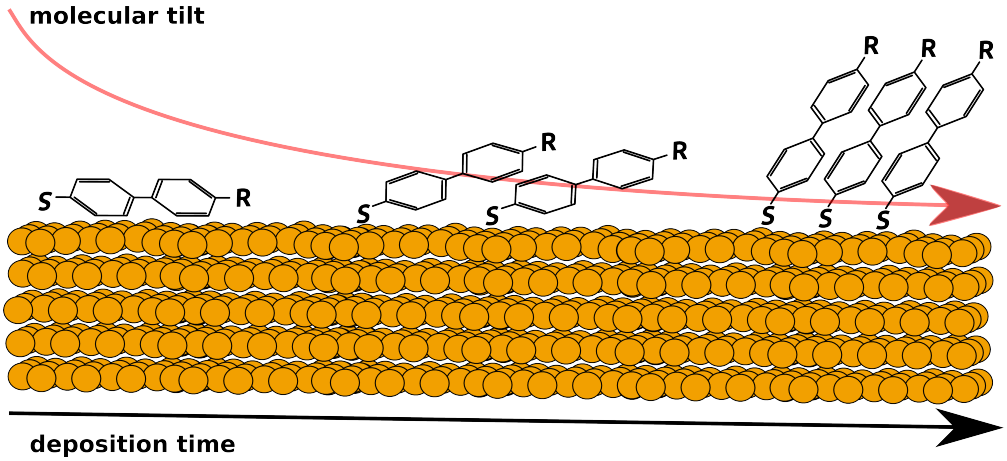

Figure 11: Sketch motivated by Azzam, W.; et al.; Langmuir 2003, 19, 4958 - 4968[149] representing the different motifs of the monolayer formed during the deposition of the molecules onto the substrate

In the first steps of adsorbing biphenylthioles onto Au(111) a low coverage phase with the molecules arranging in a lying-down fashion is reported.[47,149] Upon further deposition of biphenylthioles a hexagonal standing-up phase forms in a $3 \times \sqrt{3}$ unit cell, as schematically shown in Figure 11.[47] The transition between lying-down and standing-up phase itself leads to a more energetically favorable state for the entire layer, since more molecules are accommodated by the same area. But at the same time, intermolecular interactions gain importance concerning the arrangement on the surface with increasing coverage.[47,149] The system has to overcome a certain energetic threshold, which can act as kinetic trap if it is too high, generating e.g. polymorphism and disordered films.[150,151] Therefor, the structural quality of the standing-up phase is limited, resulting in small domain sizes and no features of an ordered structure when investigating the systems via GIXD, LEAD or STM).[30,62,67,137,138,152,153]

The appearance of multiple phases for biphenylthiole-SAM during the deposition process[30,47,149] motivated the investigation of the electronic properties of such a SAM as a function of surface coverage. The comprised results can be found in Publication I. In this Publication the combined effects of dipolar tail-groups and surface coverage on the work-function modification are investigated.

Furthermore, an origin of polymorphism to occur in such systems is a lattice mismatch between the adsorbate layer and the underlying metal substrate.[135,136,151] Thereby stress and strain is generated in the SAM.[136] The reason for this behavior

can be associated with two competing factors. i) The adsorbate tries to assemble in its energetically favored crystal lattice, typically the bulk lattice structure, for which multiple conformations ranging from planar to slightly twisted are reported.[154–158] In SAMs, however, biphenyl is suggested to occur in a planar geometry arranged in herringbone fashion.[47,138,149,150,159,160] The planarity in this case may be a result of biphenyl being spatially constricted on the surface,[156] which is a consequence of ii) the Au(111) substrate that governs the adsorbate's arrangement through its binding chemistry and periodicity. Elucidating possible motifs to occur for such a SAM and the physical effects that drive the motif-formation is the focus of Publication II.

To avoid or diminish the occurrence of polymorphism for thio-aromatic SAMs on Au(111), flexible alkyl-spacer elements are introduced between the anchoring (thiole) group and the conjugated backbone. The increased flexibility of the monolayer due to the alkyl-groups leads to an enhanced monolayer arrangement on the surface.[135,151,161,162] The spacer element between the backbone and the substrate, acts like a buffer that allows the monolayer to adopt the substrate-lattice given bonding arrangement, while at the same time enables the adsorbate to pack in an energetically more favorable crystal lattice. Moreover, transitioning between different phases during the deposition process might be facilitated.

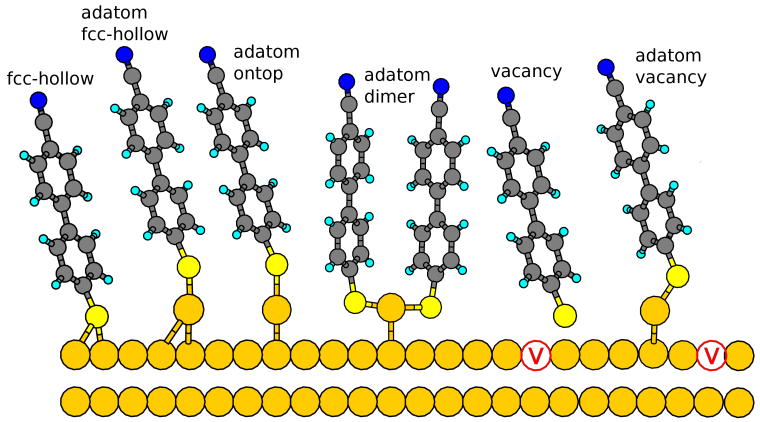

Figure 12: Schematic representation of the starting geometries of various surface reconstructions, exemplary shown for a cyano-substituted biphenylthiole SAM. For the sake of clarity only one of the two molecules in the unit cell ($3 \times \sqrt{3}$) is shown. *fcc-hollow* denotes the unreconstructed system; *adatom-fcc-hollow*, *adatom-ontop* denote one adatom per molecule being placed at either a fcc-hollow or ontop site; *adatom-dimer* depicts the staple motif known from literature[163] where two biphenylthioles bind to one adatom situated at an ontop position; *vacancy* depicts the introduction of one vacancy per molecule; *adatom vacancy* depicts one vacancy together with one adatom at a fcc-hollow per molecule.

Apart from investigating the impact of coverage or monolayer-arrangement on the electronic and structural properties of biphenylthiole-based SAMs, also the

impact of surface reconstructions was explored. Various surface reconstruction known from literature[164,165] (schematically presented in Figure 12) were generated and tested upon their impact on the work-function modification of a -CN, $-CF_3$, and $-CH_3$ substituted biphenylthiole SAM. The geometries include vacancies (*2vac*), adatoms (*adatom-ontop*, *adatom-fcc-hollow*) and the combination of adatoms and vacancies (*2ad2vac*). Testing their impact on the work-function however, revealed only minor modifications, except for the systems *adatom-ontop* and *adatom-fcc-hollow*. Therefore, further research focused on investigating these particular adatom-induced geometries.
Moreover, metal/organic interfaces containing adatoms are more and more frequently observed for low density alkylthiole-SAMs on Au(111).[25,163,166–175] However, also reconstructed surfaces in densely packed arylthioles on Au(111) are discussed in literature.[27,167,176,177] Whether such a reconstructed interface impacts the overall structural quality of a monolayer and the resulting impact on electronic properties will be extensively discussed in the following Chapter in Section II.

II Results and Publications

1 Surface Reconstructions

Allowing for a homogeneous structure of this thesis, the following chapter is written in the style of an article, containing an introduction, results and discussion, methodology and conclusion section. This way all information on the specifics of this work is embedded in one chapter.

Introduction

In search for modern molecular electronic devices, it is frequently proposed to use self-assembled monolayers (SAMs) to alter the surface properties of metals.[45,178,179] SAMs are commonly represented by well ordered densely packed structures of *organic molecules* that can easily be custom-tailored due to their rich chemistry.[180] Amongst the multitude of possible organic molecules that are investigated and used as building-blocks for SAMs, alkylthioles are one of the most studied adsorbents due to their ability of forming highly ordered stable monolayers by covalently binding to the metal substrate (RS-Au).

STM (Scanning-Tunneling Microscopy) studies investigating the adsorption behavior and geometry of such alkylthioles on Au(111) revealed the existence of adatoms,[168,169,175] which are excess substrate atoms on the metal surface. These adatoms are suggested to originate from either low coordination sites on the metal, such as step etches,[181] or are generated during the assembly process itself.[65,78,175,182]
Upon the adsorption of alkylthioles on a Au(111) surface, defects such as adatoms are generated, lifting the herringbone resonstruction of Au(111), to which the alkylthioles may bind.[25,174,183] Although gold is rather non-reactive in bulk form, its isolated atomic form has a rich ligand chemistry due to the several possible oxidation states.[184–186] Thus, thioles adsorb more easily on a reconstructed gold surface compared to a "clean" substrate, as it provides more reactive gold atoms such as undercoordinated adatoms[167,177,187] or gold atoms next to vacancies.[175] Once formed, the mobility of an adatom-thiolate complex RS-Ad (Ad = Adatom) is much higher than that of a thiole on the surface.[24] Consequently, it is reasonable to assume, that these mobile RS-Ad moieties may govern the structural assembly of the whole SAM.[24–27]

Literature agrees upon defects, especially the presence of adatoms, playing an important role in the overall assembly process.[26,65,174,182,187] Thereby in depth studies of the thiole adsorption geometry on defected surfaces is motivated. Special interest was given to methylthiole on Au(111), where contrasting results concerning the adsorption geometry were obtained. NIXSW[188] (Normal Incidence X-Ray Standing Wave) and Scanned-Energy and Scanned-Angle S 2p Photo-Electron Diffraction[189] experiments suggested Au-S bonds perpendicular to the interface, indicating ontop-site adsorption of the thiolate.
However, subsequent studies revealed that these perpendicular S-Au bonds did not originate from thiolate-*monomer* units (RS-$Au_{substrate}$), but from a *dimeric* structure incorporating one adatom (RS-Au_{Ad}-SR), the so called *staple-motif*.[163] In this configuration two thioles, each sitting on an ontop position, coordinate to one adatom, occupying a bridge position via covalent bonds parallel to the surface plane. This peculiar adsorption geometry is suggested to be the energetically most favorable configuration for methylthioles on reconstructed Au(111).[187]
The staple motif[163] was confirmed by a multitude of STM experiments[25,163,170] and by DFT analysis for a low coverage methylthiole SAM on Au(111). In the

low coverage regime the staple entities form a striped pattern on the surface.[190–192] This staple configuration, however, was also predicted to occur in a high density methylthiole SAM by Molecular Dynamics[174] and first-principle DFT[167,170,187] calculations as well as GIXRD (Grazing Incidence X-Ray Diffraction) measurements[174] and STM experiments.[170]
Moreover DFT calculations and STM experiments as well as GIXRD measurements of hexylthioles[173] and ethylthioles[167,171] on Au(111) confirmed the staple motif to also occur in high density SAMs of long-chain alkylthioles.[172]

Since mostly studies of alkylthioles on reconstructed Au(111) exist, only little is known about aromatic thioles in that matter. The existence of surface reconstructions in rigid aryl-thioles is debated in literature.[193,194] However, DFT calculations by Rajaraman et.al. suggest surface reconstructions to also appear in low density arylthiole SAMs (Phenylthioles on Au(111)), displaying the previously mentioned staple motif.[167] Maksymovych et.al.[27,176] and Fan et.al.[177] agree on the staple motif to be the energetically most favorable adsorption configuration for phenylthioles on reconstructed Au(111).
Besides the staple motif also other adatom-thiole binding configurations were suggested to occur. Polymeric[173,191,195,196] $[\text{RS-Ad}]_n$ as well as mixed adatom-complexes, where either two different thioles form an adatom-dimer[176] (RS-Ad-SR`) or adatom-monomers and adatom-oligomers (dimers and/or polymers) coexisting within a sample,[174,191,194] were identified in low density SAMs.

As prior work focuses more on low coverage alkyl- and aryl-SAMs, the investigation of surface reconstructions in a high density regime presents a promising subject. Yet, especially experimental work on this topic seem to be scarce. This may be due to the particular difficulty in probing the metal-organic interface in such high density SAMs.[164]
In ordered high-coverage SAMs, the adsorbing molecules adopt a "standing-up" phase with the molecular backbones tightly packed in an almost vertical orientation relative the substrate surface. This close packing is motivated by long-range dispersion forces (van der Waals interactions) which increase in strength with the surface area of the backbones. Due to this tight vertical packing, the interfacial adsorption geometry is shielded from direct imaging by the dense monolayer.[164] Thus, surface-sensitive scattering spectroscopy tools such as variants of the X-ray standing wave (XSW) technique, photodiffraction, helium diffraction or electron diffraction methods have to be employed.

To support and supplement experimental work exploring the presence and effects of adatoms, which in case of such SAMs may be of peculiar difficulty, we computationally model high density arylthiole-SAMs on reconstructed Au(111). The systems of choice in this work are derivatives of the prototypical biphenylthiole-SAM, see Figure 13 as it is frequently used in studies of SAM/Au interfaces.[17,28,30,47,142–146,197,198] Since biphenylthiole-SAMs are known to form films of rather bad quality,[30,47,120,135–138] one may also assume the presence of various surface reconstructions. A set of three different adsorption configurations and their impact on easily accessible observables

such as the tilt angle, β, and the density of states (DOS) are investigated. The biphenylthioles are substituted by polar tail-groups (-CN, -CF_3, -CH_3) at the 4' position enabling the investigation of the impact of adatoms on the work-function modification, $\Delta\Phi$.

Methodology

Computational Approach. The band-structure calculations in this work employ dispersion-corrected density functional theory calculations using a modified version of the Vienna Ab-Initio Simulation Package[199] (based on VASP version 5.4.1, see below for more details).
Throughout this work, the Perdew-Burke-Enzerhof (PBE)[8,9] exchange-correlation functional was applied together with projected augmented-wave (PAW) potentials[200,201] to treat core-valence interactions.
A cutoff energy of 400 eV for the plane waves and a 8x5x1 Monkhorst-Pack[20] type k-point mesh were used for geometry optimizations. Subsequent single-point calculations were performed with a cutoff energy of 450 eV and a 11x8x1 k-point mesh.
To account for long-range dispersion forces (vdW), the PBE functional was augmented by the Tkatchenko-Scheffler scheme[202] parameterized specifically to treat adsorption on metallic surfaces (PBE+vdWsurf).[12]
The interaction between the atoms of the Au substrate was switched off, which was made possible by a special modification of the VASP code, kindly provided by Tomáš Bučko, enabling us to selectively switch off the vdW correction between specific atomic species.
An optimization scheme based on internal coordinates and the Direct Inversion in the Iterative Subspace (DIIS)[203] algorithm as implemented in the GADGET tool[21] were used to relax the geometries.
The Au(111) metal substrate was represented by a 5-layer slab, with a lattice constant set to the equilibrium value for the used methodology, which amounts to 2.928 Å.
The top two layers and the molecules including the adatoms were allowed to relax until the remaining forces where smaller than 10^{-2} eV/Åand tight convergence criteria of 10^{-6} eV were employed for the SCF procedure.
To model the self-assembled monolayer on the metallic substrate, we applied the repeated slab approach. Decoupling of the periodic replicas of the slab was achieved by inserting a 20 Åvacuum gap and a self-consistently determined dipole layer compensating for the electrostatic asymmetry.[204]

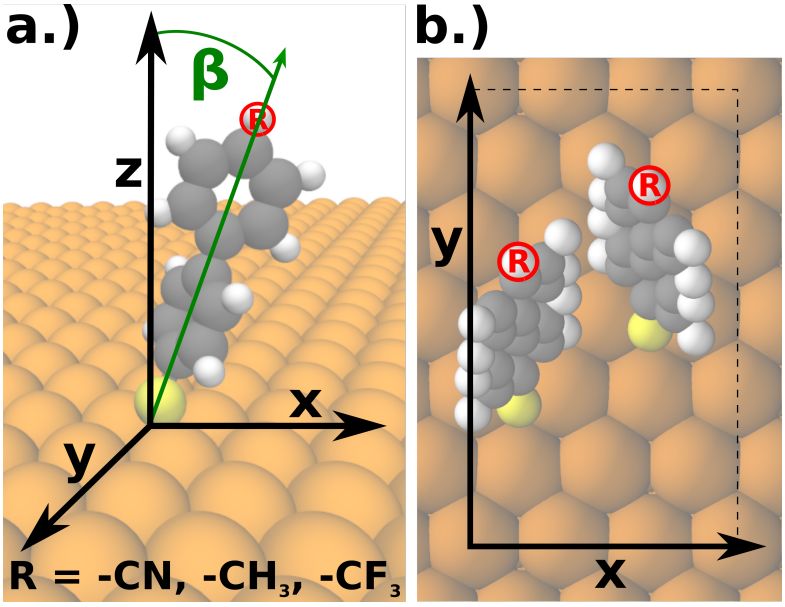

Figure 13: Schematic sketch of biphenylthiolate on Au(111). a) The substituted 4' position is marked by a red R = -CN, -CH_3, -CF_3. Z denotes the axis perpendicular to the slab, β the tilt angle between the long-molecular axis and z. b) $3 \times \sqrt{3}$ surface unit cell used in the present study containing two molecules in herringbone arrangement.

System Setup. 4`-substituted mercapto-biphenylthiols on reconstructed Au(111) were calculated with electron withdrawing-(-CN, -CF_3) as well as -donating (-CH_3) tail-groups. Two molecules were placed in a $3 \times \sqrt{3}$ surface unit cell arranged in a herringbone pattern, mimicking the typical growth of oligophenylenes at full coverage,[47,62,149] see Figure 13.
To model the reconstructed Au(111) surface, adatoms were introduced in a 1:1 and 1:2 (adatom:molecule) ratio. The starting geometry of the 1:2 ratio system closely resembles the staple-motif known from literature,[163] displayed in Figure 14 panel a). The adatom, placed at an ontop position, coordinates bonds parallel to the gold surface to each of the two biphenylthioles, situated at bridge positions (*CN-staple*, *CF_3-staple*, *CH_3-staple*). The docking positions of the thioles and the adatom however differs from the "original" staple-configuration (S-Au-S; ontop-bridge-ontop). Nevertheless we expect this initial geometry to also converge into the same local minimum geometry as the staple-motif. As literature suggests this motif to be the most stable adatom-configuration, it will serve as reference system for the other reconstructed SAMs. Additionally all SAMs were calculated on an unreconstructed gold substrate to visualize the impact of introducing adatoms on geometric as well as electronic properties (*CN-unrec*, *CF_3-unrec*, *CH_3-unrec*).

The 1:1 ratio starting geometries contain one adatom per molecule where both adatoms are either placed on an fcc-hollow site, see Figure 14 panel b) (*CN-fcc*, *CF_3-fcc*, *CH_3-fcc*) or on an ontop position, panel c) (*CN-ontop*, *CF_3-ontop*, *CH_3-ontop*). In all adatom:molecule ratios the biphenylthioles are oriented perpendicular to the surface in a herringbone arrangement, see Figure 14.

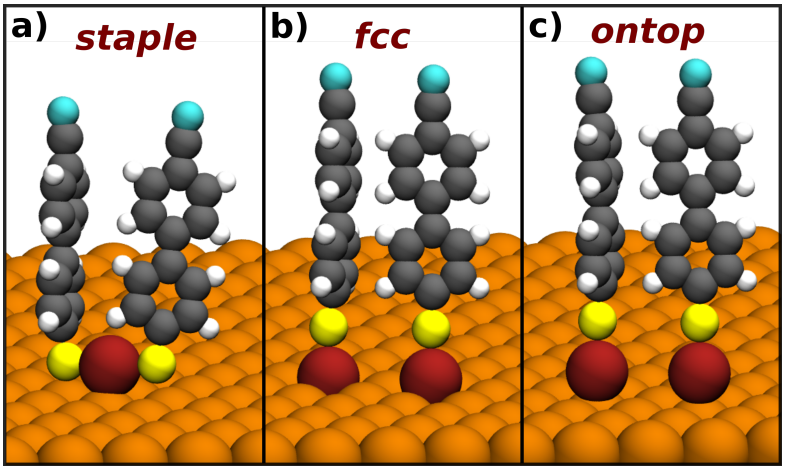

Figure 14: Starting geometries for a) the 1:2 ratio staple-motif (adatom:molecule), b) the 1:1 ratio geometry with adatoms sitting at fcc-hollow positions and c) the 1:1 ratio geometry with adatoms sitting at ontop sites; exemplary shown for the CN-substituted biphenylthiole-SAM. For the sake of clarity, only the two molecules that constitute the unit cell are shown and neighboring molecules are omitted. Adatoms are colored in red

As the adatoms are introduced in different ratios (adatoms:molecules) and on different docking sites (fcc-hollow and ontop), an according variety of interfacial architectures is expected. In the starting geometries for the adatom-fcc and adatom-ontop systems, the biphenylthiole backbone is placed almost directly ontop of the adatom, see Figure 15. Since adatom, sulfur and carbon of the backbone form an almost straight Au_{ad}-S-C line, optimizing such an initial structure leaves the resulting local minimum geometry somewhat up to chance. One might categorize this procedure as random sampling, where the straight Au_{ad}-S-C bonds represents the degree of freedom that might randomly relax into one of many possible local minimum geometries.

This sort of arbitrary approach however enables the generation of strongly varying geometries, as no geometric trajectory towards any specific local minimum is given by the starting configuration. The thereby created set of adatom-configurations will be investigated focusing on the impact of adatom-induced interfacial architectures on the physical and structural properties of the SAM.

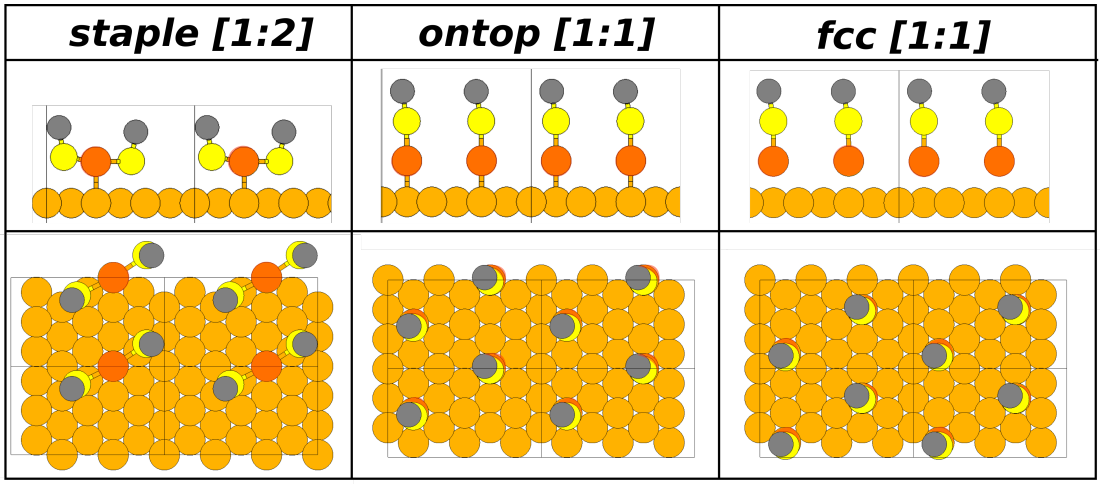

Figure 15: Schematic representation of the starting geometries for the 1:2 ratio staple-motif, the 1:1 ratio with adatoms sitting at fcc-hollow positions and the 1:1 ratio with adatoms sitting at ontop sites. Adatoms are colored in red, sulfur atoms in yellow and the first carbon atom of the backbone in gray.

Results and Discussion

Optimizing the biphenylthiole-based SAMs on an unreconstructed Au(111) surface displays the well known herringbone arrangement with the thioles occupying fcc-hollow sites slightly shifted towards a bridge position. The resulting tilt angle of the molecules is in a similar range for all three tail-groups with the -CH_3 substituted monolayer having the smallest tilt of 26°followed by the -CN substituted biphenylthioles tilting by 29°and the -CF_3 substituted ones displaying a tilt of 32°.

Introducing adatoms drastically changes the interfacial architecture, while the typical herringbone arrangement prevails. Since thiole-gold and gold-gold bonds are of similar strength, the gold-gold bonding at the metal-organic interface can be significantly modified by a thiole.[164] Depending on the coverage and adatom:molecule ratio, several adatom-induced motifs are known from literature, as already mentioned in the Introduction. The molecules may arrange in a staple-motif forming adatom dimers (RS-Au_{Ad}-SR), arrange in an adatom-polymeric form ([RS-Au_{Ad}-SR]$_n$), or simply result in adatom-monomers (RS-Au_{Ad}).

Upon comparing the final geometries, see Figure 16, one may recognize a peculiar trend regarding the formation of specific adatom-motifs. Whether this trend is based on physical effects, stemming from e.g. the tail-group, or is occurring strictly by chance, will be investigated in the following sections.

start-configuration	final-geometry		final-configuration
	top-view	side-view	
CN-staple	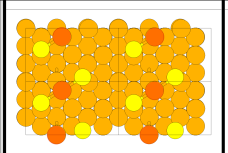		CN-staple
CN-ontop	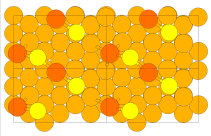	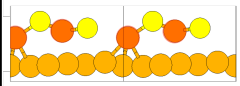	$CN\text{-}poly^{(o)}$
CN-fcc	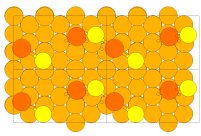	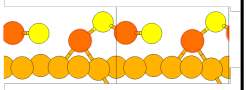	$CN\text{-}poly^{(f)}$
CF_3-staple	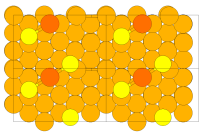	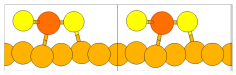	CF_3-staple
CF_3-ontop	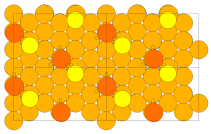	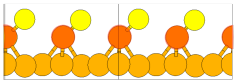	$CF_3\text{-}mono^{(o)}$
CF_3-fcc	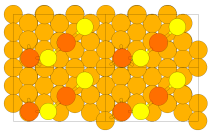	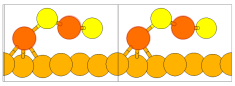	$CF_3\text{-}poly^{(f)}$
CH_3-staple	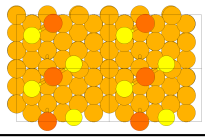	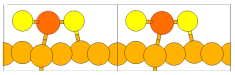	CH_3-staple
CH_3-ontop	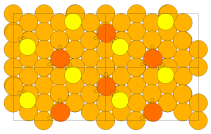	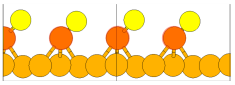	$CH_3\text{-}mono^{(o)}$
CH_3-fcc	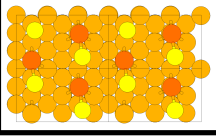	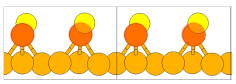	$CH_3\text{-}mono^{(f)}$

Figure 16: Schematic representation of all final geometries for the reconstructed BPTCN, $BPTCF_3$ and $BPTCH_3$ SAMs in top- and side-view. Adatoms are colored in red, sulfur atoms in yellow. The gray panel on the left contains the naming convention for the starting adatom-configurations while the naming convention for the relaxed adatom-motifs are given in red in the right panel

Geometry. While the staple-motif (1:2, adatom:molecule) remains in the predicted configuration for all tail-group substitutions, the 1:1 ratio systems (Figure 14 b, c) converge into more unexpected geometries. Both *CN-fcc* and *CN-ontop* relax from the initial adatom-monomers RS-Au_{Ad}, into almost identical configurations, resembling a mixture of an adatom-polymeric form [RS-Au_{Ad}-SR]$_n$ and the staple-motif RS-Au_{Ad}-SR, see Figure 17. The resulting adatom configurations will in the following be referred to as *CN-poly*$^{(f)}$ and *CN-poly*$^{(o)}$.

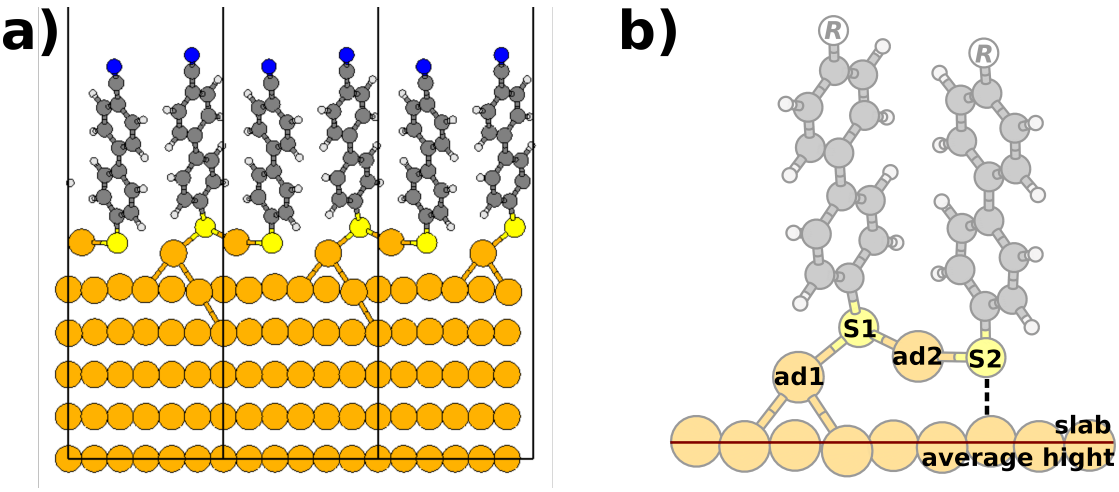

Figure 17: a) Three unit cells of the CN-substituted biphenylthiole-SAM in an adatom-polymer configuration, *CN-poly*$^{(f)}$ b) Sketch of the adatom-polymer configuration. Atoms for which computed bond distances are discussed in the text and given in Table 1 are labeled with ad1 for adatom1, ad2 for adatom2, S1 for sulfur1, S2 for sulfur2 and slab, referring to the average hight of the first substrate layer.

While one adatom remains closely attached to the substrate at a hollow site, binding to a single thiole group, the second adatom, bridged by the two biphenylthioles, is lifted up from the substrate surface (for details of distances and bond lengths see Table 1).
One of the two thioles is covalently bound to two adatoms and only weakly interacting with the gold surface, while the other thiole is covalently bound to only one adatom interacting more strongly with the substrate. This may indicate a sp3-hybridisation for the sulfur atoms, each desiring to form three bonds; one to the backbone-carbon, and one to each of the two non-equivalent gold atoms (Au-substrate, Au-adatom).[75,164] Resulting bondlengths for the thiolate (Au-S) compare nicely to literature, especially in case of the staple-motif, see Table 1.

Similar to the CN-adatom systems, relaxing *CH_3-ontop* and *CH_3-fcc* results in almost identical geometries. Nonetheless, they drastically differ from their -CN analogues. While both *CN-fcc* and *CN-ontop* end up in "polymeric" adatom geometries, *CN-poly*$^{(f)}$ and *CN-poly*$^{(o)}$ (see Figure 17), *CH_3-ontop* and *CH_3-fcc* solely converge into adatom-monomers (RS-Au_{Ad}), *CH_3-mono*$^{(f)}$ and *CH_3-mono*$^{(o)}$

see Figure 16. In this configuration both adatoms remain strongly bound at fcc-hollow sites while the thioles shift from their initial position ontop of the adatom to its side in an 110°angle (Au_{ad}-S-C), strongly suggesting a sp3-hybridization for the sulfur atoms.[75,205] This angle however, is too small to allow the sulfur atom to strongly interact with the underlying substrate due to a distance of 3.10Å(fcc) - 3.50Å(ontop), thus both thioles and adatoms only form two bonds each (ad-slab, ad-S, S-C).

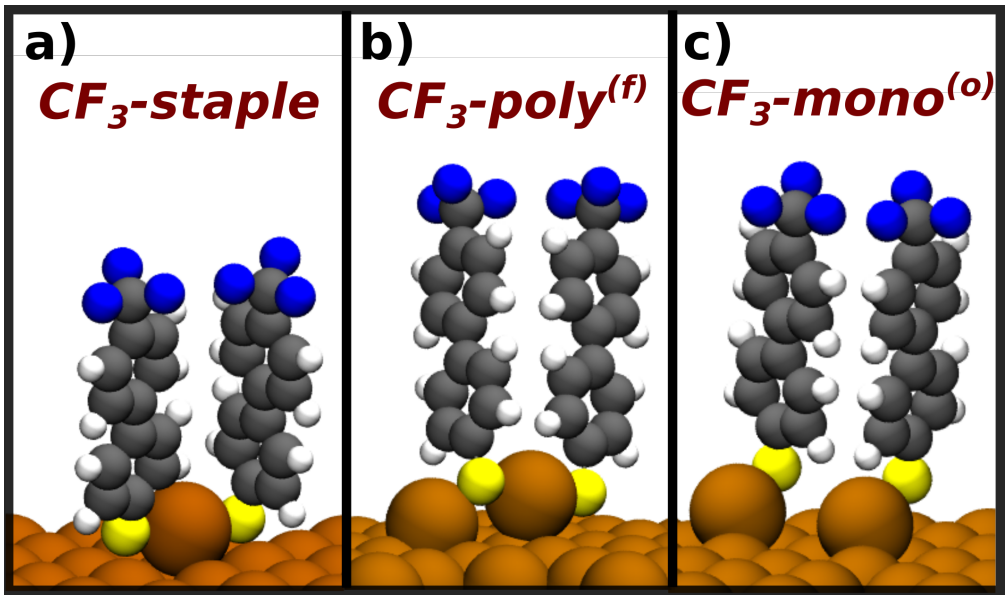

Figure 18: End geometries for the three adatom-motifs: a) staple-motif, *CF_3-staple* b) polymer-motif, *CF_3-poly$^{(f)}$* and c) the monomer-motif, *CF_3-mono$^{(o)}$*; exemplary shown for one unit cell of the CF_3- substituted biphenylthiole

While *CN-fcc* and *CN-ontop*, respectively *CH_3-fcc* and *CH_3-ontop* converge into almost identical polymeric, respectively monomeric adatom geometries, the relaxation of *CF_3-fcc* and *CF_3-ontop* results a mixture of the two configurations discussed above, see Figure 18. The *CF_3-ontop* geometry converges to the monomer-motif, *CF_3-mono$^{(o)}$* while *CF_3-fcc* displays an adatom-polymer, *CH_3-poly$^{(f)}$*, each closely resembling the -CH_3,respectively -CN analogues with only minor differences in bond lengths of less than 0.2 Å.

The final geometries for all tail-groups assume a trend in the formation of the adatom-polymer motif as shown in Figure 16. This raises the question of what dictates the trend in converging into certain configurations or whether it is rather up to chance due to the flexible nature of the starting geometry (see Figure 15). Scrutiny of the final geometries and their interfacial bonding configuration might answer this question.

Table 1: Calculated bond lengths for the reconstructed- and unreconstructed- systems. The used labels are illustrated in Figure 17. The given values are averaged for the two molecules per unit cell. Adatom-configurations that result in a polymeric, or staple form are labeled in italic.
Bond lengths and distances from literature: ad-S 2.33Å[25,187] / S-slab 2.49Å[25] / 2.45Å[205] / ad-slab 2.53Å[187]

Systems	[Å]	[Å]	[Å]	[Å]	[Å]	[Å]	[Å]	[Å]	[°]	[Å]
-CN	**ad1-slab**	**ad1-S1**	**S1-slab**	**S1-ad2**	**ad2-slab**	**ad2-S2**	**S2-slab**	**ad1-S2**	**∠ad-S-C**	**S-C**
CN-staple	2.75	2.33	2.51	-	-	-	2.56	2.32	97.0	1.78
CN-poly$^{(o)}$	2.11	2.36	3.40	2.37	2.64	2.34	2.86	-	102	1.77
CN-poly$^{(f)}$	2.07	2.34	3.55	2.35	2.69	2.35	2.65	-	101	1.78
CN-unrec	-	-	1.84	-	-	-	1.87	-		1.78
-CH_3	**ad1-slab**	**ad1-S1**	**S1-slab**	**S1-ad2**	**ad2-slab**	**ad2-S2**	**S2-slab**	**ad1-S2**	**∠ad-S-C**	S-C
CH_3-staple	2.39	2.32	2.55	-	-	-	2.52	2.33	97.0	1.78
CH_3-mono$^{(o)}$	2.14	2.32	3.55	-	2.15	2.33	3.44	-	107	1.76
CH_3-mono$^{(f)}$	2.19	2.39	3.07	-	2.21	2.39	3.10	-	110	1.76
CH_3-unrec	-	-	1.82	-	-	-	1.87	-		1.77
-CF_3	**ad1-slab**	**ad1-S1**	**S1-slab**	**S1-ad2**	**ad2-slab**	**ad2-S2**	**S2-slab**	**ad1-S2**	**∠ad-S-C**	S-C
CF_3-staple	2.40	2.32	2.58	-	-	-	2.51	2.32	97.1	1.78
CF_3-mono$^{(o)}$	2.16	2.32	3.55	-	2.17	2.32	3.48	-	108	1.76
CF_3-poly$^{(f)}$	2.08	2.32	3.60	2.35	2.89	2.33	2.86	-	101	1.78
CF_3-unrec	-	-	1.79	-	-	-	1.89	-		1.77

As the thiole-gold interaction significantly depends on interfacial geometric parameters such as this ∠Au_{ad}-S-C angle, the S-C bond length, the S-slab and the S-ad distance,[205] it comes of no surprise that within the converged polymer-motif, respectively monomer-motif structures, very similar parameters occur, see Table 1. Albeit the strongly diverging interfacial architectures of the polymeric-/monomeric- motifs, the calculated ∠Au_{ad}-S-C angles remain in a range (100-110°) where a sp3-hybridisation for all sulfur atoms can tentatively be suggested.[75,205] The decrease of ∠Au_{ad}-S-C in the staple- and polymeric-motifs might origin from the arrangement of the biphenyl-monolayer, displaying molecules with an increased tilt angle.
A connection between the Au_{ad}-S-C angle of the sulfur atom, the tilt angle and the final adatom-configuration becomes evident. The subsequent interpretations for the adatom-configuration formation are twofold. Either i) the interfacial architecture converges into a random local minimum displaying a specific thiole-adatom bonding-configuration, thus, specific Au_{ad}-S-C and tilt angle. In short, the randomly generated interfacial configuration determines the structure of the monolayer.
Or, ii) as the converged motifs only differ in their tail-group substitution, their electronic and steric impact might determine the arrangement of the biphenyl-backbones, the resulting tilt-angle of the molecules and in turn the interfacial architecture by defining the Au_{ad}-S-C angle. In short, the tail-group determines the structure of the monolayer and subsequently the interfacial configuration.

Addressing the latter, it is known that different substituents at the 4´ position of biphenylthioles, have been proven to result in different packing arrangements of SAMs on gold.[137]
Since these tail-groups are of dipolar nature, their electron-donating (-CH_3), respectively -accepting (-CN, -CF_3) character might affect the chemistry of the thiole docking-group through the aromatic biphenyl backbone.[160,206]
As the thiole docking-group is of electron-donating nature, a combination with an electron-attracting substituent (-CN, -CF_3) at the 4` -position of the biphenyl backbone, results in a significant molecular dipole moment (calculated for the isolated molecules; BPTCN: 5.1 D; BPTCF_3: 2.8 D; BPTCH_3: 1.5 D). This strong dipole may alter the bonding configuration at the interface.[160,206]
While the donor substituted SAMs (*CH_3-fcc*, *CH_3-ontop*) result in monomeric geometries, the strongly electron-accepting substituted thioles (*CN-fcc*, *CN-ontop*) converge exclusively into polymeric structures, correlating with the previously stated theory. The lesser electron accepting -CF_3 substituted thioles (*CF_3-fcc*, *CF_3-ontop*) display a mixture of the two variations.

However, within a densely packed monolayer, collective electrostatic effects[44,101,207] strongly diminish the possible electronic impact of the tail-group on the thiole docking-group.
Nevertheless, to test the possible impact of the tail-group, the strongest electron-acceptor -CN was placed on a monomeric adatom geometry (*CH_3-mono$^{(o)}$*) and the electron-donating tail-group -CH_3 was placed on a polymeric structure (*CN-poly$^{(o)}$*), relaxing both systems until convergence is reached. This switch was done to test whether the change in electron-accepting, respectively -donating character of the tail-group might influence the bonding behavior of the docking thiole, leading to a rearrangement of the adsorption geometry to the respective other adatom-motif. One, thus, would expect a dimer for the -CN tail-group and a monomer for the -CH_3 substituted biphenylthioles.
The resulting geometries remain close to their initial conformation as the energetic barrier to overcome each local minimum geometry may be too high. While the -CN substituted SAM in the adatom-monomer configuration (-CN on *CH_3-mono$^{(o)}$*, E_{sys} = -417.83 eV) becomes less energetically favorable compared to the adatom-polymer motif (*CN-poly$^{(o)}$*, E_{sys} = -418.26 eV), the -CH_3 substituted SAM in the adatom-polymer configuration (CH_3 on *CN-poly$^{(o)}$*, E_{sys} = -426.25 eV) becomes more favorable in energy compared to the adatom-monomer (*CH_3-mono$^{(o)}$*, E_{sys} = -425.74 eV) configuration. This simply states the fact that the polymeric adatom-motif is energetically more favorable than the adatom-monomer motif.

Declaring that the different tail-group substitutions may not have a primary effect on the resulting interface-geometries proves theory i) stating that the arbitrarily generated interfacial adatom-configuration determines the structure of the monolayer.

Electronic Properties. The adsorption energy, E^{ads}, is a correlating quantity to the total stability of the calculated SAM. Nevertheless, it may serve as qualitative parameter to estimate the likeliness of the presented adatom-configurations to occur in real SAMs. Therefore E^{ads} is calculated following equation 18.

We define E^{ads} (following the procedure by Otálvaro et.al.[165]) per molecule for a SAM with M molecules in the unit cell as

$$E^{\text{ads}} = \frac{1}{M}[E_{\text{sys}} - E_{\text{Au}} - M \times E_{\text{mol}} - N \times E_{\text{adatom}} + E_{\text{H}_2}] \tag{18}$$

where E_{sys} is the total energy of the SAM, E_{Au}, is the energy of the clean unreconstructed gold substrate, E_{mol} is the energy of one isolated saturated molecule, E_{adatom} is the energy of N gold atoms and E_{H_2} is the energy on a free H_2 molecule. E_{adatom} is defined as the energy of a clean slab divided by the number of gold atoms it contains.
Equation (1) is defined so that negative values for E^{ads} indicate a favorable adsorption process upon replacing a covalent bond (S-H to S-Au).

The adsorption energy may be influenced by whether an electron-accepting or -donating substituent is placed on the 4´ position of the biphenylthiole,[160] where the -CN substituted SAMs display the lowest (highest negative) values for E^{ads}. However, albeit the opposite accepting-/donating- character for the $-CF_3$ respectively $-CH_3$ tail-groups, the according systems display comparable values for E^{ads}. The primary reason for a more or less favorable E^{ads} might thus originated from the interfacial architecture.

Independent of tail-group substitution, a general trend towards a more favorable E^{ads} for the polymer- and staple-motif compared to the monomer-motif and even to the unreconstructed SAMs occurs. These results agree nicely with literature where the staple-motif has been confirmed to be the most stable adsorption configuration for a variety of SAMs on gold.[25,163,170,190–192] Thus, additional energetic gain may stem from a particular bonding arrangement between the adatoms and the thioles, which allows for a higher coordination of strong thiolate-bonds compared to the arrangement in the monomer-motif or the unreconstructed system.

Table 2: Adsorption energy, E^{ads}, work-function modification,$\Delta\Phi$, and tilt angle,β, for the converged reconstructed and unreconstructed systems.

System	$\mathbf{E^{ads}}$ **[eV]**	$\Delta\Phi$ **[eV]**	β [°] / **cos(**β**)** [ ]
CN-staple	-1.81	2.07	31.99 / 0.85
***CN-poly*$^{(o)}$**	-1.67	2.29	30.17 / 0.86
***CN-poly*$^{(f)}$**	-1.78	2.19	30.57 / 0.85
CN-unrec	-1.67	2.21	29.05 / 0.87
exp			40.40[208]
CF_3-staple	-1.54	0.83	28.93 / 0.88
CF_3-mono$^{(o)}$	-1.20	1.34	23.01 / 0.92
***CF_3-poly*$^{(f)}$**	-1.45	1.15	24.75 / 0.91
CF_3-unrec	-1.40	0.98	32.14 / 0.85
CH_3-staple	-1.57	-1.72	30.14 / 0.86
CH_3-mono$^{(o)}$	-1.22	-1.17	21.79 / 0.93
CH_3-mono$^{(f)}$	-1.29	-1.36	21.63 / 0.93
CH_3-unrec	-1.45	-1.71	25.75 / 0.90
exp			$\leq$19.00[47, 160, 209]

A quantity of interest suitable for comparison with experimental work, as it is of special interest in the field of organic monolayers on metal substrates, is the work-function modification of the underlying metal, $\Delta\Phi$. In theory $\Delta\Phi$ can be split into two potential energy steps,[44]

$$\Delta\Phi = BD + \Delta E_{vac} \tag{19}$$

where the bond dipole, BD, describes the binding induced dipole at the metal/organic interface and ΔE_{vac}, the potential jump that originates from the shift of the vacuum level induced by the dipolar monolayer. The magnitude of ΔE_{vac} depends on the dipole contribution of the monolayer according to the Helmholtz equation,

$$\Delta E_{vac} = \frac{e\mu_0 cos(\beta)}{\varepsilon^{eff}\varepsilon_0 A} \tag{20}$$

with the elementary charge, e, the dipole moment of the isolated molecule, μ_0, the cosine of the tilt angle of the molecules, $cos(\beta)$, a depolarization factor, ε^{eff} and the area per molecule, A.
Following equation 20, it becomes evident that the tilt, β, of the dipolar substituted molecules, that constitute the monolayer, strongly affects ΔE_{vac}. The expression $\mu_0 cos(\beta)$ signifies that only the dipole-contribution in z-direction affects ΔE_{vac}, thus, the larger(smaller) the tilt angle, the smaller(larger) the contribution to ΔE_{vac}.

Upon investigating the different adatom-induced systems, one would assume the changes at the interface (affecting BD) and changes of the molecular tilt angle (affecting ΔE_{vac}) to impact the resulting $\Delta\Phi$ of the total SAM. Any adatom-induced

impact on $\Delta\Phi$ becomes evident when comparing the unreconstructed and reconstructed systems. This comparison however reveals a somewhat surprising result. In the majority of the investigated systems only a minor impact on $\Delta\Phi$ occurs. The dimeric- and polymeric-adatom configurations leave $\Delta\Phi$ relatively unaltered, which can be rationalized when analyzing at its contributions ΔE_{vac} and BD separately.
The values for $cos(\beta)$ of all calculated systems remain in a very similar range, with deviations of less than 9%, see Table 2. Therefor, ΔE_{vac} will be ruled out to have a primary impact on $\Delta\Phi$, leaving only the bond-dipole as responsible factor according to equation 19.

A strong change in $\Delta\Phi$ (0.4 - 0.5 eV) originates only from the monomeric adatom-configurations *CF_3-ontop*, *CH_3-ontop* and *CH_3-fcc*.
As the BD originates from the monolayer-to-substrate induced bonding at the metal/organic interface, the arrangement of the adatom-sulfur bonds (Au_{ad}-S) must have a crucial impact on BD and subsequently $\Delta\Phi$. Taking a closer look at the orientation of the thiolate bonds at the interface reveals a more surface-parallel Au_{ad}-S orientation for the polymeric motifs, while especially in the adatom-ontop systems, *CF_3-ontop* and *CH_3-ontop*, the thiolate Au_{ad}-S bonds assume a more "vertical" configuration. As only the z-component of the dipoles affects $\Delta\Phi$, the contribution of the thiolate Au_{ad}-S bonds to the resulting potential jump increases with a more vertical arrangement. This might explain the relatively unchanged $\Delta\Phi$ for the polymeric-/dimeric- adatom configurations while the adatom-monomer motifs display a considerable impact.

Although this relatively strong change in $\Delta\Phi$ would be of great interest when tailoring the underlying metal substrate, it would not be reasonable trying to force a SAM in that peculiar configuration, as it has the least favorable adsorption energy and may not be the most stable arrangement.

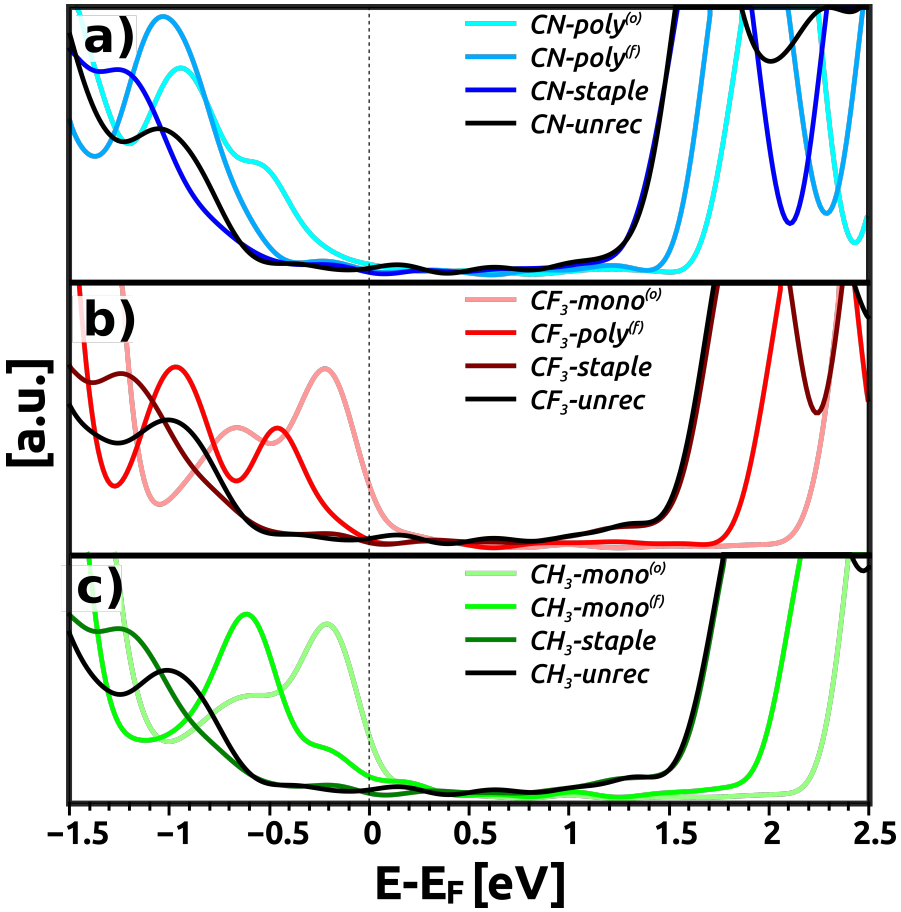

Figure 19: Density of states for the *staple-*, *ontop-*, *fcc-adatom* and unreconstructed configuration for a) the -CN (blue), b) the -CF_3 (red) and c) the -CH_3 (green) substituted biphenylthiole SAMs. The DOS of the respective unreconstructed SAMs is displayed in black. The dashed line signifies E_F.

Introducing adatoms into the metal-organic interface significantly changes the bonding-geometry and -chemistry. Thus, one may expect a correlation between the bonding-configuration of the monolayer to the substrate and features in the Density of States (DOS) to occur.[173,210]
Potential deviations in the distribution of states between the calculated DOS of a reconstructed and unreconstructed system might enable or facilitate the identification of a present adatom or even the resulting interfacial adatom-geometry. In that respect the DOS of each reconstructed and unreconstructed SAM was calculated and compared as shown in Figure19.
The most crucial observations, regarding all tail-group substitutions, are twofold. First, comparing the DOS for the unreconstructed SAM (black) and the staple-motif reveals an almost identical distribution of states. Thus, whether a staple-motif or a SAM on a 'clean' gold surface is at present, would not be distinguishable. Since this staple-motif has the most favorable adsorption energy (including the unreconstructed systems) and is frequently reported in literature to also occur in high

density SAMs,[167,170,172,173] one must acknowledge the significant possibility of its presence in real life samples.

The second crucial observation is that in monomeric adatom-configurations (*CH_3-fcc*, *CH_3-ontop*, *CF_3-ontop*) the HOMO peak in the DOS is shifted towards more positive values, suggesting Fermi-level pinning.[173,210] This may be caused by the presence of chargeable states at the interface (metal-induced gap states) induced by the direct chemical bonding of the monolayer to (*under-coordinated*) adatoms.[211] The observation of Fermi-level pinning may serve as suitable indicator for the presence of a certain bonding-configuration that contains under-coordinated adatoms at the interface.
Nevertheless, it is reasonable to assume, that such interfacial-configurations might not occur in reality as the calculated adsorption energies are rather high compared to the unreconstructed systems. Further, consequential effects on electronic properties such as a strong work-function modification, would envoke a larger interest on detecting such geometries.

In general, the deviation of the DOS for a reconstructed system compared to the DOS of the 'clean' SAM, appears to be determined by the bonding-configuration of the adatom. With an increasing resemblance of this bonding-configuration to a polymeric- or staple-motif, charge distribution at the Fermi-level decreases, closely resembling the unreconstructed system. Thus, investigating the DOS of such SAMs may not reveal whether a unreconstructed or reconstructed system is at hand.

Conclusion

High-coverage, donor- (-CN, -CF_3) and acceptor- (-CH_3) substituted biphenylthiol-based SAMs on reconstructed Au(111) were modeled, focusing on the impact of introducing adatoms into the metal/organic interface.
Three different adatom-motifs were generated in a 1:1 and 1:2 (adatoms:molecule) ratio, where the 1:2 systems form the well known staple-motif. Due to a flexible initial-configuration, no geometric trajectory towards any specific local minimum is given enabling the generation of versatile adatom-induced interfacial architectures.

At first sight the final geometries assume a tail-group dependent trend in formation of a specific adatom motif, resembling a mixture of a polymeric- and staple-adatom configuration (Au_{ad}-SR-Au_{ad}-SR). While all -CN-substituted adatom geometries display the polymer-motif, the -CH_3 analogues remain in a monomeric configuration (Au_{ad}-SR).
However, due to collective electrostatic effects within densely packed monolayers diminishing the impact-reach of dipolar tail-groups, the electronic impact of the donor-/acceptor-substituents cannot be held responsible to have a primary impact. Which states that the arbitrarily generated interfacial adatom-configurations determine the structure of the monolayer.

In accordance to published literature, we find the energetically most favorable adsorption configuration, including the unreconstructed systems, to be the staple motif. Polymeric/staple adatom-motifs in general appear to increase a SAMs stability, resulting in a uniform hierarchy for all tail-group substitutions: staple $<$ polymer $<$ *unrec* $<$ monomer.
Whilst having the least favorable adsorption energy, monomeric motifs also display the strongest deviations from their unreconstructed analogues in terms of their electronic properties. We find a change of work-function modification up to 0.5 eV and Fermi-level pinning to occur for the monomer-motifs. The distribution of states close to the Fermi-level, might be rationalized by the presence of under-coordinated adatoms at the interface inducing metal-induced gap states.[211]
The observation of Fermi-level pinning may potentially serve as indicator for the presence of a specific bonding-configuration at the interface.
On the contrary, calculating the work-function modification and density of states for the polymeric-/staple- motifs, containing highly coordinated adatoms, displays a surprisingly minor deviation from the according unreconstructed systems. As these motifs also have the lowest adsorption energies, the probability of their yet undetected existence in a multitude of high-density SAMs on a Au(111) substrates is reasonably high.

2 Electronic Properties of Biphenylthiolates on Au(111): The Impact of Coverage Revisited

2.1 Author Contribution

E. Zojer conceived the idea to investigate the impact of coverage on the electronic properties of a biphenylthiole-based SAM on Au(111). E. Verwüster performed all calculations and primary analysis of the data. The data set was interpreted by all authors. E. Verwüster wrote the first version of the manuscript and prepared all figures. The manuscript was improved in cooperation with E. Zojer, O.T. Hofmann and D.A. Egger. The project was supervised by E. Zojer

The following paper is published in the Journal of Physical Chemsitry C and inserted here as original publication together with the Supporting Information. Reprinted with permission from "Verwüster E.; Hofmann O.T.; Egger D.A.; Zojer E.; Electronic Properties of Biphenylthiolates on Au(111): The Impact of Coverage Revisited, *J. Phys. Chem. C.*, vol. 119, no. 14, pp. 7817-7825, 2015" Copyright 2015 American Chemical Society

2.2 Original Article

THE JOURNAL OF PHYSICAL CHEMISTRY C

Article

pubs.acs.org/JPCC

Electronic Properties of Biphenylthiolates on Au(111): The Impact of Coverage Revisited

Elisabeth Verwüster,[†] Oliver T. Hofmann,[†] David A. Egger,[†,§] and Egbert Zojer*[,†]

[†]Institute of Solid State Physics, NAWI Graz, Graz University of Technology, Petersgasse 16, 8010 Graz, Austria

[§]Department of Materials and Interfaces, Weizmann Institute of Science, Rehovoth 76100, Israel

Supporting Information

ABSTRACT: We study the impact of coverage on the electronic structure of substituted biphenylthiolate-based self-assembled monolayers (SAMs) on Au(111) surfaces with a particular focus on SAM-induced work-function changes, $\Delta\Phi$. This is done using density functional theory accounting also for van der Waals interactions. We find that the tilt angle of the molecules increases significantly when reducing the coverage, which results in a marked decrease of the perpendicular component of the molecular dipole moment. However, $\Delta\Phi$ does not follow the trend that one would expect on purely geometrical grounds. While for donor-substituted SAMs, $\Delta\Phi$ decreases much more slowly than anticipated, for acceptor-substituted SAMs the coverage-induced reduction of $\Delta\Phi$ is clearly more pronounced than expected. In fact, in that case $\Delta\Phi$ already vanishes around half coverage. This is in part associated with the (coverage-dependent) bond dipole originating from the "Au−S−C" bond. Especially for low coverages, however, the relevance of the "Au−S−C" dipole diminishes, and we observe a significant contribution of Pauli-Pushback (also known as "cushion effect") to the interfacial charge rearrangements, an effect that hitherto received only minor attention in the discussion of covalently bonded SAMs.

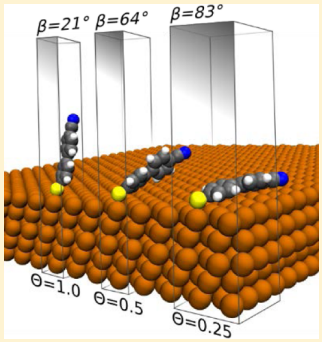

INTRODUCTION

There is an increasing use of organic self-assembled monolayers (SAMs) covalently bonded to metal surfaces in various organic electronics applications.[1−8] This raises the need for an in-depth understanding of the processes that determine the properties of the resulting metal−organic interfaces.[9−12] Especially molecules with conjugated, rigid backbones are of interest, as due to the π-conjugation they allow for moderate tunnel barriers at the metal−organic interface.[13−15] Thus, an interesting class of molecules for tuning charge injection/extraction barriers[8,16,17] in organic devices are oligophenylenethiolates substituted with polar tail groups to modify the substrate work function, Φ.[18−22] Such systems are at the heart of the present paper (see Figure 1a).

The impact of the film quality on the monolayer properties is a crucial aspect when comparing idealized perfectly ordered and infinitely extended monolayers with more realistic systems, which are encountered, e.g., on top of the electrodes in actual devices. Quantum-mechanical simulations typically study perfectly ordered and densely packed metal−SAM systems, because their 2D-periodic nature is compatible with highly efficient theoretical approaches based on density functional theory (DFT). For these systems, extraordinarily large changes of the work function, $\Delta\Phi$, and injection barrier amounting up to several electronvolts have been predicted.[23−29] Quantitative agreement between theory and experiment has, however, been achieved only for exceptionally well-ordered layers that induce moderate work-function shifts.[30,31] This calls for developing a systematic understanding of how imperfections in the structural arrangement of the SAM affect the electronic properties of the interface. Indeed, the impact of certain types of film imperfections has been recognized earlier. For instance,

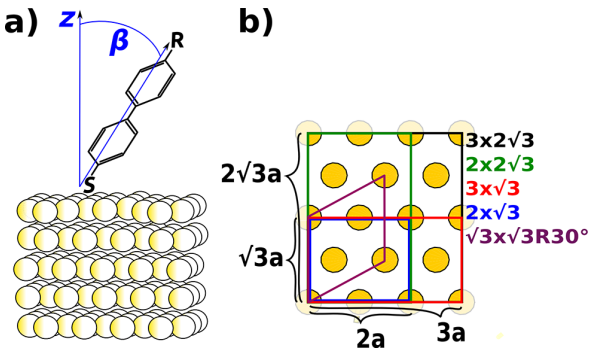

Figure 1. (a) Schematic sketch of the studied substituted biphenylthiolate on a slab of five layers of gold. z denotes the axis perpendicular to the slab, β the tilt angle between long-molecular axis and z, and R = CN, CF_3, CH_3, NH_2 (where data for the CF_3- and CH_3-substituted molecules are shown in the Supporting Information (SUI) only). (b) Surface unit cells used in the present study to simulate coverages of 1.0, 0.75, 0.5, 0.375, and 0.25; each unit cell contains one molecule (see text for details).

Received: January 30, 2015
Revised: March 11, 2015
Published: March 16, 2015

DOI: 10.1021/acs.jpcc.5b00992
J. Phys. Chem. C 2015, 119, 7817−7825

Otálvaro et al. studied the influence of deviations from a perfectly flat Au(111) surface.[32] For simple aliphatic thiolates on Au and Ag they, however, found only a minor impact on $\Delta\Phi$. Beyond that, grain boundaries[33] can have a significant influence on the internal film structure.[34] They can be caused by coverage-dependent internal stress exerted on the molecular layer by the enforced hexagonal arrangement of the thiolate docking groups.[35] Moreover, incomplete coverage SAMs and "lying-down" (face-on) phases (*vide infra*) have been observed for films grown on small-grained Au substrates.[36] Recently, low-coverage SAMs have even been prepared on purpose to tune/switch the tilt angle of the adsorbed molecules and thereby tune $\Delta\Phi$.[37,38]

Most papers modeling the impact of varying densities of molecules bearing polar substituents deal with essentially upright-standing SAMs also when the monolayer coverage is reduced.[39−43] While this provides significant fundamental insight, it does not necessarily reflect the situation occurring in an actual monolayer at low packing densities. In fact, lying-down phases of low-coverage SAMs have been found in several experiments,[44−48] which is not surprising considering the significant van der Waals (vdW) attraction between organic adsorbates and metal surfaces.[49,50]

To provide insight into the interplay between coverage, molecular tilt, and the electronic properties of the interfaces, we here fully optimize film structures of substituted 4-mercapto-biphenylthiole as a function of coverage using an advanced optimization tool. This allows us to identify the significant impact that the increasing molecular tilt at low coverages has on the SAM-induced work-function modification, $\Delta\Phi$. We show that the "falling over" of molecules causes rather unexpected findings such as a vanishing $\Delta\Phi$ already at half coverage for acceptor-substituted layers.

METHODOLOGY

Computational Approach. The calculations rely on the slab-type band-structure approach, employing density functional theory using the VASP code.[51] The cutoff energy for the plane-wave basis was set to 273.894 eV, and a tight convergence criterion of 10^{-6} eV was employed for the total energy in the self-consistent field procedure. Throughout this work, we used the Perdew−Burke−Ernzerhof (PBE) functional,[52] augmented by the Tkatchenko−Scheffler scheme,[53] in the parametrization that is specifically tailored to surfaces[54] to account for the missing long-range van der Waals interactions. For that we used the implementation described in ref 55. We applied the projector augmented-wave (PAW) method[56,57] to account for valence−core interactions. More details on the PAW potentials used here can be found in the Supporting Information (SUI).

At full coverage, we used an 8 × 8 × 1 Monkhorst−Pack[58] type k-point grid that was appropriately scaled for reduced coverages. To decouple periodic replicas of the slab, a ∼20 Å vacuum gap and a self-consistently determined dipole layer were introduced.[59] The Au(111) surface was represented by a five-layer slab, where the positions of the atoms in the bottom three layers were kept fixed in the geometry optimization process. The top two layers and the molecule were allowed to relax without any constraints until the remaining forces were smaller than 10^{-2} eV/Å. We applied an optimization scheme based on internal coordinates and the Direct Inversion in the Iterative Subspace (DIIS) algorithm as implemented in the GADGET tool[60] (which in the used implementation also features automated substrate detection).[61] This and a suitable initialization of the Hessian are important for obtaining reliable geometries at affordable computational costs, as especially the molecular tilt angle changes significantly in the course of geometry optimizations at low coverages.

System Setup. Ordered oligophenylene-thiolates on Au(111) surfaces at full coverage typically grow in a herringbone pattern with two molecules in a $3 \times \sqrt{3}$ surface unit cell.[47,48,62] A possibility to reduce the coverage preserving this herringbone motive would be to add extra rows of gold between the molecules. Adding a single row yields the $4 \times \sqrt{3}$ unit cell with a striped phase that has been observed experimentally for anthracene selenolates.[63,64] Systematically reducing the coverage even further pursuing that approach is, however, difficult. Thus, we abandoned the herringbone motive and followed a different strategy with a single molecule per unit cell (noteworthy, the trends obtained in this way are fully consistent with those for the accessible herringbone-based structures at full, 0.75, and 0.60, as shown in the SUI). We defined full coverage as a single molecule in a $(\sqrt{3} \times \sqrt{3})R30°$ surface unit cell (which gives the same area per molecule as 2 molecules in the $3 \times \sqrt{3}$ cell). Subsequently, the unit cell size was increased, as indicated in Figure 1 b. The lowest coverage considered was 0.25, corresponding to a $3 \times 2\sqrt{3}$ surface unit cell.

Interestingly, smooth trends are obtained for all quantities considered below, in spite of the fact that the aspect ratios of the unit cells change quite significantly when following this procedure. This, together with the fact that also for the above-described herringbone structures similar trends are obtained, indicates that for the effects discussed here the exact details of the packing motive are not of primary relevance. This finding is important since the studied monolayer displays a 2D translational periodicity, which will not necessarily be obtained in experimentally investigated low-coverage samples (the ordered lying-down phases mentioned above notwithstanding). Such periodic boundary conditions are, however, necessary for properly describing the metallic substrate in the simulations; they also allow for a straightforward description of collective electrostatic effects, whose consideration is absolutely crucial when studying SAMs.[14,40]

To understand differences between donor- and acceptor-substituted SAMs, we focus here on two 4-mercaptobiphenyl derivatives with either a −CN (strong acceptor) or $-NH_2$ (strong donor) tail-group substituent. These were shown to display particularly strong coverage-dependent effects.[14,41] The trends obtained when using the more weakly donating and accepting substituents, $-CH_3$ and $-CF_3$ are equivalent. Thus, for the sake of clarity, the corresponding data are contained only in the Supporting Information.

RESULTS AND DISCUSSION

The most important parameter to quantify the change of the SAM geometry upon reducing the coverage is the molecular tilt angle, β, defined as the angle between the surface normal (z) and the long molecular axis (see Figure 1a). In Figure 2a, we show its evolution when decreasing the coverage, Θ.

For both systems, we observe a pronounced increase of β up to the point where the molecules "fall over"; i.e., they lie essentially flat on the surface and $\beta \sim 90°$. To understand how this affects the SAM-induced work-function modification, it is useful to remember that $\Delta\Phi$ is commonly separated into two contributions,[14,17,65−67] denoted here as $\Delta\Phi_{BD}$ and $\Delta\Phi_{mol}$. $\Delta\Phi_{BD}$ arises from the charge rearrangements due to the metal−

DOI: 10.1021/acs.jpcc.5b00992
J. Phys. Chem. C 2015, 119, 7817−7825

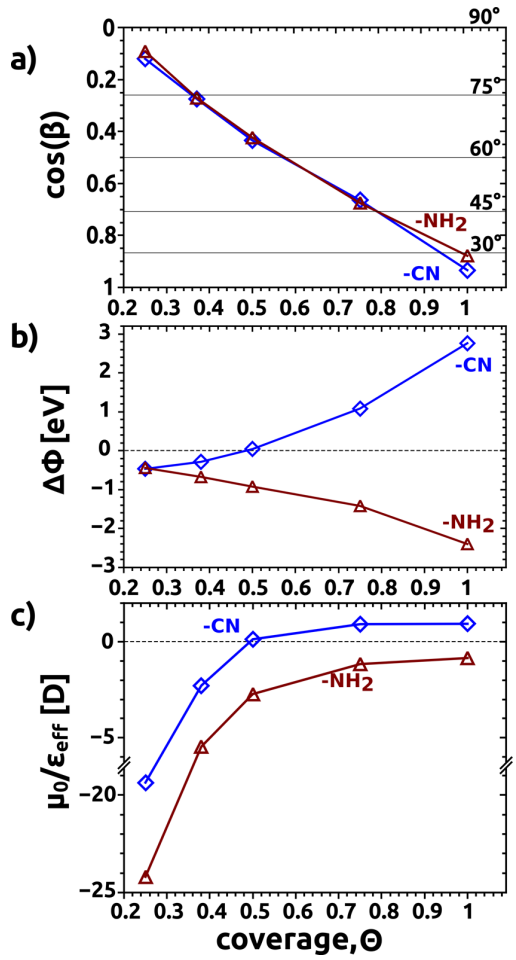

Figure 2. Coverage dependence of (a) the tilt angle (β) and cosine of the tilt angle ($\cos(\beta)$); (b) the work-function modification, $\Delta\Phi$, and (c) the quantity μ_0/ε_{eff} obtained by calculating $\Delta\Phi A_{1.0}\varepsilon_0/(e\Theta\cos(\beta))$, which can be regarded as an effective dipole moment of the combined metal−SAM system (for details see text). Results for the CN-substituted system are shown as blue diamonds and those for the $-NH_2$-substituted case as red triangles.

SAM interactions. As this is commonly associated with bonding, it is referred to as bond dipole. How it is affected by a change in the molecular tilt angle will be discussed later.

Prior to that it is useful to qualitatively analyze how $\Delta\Phi_{mol}$, which stems from the molecular dipole, is affected by a change in β. The molecular dipole and the associated work-function change are related by the Helmholtz equation

$$\Delta\Phi_{mol} = -\frac{e}{\varepsilon_0}\frac{\mu_{z,mol}}{A_{1.0}}\Theta = -\frac{e}{\varepsilon_0}\frac{\mu_{0,mol}\cos(\beta)}{\varepsilon_{eff}A_{1.0}}\Theta \quad (1)$$

Here ε_0 is the vacuum permittivity, and $A_{1.0}$ is the surface area per molecule at $\Theta = 1.0$. In the present case with one molecule per unit cell, $A_{1.0}$ is also the area of the $(\sqrt{3}\times\sqrt{3})R30°$ surface unit cell, which amounts to 22.27 Å^2. The area per molecule at reduced coverages is then given by $A_{1.0}/\Theta$. $\mu_{z,mol}$ is the (coverage-dependent) z-component of the dipole moment per molecule within the monolayer. The sign of $\mu_{z,mol}$ is taken to be positive, when the dipole moment points away from the substrate. $\mu_{z,mol}$ includes depolarization effects that originate from the polarization of the molecular electron cloud caused by the electrical fields of the surrounding molecules.[41−43,68−70] Note that these depolarization effects are intrinsically considered in our self-consistent calculations.

In the right part of eq 1, the expression is recast in terms of the intrinsic (gas-phase) dipole moment of the isolated molecule, $\mu_{0,mol}$. The appearance of $\cos(\beta)$ in the right part of eq 1 denotes that only the z- (i.e., perpendicular) component of the molecular dipole moment impacts the value of $\Delta\Phi$. In passing we note that for the actual SAM on a metal substrate the in-plane (x- and y-) components of the dipoles of the unit cell have to disappear, as a metal does not tolerate a potential gradient parallel to its surface; i.e., the corresponding dipole components of the molecule will be compensated by a polarization of the metal substrate (described by mirror charges). On more technical grounds, when applying periodic boundary conditions, the in-plane components of the molecular dipole moment in the SAM disappear also in the isolated monolayer as a consequence of the translational symmetry.

ε_{eff} is a coverage-dependent effective parameter that quantifies the decrease in the dipole moment due to depolarization effects.[41] At full coverage it is often approximated by the dielectric constant of a bulk material consisting of the same molecules as the SAM. At lower coverages ε_{eff} decreases, accounting for the fact that depolarization diminishes.[41] Finally it should be noted that in the following discussions we will frequently refer to $|\Delta\Phi_{mol}|$, where the absolute value is used because the sign of $\Delta\Phi_{mol}$ (respectively, the orientation of the dipole on the surface) differs for donor and acceptor substituents.

When decreasing Θ, $|\Delta\Phi_{mol}|$ is expected to decrease as well for two reasons: (i) the dipole density naturally decreases with decreasing molecular density, and (ii) at low coverage the tilt angle increases (see Figure 2a). This results in a smaller component of the dipole moment perpendicular to the surface as expressed through $\cos(\beta)$ in eq 1. The trend is counteracted by a decreasing depolarization at reduced coverage, but this effect is smaller than the two aforementioned ones (vide infra).

For both Au−SAM systems, the DFT-calculated evolution of (the total) work-function change, $\Delta\Phi$, as a function of Θ is shown in Figure 2b. For the $-NH_2$-substituted SAM, $|\Delta\Phi|$ decreases with coverage as qualitatively expected from the above considerations regarding the molecular contribution, $|\Delta\Phi_{mol}|$. What can, however, not be explained in terms of molecular electrostatics alone is that a significant value of $|\Delta\Phi|$ (0.44 eV) still remains at 0.25 coverage, when the molecules lie almost flat on the surface (cf. Figure 2a). For the −CN case, the dependence of $|\Delta\Phi|$ on Θ deviates even more significantly from the trend arising from the molecular dipole: A decrease of $|\Delta\Phi|$ is observed only for $\Theta \geq 0.5$; at $\Theta = 0.5$, $|\Delta\Phi|$ vanishes, and $\Delta\Phi$ even changes sign for lower coverages reaching essentially the same value as in the $-NH_2$-substituted SAM at $\Theta = 0.25$.

The deviation of the behavior of the actual interface from that of an assembly of conventional dipoles can be illustrated more clearly by calculating

$$\frac{\mu_0}{\varepsilon_{eff}} = \frac{\Delta\Phi A_{1.0}\varepsilon_0}{e\Theta\cos(\beta)} \quad (2)$$

It can be regarded as the quantity one obtains when modeling the metal−SAM system by an effective dipole moment, μ_0/ε_{eff}, pointing in the same direction as the long molecular axis. Note, that μ_0 is defined in analogy to $\mu_{0,mol}$ with the difference that it

DOI: 10.1021/acs.jpcc.5b00992
J. Phys. Chem. C 2015, 119, 7817−7825

represents the entire metal−molecule system rather than only the molecule. If the molecular dipoles were the only reason for $\Delta\Phi$ and in the absence of depolarization effects the coverage dependence of μ_0/ε_{eff} should yield a horizontal line. For systems in which depolarization is significant, which typically applies to SAMs,[28] $|\mu_0/\varepsilon_{eff}|$ should increase at small coverages. Qualitatively, this expectation is met for the $-NH_2$-substituted SAM, but even in that system depolarization-related effects can hardly account for the increase of $|\mu_0/\varepsilon_{eff}|$ by a factor of ∼28 between Θ = 1.0 and Θ = 0.25 (note the axis break in Figure 2c). In the −CN-substituted SAMs a behavior differing even qualitatively from the expectations for conventional dipoles with a sign change at Θ = 0.5 is found (see Figure 2c).

These considerations show that the behavior of the actual system significantly deviates from that of an assembly of conventional dipoles aligned along the long molecular axes. This means that the second contribution to $\Delta\Phi$, which is the above-mentioned interfacial charge-rearrangement-related work-function shift, $\Delta\Phi_{BD}$, must display a peculiar coverage dependence. In this context, it is interesting to mention that, when previously studying the coverage dependence for an analogous −CN-substituted SAM on Au(111) at small (essentially constant) molecular tilt angles, a vanishing or even negative value of $\Delta\Phi$ was not observed.[41] This implies that the peculiar evolution of $\Delta\Phi_{BD}$ must be rooted in the "falling-over" of the molecules at low coverages.

For thiolate-bonded SAMs, $\Delta\Phi_{BD}$ is frequently associated with the charge rearrangements due to the formation of a chemical bond between the thiols and the metal−surface, which can be viewed as the replacement of the S−H bonds by S−Au bonds[71] or as the formation of a bond between the −S* radical and the Au surface[65] (for a comparison of the two views see ref 72). We, here, refrain from a numerical evaluation of the coverage dependence of $\Delta\Phi_{BD}$, as, when adopting the "bond-replacement" point of view in systems with changing tilt angles, the relevant information is masked by the dependence of the S−H dipole on the on the tilt and on the relative position of the H atom.[72] For the "bond-formation approach" one mostly analyzes the charge rearrangements that originate from the transition from an open to a closed-shell electronic structure of the adsorbed molecules. That is, in this case the sought-after bonding-related charge redistributions at the metal−molecule interface are superimposed with those associated with the loss of radical character of the adsorbing molecules.[72]

Instead, we adopt a different approach to more clearly elucidate the reason for the peculiar coverage dependence of $\Delta\Phi_{BD}$: In a *Gedankenexperiment* we simply eliminate the contribution of the charge rearrangements associated with the thiolate by replacing it with a hydrogen atom. This is indicated in the inset of Figure 3a. To achieve this technically, only the geometric parameters of the C−H bond replacing the C−S bond are optimized. We denote quantities calculated for the surrogate system with primes (′). The differences in the evolution of the work-function change due to this hypothetical model system and the complete SAM can be associated with the contribution of the Au−thiolate bond to $\Delta\Phi_{BD}$. As the smallest Au−H distance is 2.24 Å, the "chemical" contributions of the interaction between the extra H atom and the surface to $\Delta\Phi_{BD}'$ can be expected to be very small. Interestingly, as shown in Figure 3a, when calculating the coverage dependence of $\Delta\Phi'$, one obtains an evolution qualitatively very similar to that of $\Delta\Phi$ shown in Figure 2b. Only at full coverage, where the density of thiolate−Au bonds is highest, $\Delta\Phi$ is clearly less

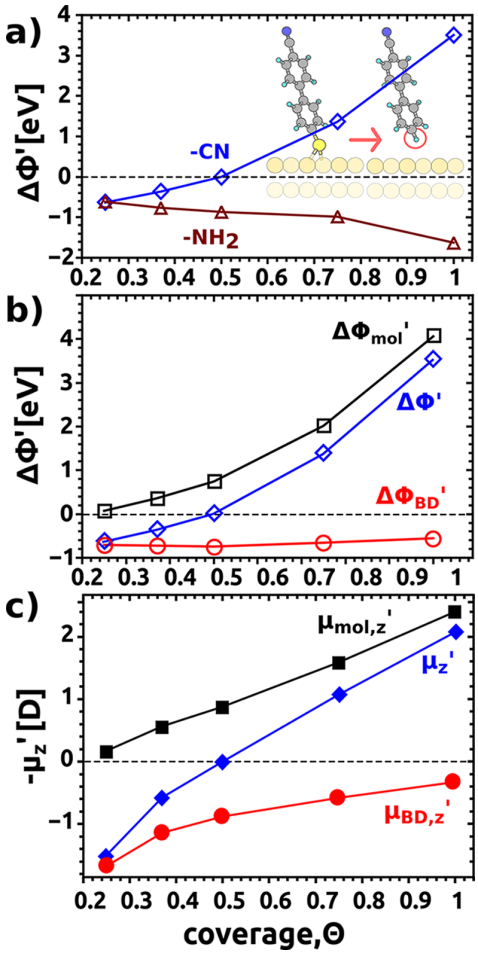

Figure 3. (a) Coverage dependence of the work-function modification in the hydrogen-substituted model systems bearing −CN (blue diamonds) and $-NH_2$ (red triangles) tail groups. The inset shows the substitution of the sulfur by a hydrogen atom as part of our gedanken experiment. (b) Coverage-dependent decomposition of the total work-function change in the −CN-substituted model system, $\Delta\Phi'$ (blue diamonds), into contributions from the (free-standing) monolayer, $\Delta\Phi_{mol}'$ (black squares), and from the interfacial charge rearrangements, $\Delta\Phi_{BD}'$ (red circles). (c) Analogous decomposition into contributing dipoles per molecule. The energetic shifts in (b) are proportional to those in (c) divided by the surface area per molecule ($\Delta\Phi' \propto \mu_z'\Theta/A_{1.0}$).

positive (more negative) than $\Delta\Phi'$ for the −CN ($-NH_2$) substituted SAM (cf., Figure 2b and Figure 3a). This comparison shows that the main reason for the deviation between the "conventional" polarizable dipole picture described by eq 1 and the actual evolution of $\Delta\Phi$ when approaching the dilute limit is not directly related to the Au−S bond formation.

An advantage of the chosen model system is that here the individual contributions of $\Delta\Phi_{mol}'$ and $\Delta\Phi_{BD}'$ to $\Delta\Phi'$ can be separated unambiguously.[73] The results for the −CN-substituted SAM are shown in Figure 3b; those for the $-NH_2$ case are contained in the SUI. As expected (cf., eq 1) for polarizable dipoles, $\Delta\Phi_{mol}'$ decreases continuously with decreasing coverage approaching zero for the close to flat-lying molecules at Θ = 0.25. Interestingly, the work-function modifications caused by the molecule−metal interaction,

DOI: 10.1021/acs.jpcc.5b00992
J. Phys. Chem. C 2015, 119, 7817−7825

$\Delta\Phi_{BD}'$, show essentially no coverage dependence. What this means becomes more evident when considering the corresponding quantities per surface area occupied by each molecule (i.e., per $A_{1.0}/\Theta$). To ensure that the resulting quantities (displayed in Figure 3c) represent dipole moments, they are defined as (cf., eq 1)

$$\mu_{X,z}' = \frac{\varepsilon_0}{e}\Delta\Phi_X'\frac{A_{1.0}}{\Theta} \quad (3)$$

μ_z' (derived from $\Delta\Phi'$) then represents the total dipole moment associated with each molecule, and $\mu_{mol,z}'$ and $\mu_{BD,z}'$, respectively, denote the contributions from the molecular dipole and the molecule−substrate interaction. While $|\mu_{mol,z}'|$ decreases strongly with coverage, one sees a pronounced *increase* of $|\mu_{BD,z}'|$ at low coverage (by a factor of ∼5 between Θ = 1.0 and Θ = 0.25). These opposite trends explain, why, for the −CN-substituted SAM μ_z' and also $\Delta\Phi'$ disappear at half coverage, where $\mu_{mol,z}'$ and $\mu_{BD,z}'$ cancel, as schematically indicated in the left panel of Figure 4a. For smaller Θ, the

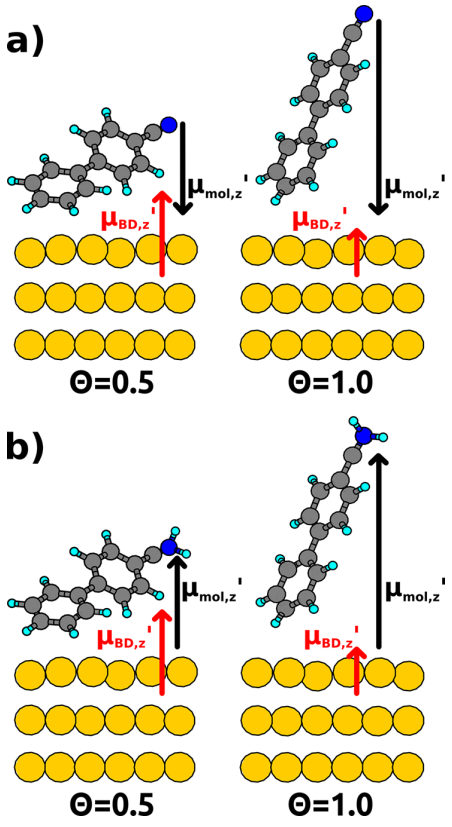

Figure 4. Schematic illustration of the resulting interplay of $\mu_{mol,z}'$ and $\mu_{BD,z}'$ when going from full to half coverage for the hydrogen-substituted model system either bearing (a) an electron-accepting substituent (−CN) or (b) an electron-donating substituent ($-NH_2$) (panel b).

combination of the different orientation of the dipoles and the larger absolute magnitude of $\mu_{BD,z}'$ explains why then the adsorption of the SAM reduces the work function in spite of the acceptor substituent. In the NH_2-substituted case the absolute value of $\mu_{mol,z}'$ and $\mu_{BD,z}'$ displays a similar coverage dependence as the one discussed above (see SUI). For this case, however, the dipoles add up, and no cancellation of dipole moments or changes in the sign of $\Delta\Phi'$ occur. This is illustrated in Figure 4b. Bearing in mind the similar evolutions of $\Delta\Phi$ and $\Delta\Phi'$ (vide supra) with coverage, the strong increase of $\mu_{BD,z}'$ at small coverage can also be held responsible for the trends observed for the thiolate-bonded SAMs in Figure 2 especially at small Θ.

What remains to be explained is the strong increase of $\mu_{BD,z}'$ in diluted SAMs. By definition, the bond dipole originates from the charge rearrangements $\Delta\rho'$ induced by the metal−molecule interaction. For the model system, we define them as

$$\Delta\rho' = \rho_{sys}' - (\rho_{slab}' + \rho_{mol}') \quad (4)$$

with ρ_{sys}' being the electron density of the combined system, ρ_{slab}' the electron density of the metal slab, and ρ_{mol}' the electron density of the isolated molecular monolayer. To calculate $\Delta\rho$ for the thiolate-containing systems in the bond-replacement picture (vide supra), one additionally needs to consider the charge densities associated with the H atoms that are removed in the course of the bond formation

$$\Delta\rho = \rho^{sys} - (\rho^{slab} + \rho^{mol} + \rho^{H}) \quad (5)$$

For Θ = 0.25, the $\Delta\rho$'s for a hydrogen-substituted model system and the corresponding thiolate system are compared in Figure 5 (plots for Θ = 1.0 and Θ = 0.5 are contained in the SUI). Figure 5a provides a side view of both systems, where the plotted quantity corresponds to $\Delta\rho$ integrated over the unit cell in the direction along the viewing axis. In the model as well as in the thiolate system one sees strong charge depletion (blue region) around the molecular backbone accompanied by an accumulation of charge directly underneath the molecule (red region). The charge depletion close to the S atom is stronger in the actual SAM than that in the C−H region of the model system, an observation to which we will return later.

In Figure 5b, we provide the corresponding top view for both systems, again integrated along the viewing axis. A decrease of (integrated) charge around the molecular backbone can be seen for the thiolate system as well as for the model system (light blue area). An increase of the integrated electron density is seen mostly in the areas between the organic moieties. Qualitatively, both systems again show the same behavior with the exception of a particularly strong charge depletion (enhancement) close the S atom of the thiolate.

We attribute the depletion of electron density around the molecular backbone and the concomitant shift to below and between the organic molecules to the so-called Pauli-Pushback effect[9,10,12,74−77] (also termed cushion effect). It is an effect originating from the repulsion of the overlapping electron densities of the adsorbate layer and the substrate caused by exchange interaction,[77] which leads to a reduction of the surface dipole of the metal substrate. Thus, it results in a significant work-function reduction upon monolayer adsorption. It is discernible from charge transfer between the molecules and metal by the fact that there is essentially no molecular density of states at the metal Fermi level.[78] This is indeed the case here (see SUI). While Pauli-Pushback is well-known in the context of flat-lying molecules on various metal surfaces,[10,74−76] it has rarely been considered for covalently bonded SAMs.[44] Still, Nouchi et al. found it to be crucial for understanding the experimental properties of their (intentionally) disordered systems.[37]

Since the extent of Pauli−Pushback (and the concomitant work-function reduction) depends on the magnitude of the

DOI: 10.1021/acs.jpcc.5b00992
J. Phys. Chem. C 2015, 119, 7817−7825

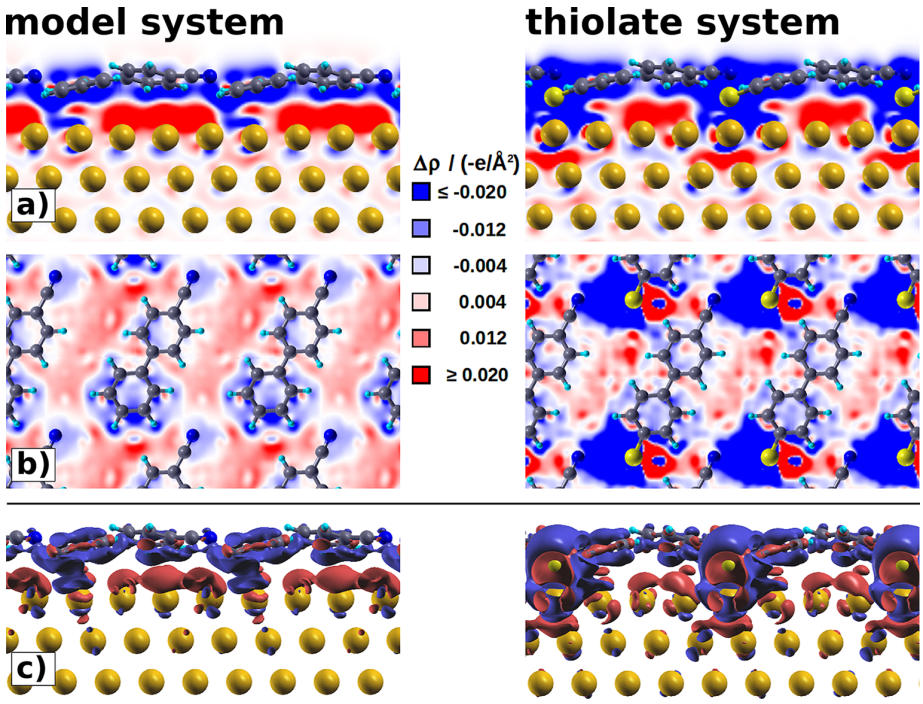

Figure 5. Charge rearrangements arising from the interaction between the metal and the monolayer for the −CN-substituted SAMs at Θ = 0.25. In (a) and (b) charge-density redistributions integrated over the unit cell in the viewing direction are shown. Red areas denote charge accumulation and blue areas depletion; only part of the five Au layers of the metal slab are shown. Panel (a) contains side views for the H-terminated model system and the corresponding thiolate system. In panel (b) the respective top views are shown. Panel (c) contains 3D isodensity plots (with an isovalue of 0.003 e/Å^3).

overlap of the molecular and substrate's electron clouds, it becomes larger when the distance between the backbone and the surface is reduced. This is the case at low coverage, where the molecular tilt angles increase enormously ("falling over" of the molecules).

We can now return to the main difference between the model system and the thiolate in Figure 5, which is the strong charge rearrangements occurring in the vicinity of the S atoms. As Figures 2b and 3b show, ΔΦ is essentially the same at Θ = 0.25 for both systems. This indicates that charge rearrangements directly associated with the thiolate−gold bond must have an only minor contribution to ΔΦ at low coverage. To understand and corroborate this finding, Figure 5c shows Δρ without integration in the form of isodensity plots. The charge rearrangements in the vicinity of the thiolate are massive but to a significant extent are associated with charge redistributions occurring parallel to the surface.[79] Considering that only the components of charge rearrangements perpendicular to the surface contribute to work-function changes one can understand that the S−Au bond formation dominates the interface energetics only at high coverage where the lateral density of thiolates on the surface is large.

SUMMARY AND CONCLUSION

In the present paper, the nontrivial dependence of SAM-induced modification of Au work-functions, ΔΦ, on molecular coverages has been discussed. While the assembly of −CN-substituted 4-mercaptobiphenyls increases the work function of a Au(111) surface by ∼2.8 eV at full coverage, no work-function change is observed for half coverage (Θ = 0.5). At lower values of Θ, ΔΦ even becomes negative in spite of the strongly electron-accepting character of the −CN group. Conversely, for a donor (i.e., $-NH_2$) substituted SAM, ΔΦ does not change its sign as a function of coverage and at Θ = 0.25 approaches −0.5 eV, which is the same value as for the −CN-substituted layer. These observations are shown to be a direct consequence of the increased molecular tilt angles occurring at lower coverages, where besides the tilt-angle dependence of the perpendicular component of the molecular dipoles, Pauli-Pushback (also termed cushion effect) plays a crucial role. At low coverages, where the overlap between the π-system of the molecule and the electron-cloud tailing from the metal surface is largest, it is even the dominant effect determining the SAM-induced work-function change. On the basis of these insights, we surmise that in imperfectly packed systems of thiolates on a metal surface the "SAM-character" (i.e., molecular dipoles and dipoles related to the Au−S bond formation dominating the interface energetics) is increasingly lost, and the film properties start resembling those of a rather inert physisorbed molecular monolayer.

ASSOCIATED CONTENT

Supporting Information

Further details of the computational methodology, additional data for systems with two molecules in the unit cell and for $-CF_3$ and $-CH_3$ substituted SAMs, the partitioning into monolayer and interaction-derived contributions to the work-function change for the $-NH_2$-substituted model system, selected densities of states, and charge rearrangement plots for half and full coverage. This material is available free of charge via the Internet at http://pubs.acs.org.

DOI: 10.1021/acs.jpcc.5b00992
J. Phys. Chem. C 2015, 119, 7817−7825

AUTHOR INFORMATION

Corresponding Author
*E-mail: egbert.zojer@tugraz.at.

Notes
The authors declare no competing financial interest.

ACKNOWLEDGMENTS

Financial support by the Austrian Science Fund (FWF), P24666-N20, is gratefully acknowledged. The work of D.A.E. has been partly supported by a DOC fellowship of the Austrian Academy of Sciences. The computational studies presented have been performed using the clusters of the division for high performance computing at the Graz University of Technology. O.T.H. acknowledges support though the Austrian Science Fund (FWF): J-3285.

REFERENCES

(1) Margapoti, E.; Li, J.; Ceylan, Ö.; Seifert, M.; Nisic, F.; Anh, T. L.; Meggendorfer, F.; Dragonetti, C.; Palma, C.-A.; Barth, J. V.; et al. A 2D Semiconductor−Self-Assembled Monolayer Photoswitchable Diode. *Adv. Mater.* **2015**, DOI: 10.1002/adma.201405110.
(2) Kim, C.-H.; Hlaing, H.; Hong, J.-A.; Kim, J.-H.; Park, Y.; Payne, M. M.; Anthony, J. E.; Bonnassieux, Y.; Horowitz, G.; Kymissis, I. Decoupling the Effects of Self-Assembled Monolayers on Gold, Silver, and Copper Organic Transistor Contacts. *Adv. Mater. Interfaces* **2014**, DOI: 10.1002/admi.201400384.
(3) Crivillers, N.; Osella, S.; Van Dyck, C.; Lazzerini, G. M.; Cornil, D.; Liscio, A.; Di Stasio, F.; Mian, S.; Fenwick, O.; Reinders, F.; et al. Large Work Function Shift of Gold Induced by a Novel Perfluorinated Azobenzene-Based Self-Assembled Monolayer. *Adv. Mater.* **2013**, *25*, 432−436.
(4) Newton, L.; Slater, T.; Clark, N.; Vijayaraghavan, A. Self Assembled Monolayers (SAMs) on Metallic Surfaces (gold and Graphene) for Electronic Applications. *J. Mater. Chem. C* **2013**, *1*, 376.
(5) Halik, M.; Hirsch, A. The Potential of Molecular Self-Assembled Monolayers in Organic Electronic Devices. *Adv. Mater.* **2011**, *23*, 2689−2695.
(6) Ma, H.; Yip, H.-L.; Huang, F.; Jen, A. K.-Y. Interface Engineering for Organic Electronics. *Adv. Funct. Mater.* **2010**, *20*, 1371−1388.
(7) Marmont, P.; Battaglini, N.; Lang, P.; Horowitz, G.; Hwang, J.; Kahn, A.; Amato, C.; Calas, P. Improving Charge Injection in Organic Thin-Film Transistors with Thiol-Based Self-Assembled Monolayers. *Org. Electron.* **2008**, *9*, 419−424.
(8) De Boer, B.; Hadipour, A.; Mandoc, M. M.; van Woudenbergh, T.; Blom, P. W. M. Tuning of Metal Work Functions with Self-Assembled Monolayers. *Adv. Mater.* **2005**, *17*, 621−625.
(9) Braun, S.; Salaneck, W. R.; Fahlman, M. Energy-Level Alignment at Organic/Metal and Organic/Organic Interfaces. *Adv. Mater.* **2009**, *21*, 1450−1472.
(10) Koch, N. Organic Electronic Devices and Their Functional Interfaces. *ChemPhysChem* **2007**, *8*, 1438−1455.
(11) Love, J. C.; Estroff, L. A.; Kriebel, J. K.; Nuzzo, R. G.; Whitesides, G. M. Self-Assembled Monolayers of Thiolates on Metals as a Form of Nanotechnology. *Chem. Rev.* **2005**, *105*, 1103−1170.
(12) Ishii, H.; Sugiyama, K.; Ito, E.; Seki, K. Energy Level Alignment and Interfacial Electronic Structures at Organic/Metal and Organic/Organic Interfaces. *Adv. Mater.* **1999**, *11*, 605−625.
(13) Karthäuser, S. Control of Molecule-Based Transport for Future Molecular Devices. *J. Phys.: Condens. Matter* **2011**, *23*, 013001.
(14) Heimel, G.; Rissner, F.; Zojer, E. Modeling the Electronic Properties of Π-Conjugated Self-Assembled Monolayers. *Adv. Mater.* **2010**, *22*, 2494−2513.
(15) Shamai, T.; Ophir, A.; Selzer, Y. Fabrication and Characterization of "on-Edge" Molecular Junctions for Molecular Electronics. *Appl. Phys. Lett.* **2007**, *91*, 102108.
(16) Bock, C.; Pham, D. V.; Kunze, U.; Käfer, D.; Witte, G.; Wöll, C. Improved Morphology and Charge Carrier Injection in Pentacene Field-Effect Transistors with Thiol-Treated Electrodes. *J. Appl. Phys.* **2006**, *100*, 114517.
(17) Campbell, I. H.; Rubin, S.; Zawodzinski, T. A.; Kress, J. D.; Martin, R. L.; Smith, D. L.; Barashkov, N. N.; Ferraris, J. P. Controlling Schottky Energy Barriers in Organic Electronic Devices Using Self-Assembled Monolayers. *Phys. Rev. B* **1996**, *54*, R14321−R14324.
(18) Waske, P.; Wächter, T.; Terfort, A.; Zharnikov, M. Nitro-Substituted Aromatic Thiolate Self-Assembled Monolayers: Structural Properties and Electron Transfer Upon Resonant Excitation of the Tail Group. *J. Phys. Chem. C* **2014**, *118*, 26049−26060.
(19) Xie, Y.; Cai, S.; Shi, Q.; Ouyang, S.; Lee, W.-Y.; Bao, Z.; Matthews, J. R.; Bellman, R. A.; He, M.; Fong, H. H. High Performance Organic Thin Film Transistors Using Chemically Modified Bottom Contacts and Dielectric Surfaces. *Org. Electron.* **2014**, *15*, 2073−2078.
(20) Fracasso, D.; Muglali, M. I.; Rohwerder, M.; Terfort, A.; Chiechi, R. C. Influence of an Atom in EGaIn/Ga2O3 Tunneling Junctions Comprising Self-Assembled Monolayers. *J. Phys. Chem. C* **2013**, *117*, 11367−11376.
(21) Kim, H.; Meihui, Z.; Battaglini, N.; Lang, P.; Horowitz, G. Large Enhancement of Hole Injection in Pentacene by Modification of Gold with Conjugated Self-Assembled Monolayers. *Org. Electron.* **2013**, *14*, 2108−2113.
(22) Hamadani, B. H.; Corley, D. A.; Ciszek, J. W.; Tour, J. M.; Natelson, D. Controlling Charge Injection in Organic Field-Effect Transistors Using Self-Assembled Monolayers. *Nano Lett.* **2006**, *6*, 1303−1306.
(23) Zhang, T.; Ma, Z.; Wang, L.; Xi, J.; Shuai, Z. Interface Electronic Structures of Reversible Double-Docking Self-Assembled Monolayers on an Au(111) Surface. *Philos. Trans. R. Soc. London Math. Phys. Eng. Sci.* **2014**, *372*, 20130018.
(24) Benassi, E.; Corni, S. Work Function Changes of Azo-Derivatives Adsorbed on a Gold Surface. *J. Phys. Chem. C* **2014**, *118*, 26033−26040.
(25) Hofmann, O. T.; Egger, D. A.; Zojer, E. Work-Function Modification Beyond Pinning: When Do Molecular Dipoles Count? *Nano Lett.* **2010**, *10*, 4369−4374.
(26) Egger, D. A.; Rissner, F.; Rangger, G. M.; Hofmann, O. T.; Wittwer, L.; Heimel, G.; Zojer, E. Self-Assembled Monolayers of Polar Molecules on Au(111) Surfaces: Distributing the Dipoles. *Phys. Chem. Chem. Phys.* **2010**, *12*, 4291.
(27) Rissner, F.; Rangger, G. M.; Hofmann, O. T.; Track, A. M.; Heimel, G.; Zojer, E. Understanding the Electronic Structure of Metal/SAM/Organic−Semiconductor Heterojunctions. *ACS Nano* **2009**, *3*, 3513−3520.
(28) Wang, L.; Rangger, G. M.; Romaner, L.; Heimel, G.; Bučko, T.; Ma, Z.; Li, Q.; Shuai, Z.; Zojer, E. Electronic Structure of Self-Assembled Monolayers on Au(111) Surfaces: The Impact of Backbone Polarizability. *Adv. Funct. Mater.* **2009**, *19*, 3766−3775.
(29) Sun, Q.; Selloni, A. Interface and Molecular Electronic Structure vs Tunneling Characteristics of CH3- and CF3-Terminated Thiol Monolayers on Au(111). *J. Phys. Chem. A* **2006**, *110*, 11396−11400; Erratum. *J. Phys. Chem. A* **2007**, *111*, 10170.
(30) Anna, M.; Track, F. R. Simultaneously Understanding the Geometric and Electronic Structure of Anthraceneselenolate on Au(111): A Combined Theoretical and Experimental Study. *J. Phys. Chem. C* **2010**, *114*, 2677−2684; Erratum. *J. Phys. Chem. C* **2010**, *114*, 12838.
(31) Stammer, X.; Tonigold, K.; Bashir, A.; Käfer, D.; Shekhah, O.; Hülsbusch, C.; Kind, M.; Groß, A.; Wöll, C. A Highly Ordered, Aromatic Bidentate Self-Assembled Monolayer on Au(111): A Combined Experimental and Theoretical Study. *Phys. Chem. Chem. Phys.* **2010**, *12*, 6445.
(32) Otálvaro, D.; Veening, T.; Brocks, G. Self-Assembled Monolayer Induced Au(111) and Ag(111) Reconstructions: Work Functions and Interface Dipole Formation. *J. Phys. Chem. C* **2012**, *116*, 7826−7837.
(33) Cyganik, P.; Buck, M.; Wilton-Ely, J. D. E. T.; Wöll, C. Stress in Self-Assembled Monolayers: Ω-Biphenyl Alkane Thiols on Au(111). *J. Phys. Chem. B* **2005**, *109*, 10902−10908.

(34) Yuan, L.; Jiang, L.; Thompson, D.; Nijhuis, C. A. On the Remarkable Role of Surface Topography of the Bottom Electrodes in Blocking Leakage Currents in Molecular Diodes. *J. Am. Chem. Soc.* **2014**, *136*, 6554−6557.
(35) Berger, R.; Delamarche, E.; Lang, H. P.; Gerber, C.; Gimzewski, J. K.; Meyer, E.; Güntherodt, H.-J. Surface Stress in the Self-Assembly of Alkanethiols on Gold. *Science* **1997**, *276*, 2021−2024.
(36) Godin, M.; Williams, P. J.; Tabard-Cossa, V.; Laroche, O.; Beaulieu, L. Y.; Lennox, R. B.; Grütter, P. Surface Stress, Kinetics, and Structure of Alkanethiol Self-Assembled Monolayers. *Langmuir* **2004**, *20*, 7090−7096.
(37) Nouchi, R.; Shigeno, M.; Yamada, N.; Nishino, T.; Tanigaki, K.; Yamaguchi, M. Reversible Switching of Charge Injection Barriers at Metal/organic-Semiconductor Contacts Modified with Structurally Disordered Molecular Monolayers. *Appl. Phys. Lett.* **2014**, *104*, 013308.
(38) Lahann, J.; Mitragotri, S.; Tran, T.-N.; Kaido, H.; Sundaram, J.; Choi, I. S.; Hoffer, S.; Somorjai, G. A.; Langer, R. A Reversibly Switching Surface. *Science* **2003**, *299*, 371−374.
(39) Kuzumoto, Y.; Kitamura, M. Work Function of Gold Surfaces Modified Using Substituted Benzenethiols: Reaction Time Dependence and Thermal Stability. *Appl. Phys. Express* **2014**, *7*, 035701.
(40) Natan, A.; Kuritz, N.; Kronik, L. Polarizability, Susceptibility, and Dielectric Constant of Nanometer-Scale Molecular Films: A Microscopic View. *Adv. Funct. Mater.* **2010**, *20*, 2077−2084.
(41) Romaner, L.; Heimel, G.; Zojer, E. Electronic Structure of Thiol-Bonded Self-Assembled Monolayers: Impact of Coverage. *Phys. Rev. B* **2008**, *77*, 045113.
(42) Cornil, D.; Olivier, Y.; Geskin, V.; Cornil, J. Depolarization Effects in Self-Assembled Monolayers: A Quantum-Chemical Insight. *Adv. Funct. Mater.* **2007**, *17*, 1143−1148.
(43) Natan, A.; Zidon, Y.; Shapira, Y.; Kronik, L. Cooperative Effects and Dipole Formation at Semiconductor and Self-Assembled-Monolayer Interfaces. *Phys. Rev. B* **2006**, *73*, 193310.
(44) Hong, S.-Y.; Yeh, P.-C.; Dadap, J. I.; Osgood, R. M. Interfacial Dipole Formation and Surface-Electron Confinement in Low-Coverage Self-Assembled Thiol Layers: Thiophenol and P-Fluorothiophenol on Cu(111). *ACS Nano* **2012**, *6*, 10622−10631.
(45) Zhou, J.; Yang, Y. X.; Liu, P.; Camillone, N.; White, M. G. Electronic Structure of the Thiophene/Au(111) Interface Probed by Two-Photon Photoemission. *J. Phys. Chem. C* **2010**, *114*, 13670−13677.
(46) Di Castro, V.; Bussolotti, F.; Mariani, C. The Evolution of Benzenethiol Self-Assembled Monolayer on the Cu(1 0 0) Surface. *Surf. Sci.* **2005**, *598*, 218−225.
(47) Azzam, W.; Fuxen, C.; Birkner, A.; Rong, H.-T.; Buck, M.; Wöll, C. Coexistence of Different Structural Phases in Thioaromatic Monolayers on Au(111). *Langmuir* **2003**, *19*, 4958−4968.
(48) Leung, T. Y. B.; Schwartz, P.; Scoles, G.; Schreiber, F.; Ulman, A. Structure and Growth of 4-Methyl-4′-Mercaptobiphenyl Monolayers on Au(111): A Surface Diffraction Study. *Surf. Sci.* **2000**, *458*, 34−52.
(49) Liu, W.; Tkatchenko, A.; Scheffler, M. Modeling Adsorption and Reactions of Organic Molecules at Metal Surfaces. *Acc. Chem. Res.* **2014**, *47*, 3369−3377.
(50) Ramalho, J. P. P.; Gomes, J. R. B.; Illas, F. Accounting for van Der Waals Interactions between Adsorbates and Surfaces in Density Functional Theory Based Calculations: Selected Examples. *RSC Adv.* **2013**, *3*, 13085.
(51) Kresse, G.; Furthmüller, J. Efficient Iterative Schemes for Ab Initio Total-Energy Calculations Using a Plane-Wave Basis Set. *Phys. Rev. B* **1996**, *54*, 11169−11186.
(52) Perdew, J. P.; Burke, K.; Ernzerhof, M. Generalized Gradient Approximation Made Simple. *Phys. Rev. Lett.* **1996**, *77*, 3865−3868.
(53) Tkatchenko, A.; Scheffler, M. Accurate Molecular Van Der Waals Interactions from Ground-State Electron Density and Free-Atom Reference Data. *Phys. Rev. Lett.* **2009**, *102*, 073005.
(54) Ruiz, V. G.; Liu, W.; Zojer, E.; Scheffler, M.; Tkatchenko, A. Density-Functional Theory with Screened van Der Waals Interactions for the Modeling of Hybrid Inorganic-Organic Systems. *Phys. Rev. Lett.* **2012**, *108*, 146103.
(55) Al-Saidi, W. A.; Voora, V. K.; Jordan, K. D. An Assessment of the vdW-TS Method for Extended Systems. *J. Chem. Theory Comput.* **2012**, *8*, 1503−1513.
(56) Kresse, G.; Joubert, D. From Ultrasoft Pseudopotentials to the Projector Augmented-Wave Method. *Phys. Rev. B* **1999**, *59*, 1758−1775.
(57) Blöchl, P. Projector Augmented-Wave Method. *Phys. Rev. B* **1994**, *50*, 17953−17979.
(58) Monkhorst, H. J.; Pack, J. D. Special Points for Brillouin-Zone Integrations. *Phys. Rev. B* **1976**, *13*, 5188−5192.
(59) Neugebauer, J.; Scheffler, M. Adsorbate-Substrate and Adsorbate-Adsorbate Interactions of Na and K Adlayers on Al(111). *Phys. Rev. B* **1992**, *46*, 16067−16080.
(60) Bučko, T.; Hafner, J.; Ángyán, J. G. Geometry Optimization of Periodic Systems Using Internal Coordinates. *J. Chem. Phys.* **2005**, *122*, 124508.
(61) Rissner, F. Collective Effects in Self-Assembled Monolayers of Polar Organic Molecules. *Doctoral Thesis*, Graz University of Technology, 2012.
(62) Tao, Y.-T.; Wu, C.-C.; Eu, J.-Y.; Lin, W.-L.; Wu, K.-C.; Chen, C. Structure Evolution of Aromatic-Derivatized Thiol Monolayers on Evaporated Gold. *Langmuir* **1997**, *13*, 4018−4023.
(63) Bashir, A.; Käfer, D.; Müller, J.; Wöll, C.; Terfort, A.; Witte, G. Selenium as a Key Element for Highly Ordered Aromatic Self-Assembled Monolayers. *Angew. Chem., Int. Ed.* **2008**, *47*, 5250−5252.
(64) Käfer, D.; Witte, G.; Cyganik, P.; Terfort, A.; Wöll, C. A Comprehensive Study of Self-Assembled Monolayers of Anthracenethiol on Gold: Solvent Effects, Structure, and Stability. *J. Am. Chem. Soc.* **2006**, *128*, 1723−1732.
(65) Natan, A.; Kronik, L.; Haick, H.; Tung, R. T. Electrostatic Properties of Ideal and Non-Ideal Polar Organic Monolayers: Implications for Electronic Devices. *Adv. Mater.* **2007**, *19*, 4103−4117.
(66) Rusu, P. C.; Brocks, G. Work Functions of Self-Assembled Monolayers on Metal Surfaces by First-Principles Calculations. *Phys. Rev. B* **2006**, *74*, 073414.
(67) De Renzi, V.; Rousseau, R.; Marchetto, D.; Biagi, R.; Scandolo, S.; del Pennino, U. Metal Work-Function Changes Induced by Organic Adsorbates: A Combined Experimental and Theoretical Study. *Phys. Rev. Lett.* **2005**, *95*, 046804.
(68) Sushko, M. L.; Shluger, A. L. Intramolecular Dipole Coupling and Depolarization in Self-Assembled Monolayers. *Adv. Funct. Mater.* **2008**, *18*, 2228−2236.
(69) Deutsch, D.; Natan, A.; Shapira, Y.; Kronik, L. Electrostatic Properties of Adsorbed Polar Molecules: Opposite Behavior of a Single Molecule and a Molecular Monolayer. *J. Am. Chem. Soc.* **2007**, *129*, 2989−2997.
(70) Gershevitz, O.; Sukenik, C. N.; Ghabboun, J.; Cahen, D. Molecular Monolayer-Mediated Control Over Semiconductor Surfaces: Evidence for Molecular Depolarization of Silane Monolayers on Si/SiOx. *J. Am. Chem. Soc.* **2003**, *125*, 4730−4731.
(71) Heimel, G.; Romaner, L.; Brédas, J.-L.; Zojer, E. Interface Energetics and Level Alignment at Covalent Metal-Molecule Junctions: Π-Conjugated Thiols on Gold. *Phys. Rev. Lett.* **2006**, *96*, 196806.
(72) Wang, L.; Rangger, G. M.; Ma, Z.; Li, Q.; Shuai, Z.; Zojer, E.; Heimel, G. Is There a Au−S Bond Dipole in Self-Assembled Monolayers on Gold? *Phys. Chem. Chem. Phys.* **2010**, *12*, 4287.
(73) Technically, this is achieved by calculating $\Delta\Phi'$ for the combined metal/SAM system and $\Delta\Phi_{mol}'$ for the (hypothetical) free-standing monolayer. As $\Delta\Phi' = \Delta\Phi_{mol}' + \Delta\Phi_{BD}'$, $\Delta\Phi_{BD}'$ can then be obtained as the difference of the two quantities.
(74) Terentjevs, A.; Steele, M. P.; Blumenfeld, M. L.; Ilyas, N.; Kelly, L. L.; Fabiano, E.; Monti, O. L. A.; Della Sala, F. Interfacial Electronic Structure of the Dipolar Vanadyl Naphthalocyanine on Au(111): "Push-Back" vs Dipolar Effects. *J. Phys. Chem. C* **2011**, *115*, 21128−21138.

DOI: 10.1021/acs.jpcc.5b00992
J. Phys. Chem. C 2015, 119, 7817−7825

(75) Osikowicz, W.; Jong, M. P. de; Braun, S.; Tengstedt, C.; Fahlman, M.; Salaneck, W. R. Energetics at Au Top and Bottom Contacts on Conjugated Polymers. *Appl. Phys. Lett.* **2006**, *88*, 193504.
(76) Witte, G.; Lukas, S.; Bagus, P. S.; Wöll, C. Vacuum Level Alignment at Organic/metal Junctions: "Cushion" Effect and the Interface Dipole. *Appl. Phys. Lett.* **2005**, *87*, 263502.
(77) Bagus, P. S.; Staemmler, V.; Wöll, C. Exchangelike Effects for Closed-Shell Adsorbates: Interface Dipole and Work Function. *Phys. Rev. Lett.* **2002**, *89*, 096104.
(78) Hofmann, O. T.; Rangger, G. M.; Zojer, E. Reducing the Metal Work Function beyond Pauli Pushback: A Computational Investigation of Tetrathiafulvalene and Viologen on Coinage Metal Surfaces. *J. Phys. Chem. C* **2008**, *112*, 20357−20365.
(79) Note that due to the thiolate−Au bonds also charge-density fluctuations perpendicular to the substrate surface can be resolved, when plotting $\Delta\rho$ averaged over planes parallel to the substrate surface. These, however, can be viewed as a series of comparably moderate dipoles rather than a single, particularly large one.[71]

DOI: 10.1021/acs.jpcc.5b00992
J. Phys. Chem. C 2015, 119, 7817−7825

2.3 Supporting Information

Supporting Information to

Electronic Properties of Biphenylthiolates on Au(111): The impact of coverage revisited.

*Elisabeth Verwüster †, Oliver T. Hofmann †, David A. Egger †,§, and Egbert Zojer *†*

† Institute of Solid State Physics, Graz University of Technology, Petersgasse 16, 8010 Graz, Austria

§ Department of Materials and Interfaces, Weizmann Institute of Science, Rehovoth 76100, Israel

***Corresponding Author:** Egbert Zojer, egbert.zojer@tugraz.at

1. Additional details on the applied methodology.

The Monkhorst-Pack [Monkhorst, H. J.; Pack, J. D. Special Points for Brillouin-Zone Integrations. *Phys. Rev. B* **1976**, *13*, 5188–5192] *k-point* scheme was used in all calculations. Due to the different calculated unit-cells *k*-point meshes were manually chosen for each coverage and checked for convergence, resulting in: 8x8x1, 8x6x1, 8x5x1, 4x6x1 and 4x5x1 for Θ=1, 0.75, 0.50, 0.37 and 0.25.

Table S1: In the present study following PAW potentials were used

Au	PAW_PBE Au 06Sep2000
S	PAW_PBE S 17Jan2003
C	PAW_PBE C_s 06Sep2000
H	PAW_PBE H 15Jun2001
N	PAW_PBE N_s 07Sep2000
F	PAW_PBE F 08Apr2002

To avoid spurious surface reconstructions, the Au(111) lattice constant was set to the equilibrium value for the used methodology, which amounts to 2.928 Å was used.

2. Properties of all investigated thiolate-bonded SAMs

In Figure S1 the dependence of the tit angle, the work-function modification and the effective long-axis dipole are shown for all studied molecules as a function of coverage. It is analogous to Fig. 2 from the main manuscript, but contains data for many more systems.

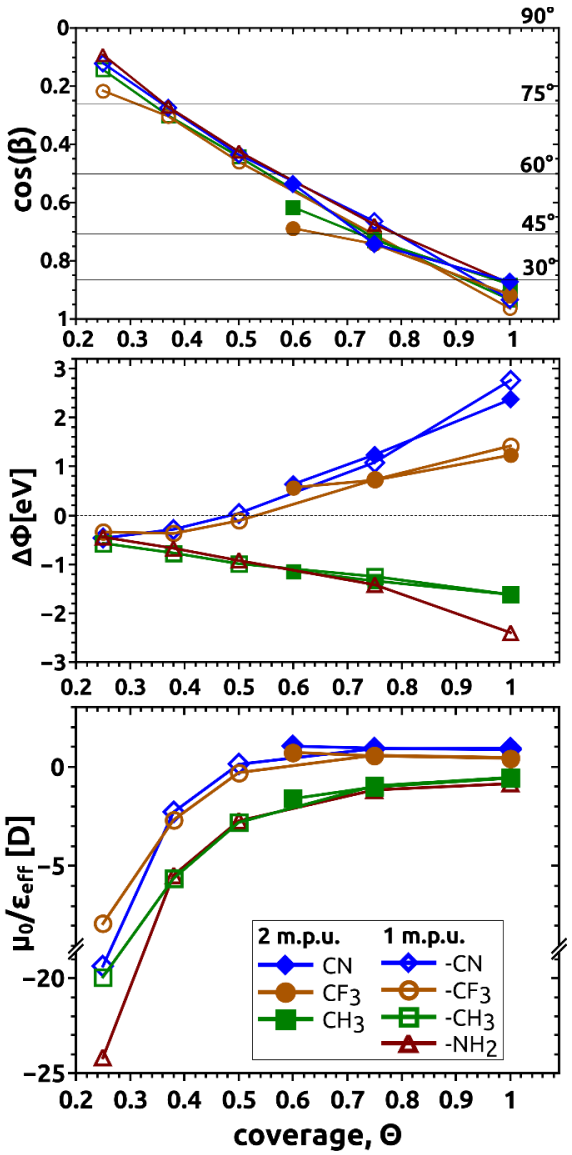

Figure S1: *Coverage dependence of a.) the tilt angle (β) and cosine of the tilt angle (cos(β)); b.) the work-function modification, ΔΦ, and c.) the quantity* μ_0/ε_{eff} *obtained by calculating* $\Delta\Phi A_{1.0}\varepsilon_0/(e\Theta\cos(\beta))$*, which can be regarded as an effective dipole moment of the combined metal-SAM system. Results for the CN-substituted system are shown as blue diamonds; for* $-CF_3$

in brown circles, for CH_3 in green squares and those for the $–NH_2$ substituted case as red triangles. The full symbols denote the unit cells containing two molecules in a herringbone arrangement.

3. Decomposition of the electronic properties of the H-terminate, NH2 tail-group substitute SAM into monolayer and interaction-based contributions

The following plot corresponds to Fig. 3b) and c) of the main manuscript for the NH_2 instead of CN substituted monolayer.

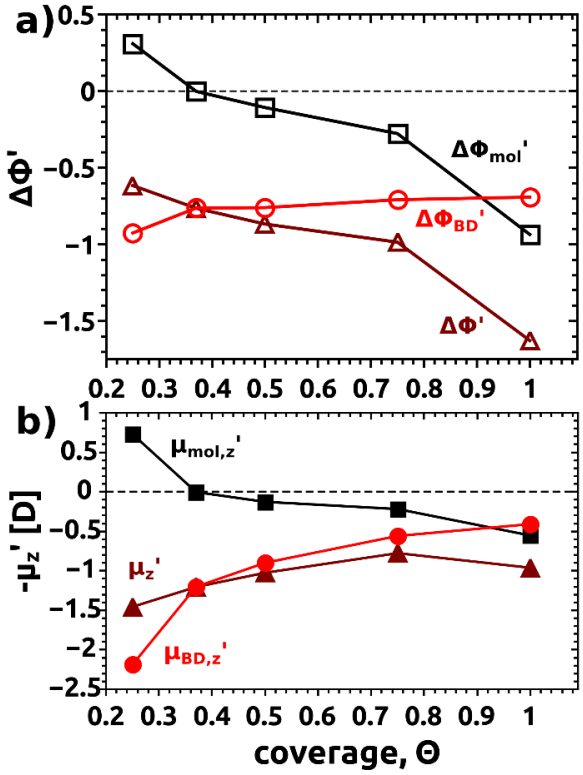

Figure S2: *a) coverage-dependent decomposition of the total work-function change in the $–NH_2$ substituted model system, $\Delta\Phi$', (dark red triangles) into contributions from the (free-standing) monolayer, $\Delta\Phi_{mol}$', (black squares) and from the interfacial charge-rearrangements, $\Delta\Phi_{BD}$', (red circles); b) analogous decomposition into contributing dipoles per molecule. The energetic shifts in a) are proportional to those in b) divided by the surface area per molecule ($\Delta\Phi' \propto \mu_z'\Theta/A_{1.0}$).*

There are two differences in the evolution of the monolayer-related quantities $\mu_{mol,z}$' and $\Delta\Phi_{mol,z}$' compared to the case of the –CN substituted SAM in the main manuscript: (i) The different signs at high coverages owing to the donating instead of accepting character of the tail-group substituent. (ii) A change in sign of $\mu_{mol,z}$' and $\Delta\Phi_{mol,z}$' at Θ=0.25, which does not occur in the –CN substituted SAMs. It is the consequence of an off-axis component of the dipole moment of the substituent caused by the pyramidalization of the bonds in the C-N-H_2 part of the molecule. This component determines the z-component of the monolayer dipole of the essentially flat-lying molecules for the conformation studied here (see Fig. S3). As far as the relative large magnitude of the dipole compared to the dipole of the essentially upright-standing SAM at full coverage is concerned, one needs to keep in mind that at low packing densities depolarization effects are significantly reduced.

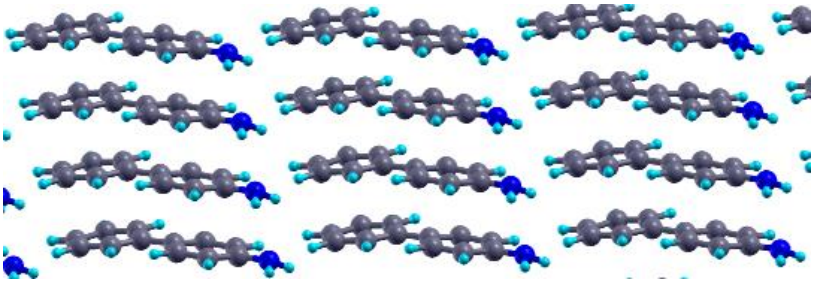

Figure S3: Structure of the isolated H-terminated monolayer of the -NH_2 tail-group substituted monolayer at Θ=0.25 used to calculate $\mu_{mol,z}$' and $\Delta\Phi_{mol,z}$' shown in Fig. S2.

4. Densities of States

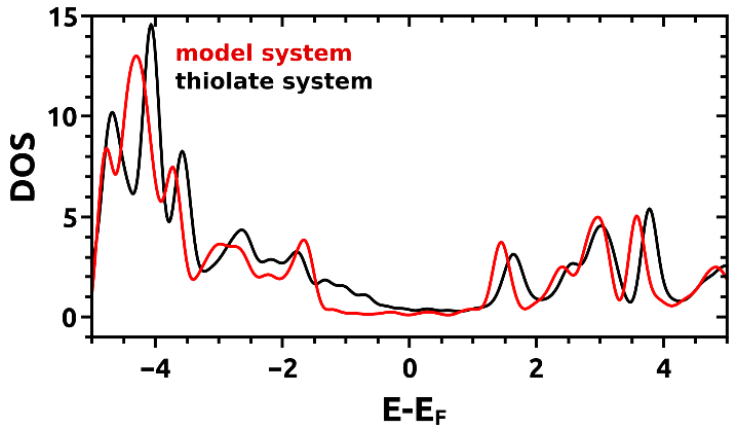

Figure S4: *Density of states (DOS) of the –CN substituted model(red) and thiolate(black) systems at Θ=0.25. The energy is plotted relative to the Fermi-energy.*

5. Charge-density rearrangements at half and full coverage

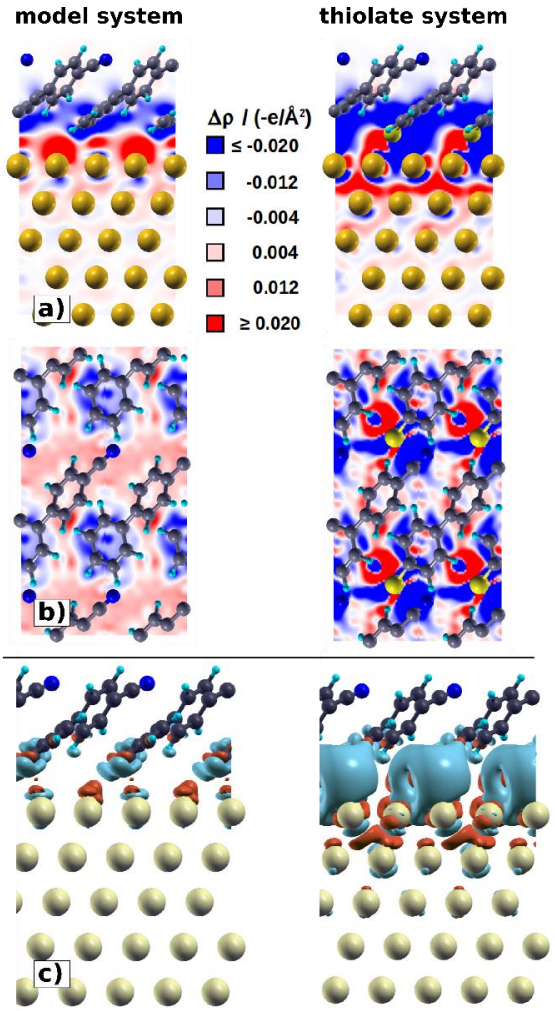

Figure S5: *Charge rearrangements arising from the interaction between the metal and the monolayer for the –CN substituted SAMs at Θ=0.5. In the first and central panels a) and b) charge-density redistributions integrated over the unit cell in the viewing direction are shown. Red areas denote charge accumulation, blue areas depletion; only part of the five Au layers of the metal slab are shown. a) contains plots for the H-terminated model system and the corresponding thiolate system in a side-view manner. In panel b) the top view of the integrated charge rearrangements for both the model- and the thiolate-system are shown. Panel c) contains 3D isodensity-plots (with an isovalue of 0.005 e/Å^3).*

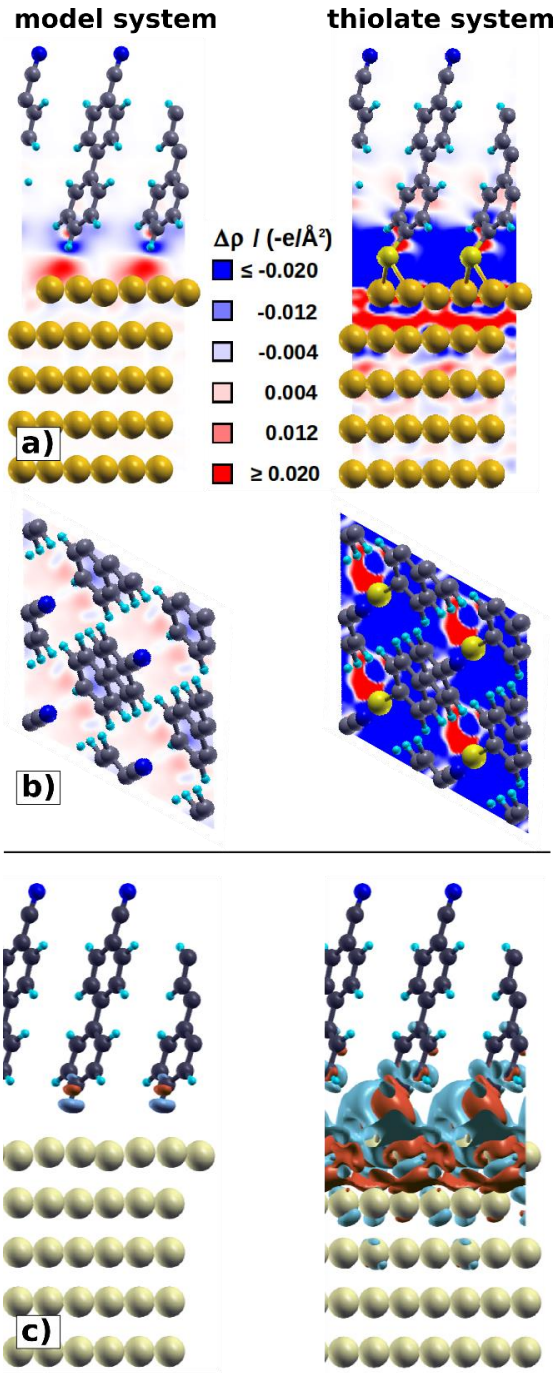

Figure S6: *Charge rearrangements arising from the interaction between the metal and the monolayer for the –CN substituted SAMs at Θ=1.0. In the first and central panels a) and b) charge-density redistributions integrated over the unit cell in the viewing direction are shown. Red areas denote charge accumulation, blue areas depletion; only part of the five Au layers of*

the metal slab are shown. a) contains plots for the H-terminated model system and the corresponding thiolate system in a side-view manner. In panel b) the top view of the integrated charge rearrangements for both the model- and the thiolate-system are shown. Panel c) contains 3D isodensity-plots (with an isovalue of 0.005 e/Å^3).

3 Exploring the driving forces behind the structural assembly of biphenylthiolates on Au(111)

3.1 Author Contribution

O.T. Hofmann conceived the idea to investigate the physical aspects that drive motif-formation upon the assembly of various polymorphs of biphenylthioles on Au(111). E. Verwüster performed all calculations and primary analysis of the data. The data set was interpreted by all authors. The used VASP code was modified by Tomáš Bučko from the Comenius University in Bratislava, Slovakia, enabling the vibrational analysis employing density-functional perturbation-theory (DF-PT) including vdW-corrections. He, however, considered his contributions to be insufficient to be included as contributing author. All authors extensively contributed to the analysis and interpretation of the calculated data. E. Verwüster wrote the first version of the manuscript and prepared all figures. The manuscript was improved in cooperation with E. Zojer, O.T. Hofmann and E. Wruss. The project was supervised by E. Zojer and O.T. Hofmann

The following paper is published by the Journal of Chemical Physics and inserted here as original publication together with the Supporting Information. Reproduced from "Verwüster, Elisabeth and Wruss, Elisabeth and Zojer, Egbert and Hofmann, Oliver T.; Exploring the driving forces behind the structural assembly of biphenylthiolates on Au (111), *J. Chem. Phys.*, vol. 147, no. 2, p. 024706, 2017" with the permission of AIP Publishing.

3.2 Original Article

Exploring the driving forces behind the structural assembly of biphenylthiolates on Au(111)

Elisabeth Verwüster, Elisabeth Wruss, Egbert Zojer, and Oliver T. Hofmann

Citation: The Journal of Chemical Physics **147**, 024706 (2017); doi: 10.1063/1.4991344
View online: http://dx.doi.org/10.1063/1.4991344
View Table of Contents: http://aip.scitation.org/toc/jcp/147/2
Published by the American Institute of Physics

THE JOURNAL OF CHEMICAL PHYSICS **147**, 024706 (2017)

Exploring the driving forces behind the structural assembly of biphenylthiolates on Au(111)

Elisabeth Verwüster, Elisabeth Wruss, Egbert Zojer, and Oliver T. Hofmann[a)]
Institute of Solid State Physics, NAWI Graz, Graz University of Technology, Petersgasse 16, 8010 Graz, Austria

(Received 21 April 2017; accepted 20 June 2017; published online 13 July 2017)

In this contribution, we use dispersion-corrected density functional theory to study inter- and intramolecular interactions in a prototypical self-assembled monolayer (SAM) consisting of biphenylthiolates bonded to Au(111) via thiolate groups. The goal is to identify the nature of the interactions that drive the monolayer into a specific conformation. Particular focus is laid on sampling realistic structures rather than high symmetry model configurations. This is achieved by studying conceptually different local minimum structures of the SAM that are obtained via exploring the potential energy surface from systematically varied starting geometries. The six obtained packing motifs differ in the relative arrangement of the two molecules in the unit cell (co-planar *versus* herringbone) and in the intramolecular configuration (twisted *versus* planar rings). We find that van der Waals interactions within the organic adsorbate and between the adsorbate and substrate are the main reason that these molecular assemblies can form stable structures at all. The van der Waals interactions are, however, very similar for all observed motifs; by analyzing various types of interactions in the course of three notional SAM-formation steps, we find that the main driving force stabilizing the actual global minimum structure originates from electrostatic interactions between the molecules. *Published by AIP Publishing.* [http://dx.doi.org/10.1063/1.4991344]

INTRODUCTION

Surface modification via organic self-assembled monolayers (SAMs) provides a versatile technique to tune the properties of metal substrates, with important technological applications, e.g., in organic electronic devices,[1–8] as corrosion protection,[9] and as active material in bio-sensing.[10,11] The impact of the SAM on the system properties does not depend solely on the chemical structure of the molecule. Rather, also the way the molecules arrange on the surface, i.e., the polymorph the SAM adopts, plays a decisive role.[12–20]

Presently, very little is known about the relation between the molecular structure and the formed adsorption motif[21–23] or the nature of the interaction that relates these two. Also in computational studies, the surface polymorph that is eventually found significantly depends on the chosen initial geometry prior to geometry optimization and on numerical details, such as the initialization of the Hessian.[22] The corresponding properties of interest can, however, vary significantly depending on which structure is found.[12,24]

In this work, we employ density-functional theory (DFT) to investigate the energy landscape of the prototypical biphenylthiolate SAM on Au(111). The focus is not so much on systematically calculating every possible polymorph structure but rather on what type of interactions is crucial for stabilizing/destabilizing a specific configuration and how these interactions depend on the specific arrangement of the molecules. Here, the various conceptually different adsorption motifs identified in our structure search serve as ideal, realistic test structures for performing that comparison.

The investigated system is illustrated in Fig. 1. Biphenylthiol derivatives bonded to the Au surface via thiolate docking groups are frequently used as models to demonstrate the physical effects at work at SAM/Au interfaces.[13,25–34] We will show in the following that even for such a comparably simple system, a variety of intermolecular and intramolecular arrangements are conceivable, for which fundamental differences in the various types of interaction energies can be expected. These are explored by defining a hypothetical SAM-formation process occurring in several well-defined steps (molecular deformation, self-assembly, and bonding to the substrate, see below). In this way, we find that although van der Waals (vdW) interactions are the main driving force for SAM formation, electrostatic interactions between the molecular backbones determine what is the most stable surface polymorph.[35–39]

METHODOLOGY

Computational details

The band-structure calculations in this work employed dispersion-corrected density functional theory using a modified version of the Vienna *Ab Initio* Simulation Package[40] (based on VASP version 5.4.1, see below for more details). Throughout this work, the Perdew-Burke-Ernzerhof (PBE)[41,42] exchange-correlation functional was applied together with "standard" projected augmented-wave (PAW) potentials[43,44] to treat core-valence interactions. To account for long-range dispersion forces (vdW), the PBE functional

a)Author to whom correspondence should be addressed: o.hofmann@tugraz.at

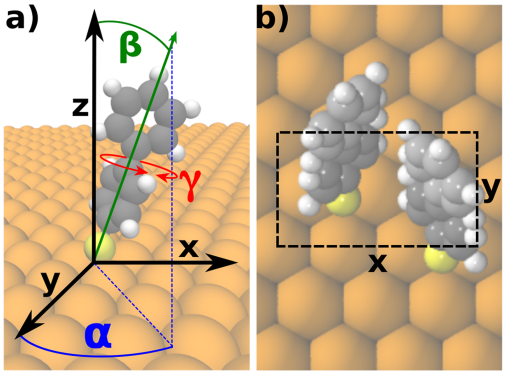

FIG. 1. (a) Schematic representation of the angles, which have been modified for generating a variety of starting configurations: The tilt angle, β, between the long molecular axis and the z-axis of the unit cell, the inter-ring twist, γ, between the top and bottom phenyl ring of the biphenylthiolate molecule, and the azimuthal angle, α, between the y-axis of the unit cell and the projection of the long molecular axis onto the surface plane. (b) Top view of the $3 \times \sqrt{3}$ unit cell containing two molecules. White spheres correspond to H, gray to C, yellow to S, and gold to Au atoms.

was augmented by the Tkatchenko-Scheffler scheme[45] parameterized specifically to treat adsorption on metallic surfaces (PBE+vdW^{surf}).[46] The vdW-correction between the atoms of the Au substrate was switched off.

A cutoff energy of 400 eV for the plane waves and an $8 \times 5 \times 1$ Monkhorst-Pack[47] type k-point mesh were used. To model the self-assembled monolayer on the metallic substrate, we applied the repeated slab approach. Decoupling of the periodic replicas of the slab was achieved by inserting a 20 Å vacuum gap and a self-consistently determined dipole layer compensating for the electrostatic asymmetry.[48] While systematically exploring the potential energy surface of biphenylthiolate on Au(111), the gold surface was represented by a 3-layer slab to reduce the computational cost. Calculations for the notional SAM-formation were done with a 5-layer slab for a higher accuracy. Test calculations show a difference of 15-60 meV in the total adsorption energy between the 3-layer and 5-layer slabs (see Table S1 in the supplementary material). To avoid spurious surface reconstructions, the Au(111) nearest-neighbor distance was set to the equilibrium value for the used methodology, which amounts to 2.928 Å. An optimization scheme based on internal coordinates and the Direct Inversion in the Iterative Subspace (DIIS)[49] algorithm as implemented in the GADGET tool[50] was used to relax the geometries. The top two layers of the slab and the molecules were allowed to relax until the remaining forces were smaller than 10^{-2} eV/Å and tight convergence criteria of 10^{-6} eV were employed for the SCF (self-consistent field) procedure.

The vibrational analysis was done via "analytical frequencies," i.e., employing density-functional perturbation-theory (DF-PT) including vdW-corrections, which was kindly implemented into our modified VASP version by Tomáš Bučko. For these calculations, the dipole correction was switched off, as it caused a strong (artificial) imaginary frequency corresponding to a translational mode towards the correcting dipole layer. More details regarding the computational settings for the vibrations can be found in the supplementary material.

For gas-phase calculations of the isolated molecules, the geometry in the gas-phase was obtained via pre-optimization with Gaussian09[51] using the PBE functional and the 6-311++G** basis set and subsequently placing the molecule in a 40 Å × 40 Å × 40 Å unit cell, recalculating it with VASP to obtain consistent energies.

RESULTS AND DISCUSSION

System setup

Our study focusses on a self-assembled monolayer of biphenylthiolates adsorbed on Au(111). Biphenyl(thiole) suggests itself for the present study, since it is well known to exhibit a strongly twisted conformation in the gas-phase ($\gamma \approx 45°$)[52] while as a bulk material, the twist angle is strongly reduced (typically to 10° or less).[52–57] In other words, the twist angle between the rings is a clear source for structural variations.

On the surface, scanning tunneling microscopy (STM)[20,58,59] experiments propose a herringbone arrangement of the bonded biphenylthiolate molecules. Typically, the STM tips cannot penetrate the material deep enough to yield authoritative information on the planarity. Still, DFT calculations imply that the molecules ought to be planar, which has been attributed to spatial constraints due to the presence of the Au surface.[55] As we show in this paper, for biphenylthiolate changes in the tilt as well as variations in the relative arrangement of the molecules in the unit cell indeed result in several possible, local minima on the surface.

To assess the structural diversity of biphenylthiolates on Au(111), we systematically explored the potential energy surface (PES) of the metal/organic interface. We focus our efforts on the $c(3 \times \sqrt{3})$ unit cell containing two molecules, which is the unit cell commonly found in experiments for oligophenylene-thiolates on Au(111) at full coverage.[18,20,58] Although studying the PES for other supercells would be highly interesting, performing an exhaustive search that explores the huge diversity of potential supercells at the same time as the potential inter- and intramolecular interactions is presently not tractable and would also go beyond the scope of the present paper.

To explore the PES, a set of suitable starting geometries (140 in total) was generated by varying the following three structural parameters [also shown in Fig. 1(a)]:

(i) The azimuthal angle, **α**, which determines the intermolecular arrangement of the two biphenylthiolates in the unit cell. It is defined as the angle between the projection of the long molecular axis of the molecule onto the gold surface and the y-axis of the unit cell. Given the orthogonal orientation of the unit cell vectors, we scan this angle between 0° and 90° in steps of 30°.

(ii) The tilt angle, **β**, between the long molecular axis and the z-axis of the unit cell. Experimental NEXAFS-studies suggest a tilt of 27° ± 5°.[60] To capture as many conformations as possible, we scanned β in the range between 0° and 45° in steps of 15°. Larger tilt angles are not sensible due to the dense packing at full coverage and would result in unphysical interpenetration of the

molecules. The tilt angle was either set symmetrically, i.e., with both molecules tilted in the same direction, or alternatingly, i.e., with the two molecules in the unit cell tilted in opposite directions.

(iii) The inter-ring twist angle, **γ**, between the two rings in each biphenyl backbone. It was varied between −90° and 90° in steps of 45°. The need to investigate γ at positive and negative values originates from having two non-equivalent biphenyl moieties in the unit cell. We chose this particular range for γ to fully include the competition between the repulsion of the *ortho*-substituted hydrogens (that would be minimized for γ = 90°) and the drive for maximizing π-conjugation (that would be maximized for γ = 0°[52,61]).

Unless otherwise noted, all geometric changes were applied in parallel to both molecules in the unit cell. Out of 140 starting geometries generated this way, we discarded 45 structures because they would be either symmetry equivalent to other configurations or unphysical due to the interpenetration of the molecules. Subsequently, the remaining 95 geometries were relaxed towards the nearest local minimum for 20 optimization steps. The target of this pre-optimization is to determine the nearest "catch-basin," i.e., the nearest minimum structure, as indicated in Fig. 2(a). We note in passing that after these 20 steps, the maximum residual force has fallen below 10^{-1} eV/Å (but not reached the final convergence criterion of 10^{-2} eV/Å), indicating that all these structures are already reasonably close to a structural minimum geometry. Visual inspection of the geometry after this "pre-relaxation" allows us to systematically capture the structural diversity of the SAM and to identify the key packing motifs that we need in a second step to analyze the relevance of the different interactions at work in the SAMs.

Already at the "pre-relaxation" stage, it becomes clear that not all starting geometries head towards the planar herringbone structure, which is the motif typically suggested by experiments.[18,20,58,59] Consequently, all pre-relaxed geometries are categorized depending on (a) whether the molecules are planar or twisted and (b) whether the top, respectively, bottom rings of the two molecules pack in a co-planar or herringbone arrangement. This gives rise to six different primary structural categories. Throughout this paper, each category is named according to the relative arrangement of the upper and lower phenyl rings of the two molecules in the unit cell (herringbone denoted as **HB** and co-planar denoted as **CP**). Additionally, we determined the inter-ring twist angle in each molecule; here, 0 indicates that both molecules are planar, 1 signifies that one molecule is non-planar, and 2 denotes a situation in which both molecules are twisted. To assess the planarity, we defined a threshold of γ < 20° after the first 20 steps of the optimization. In the final nomenclature, the structural parameters are then separated by a slash. In this way, *HB*/*HB*/0, for example, denotes two planar molecules, where both phenyl rings are arranged in a herringbone fashion. A schematic sketch of all six motifs, along with the relative energy of all group members, is given in Fig. 2(b).

We emphasize that although the energies of the non-converged geometries are not quantitatively reliable, as mentioned above, they are already close to, but not yet at, a

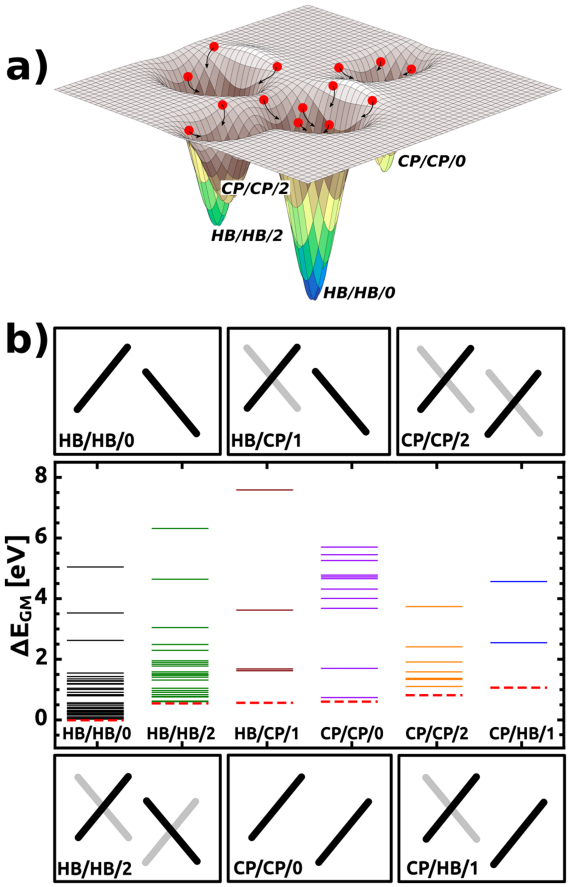

FIG. 2. (a) Schematic potential energy surface presenting the four local minima of the motifs *HB*/*HB*/0, *HB*/*HB*/2, *CP*/*CP*/0, and *CP*/*CP*/2. The red dots illustrate a set of starting geometries with their trajectories (black arrows) towards the closest local minima. (b) Energy of all calculated (not converged) geometries categorized in the six main motifs. Structures within the same categories vary in the arrangement with respect to the surface normal. The dashed red lines correspond to the energy of the obtained minimum after the final relaxation of the corresponding motif, as discussed in detail in the main text. The panels above and below the plot contain schematic sketches of the six categories with the upper (lower) phenyl ring drawn in black (gray) and the naming convention (*HB* = herringbone, *CP* = co-planar, 0/1/2 = number of inter-ring twists per unit cell).

minimum geometry. Still, it is noteworthy that only 43% of the starting structures converge towards a HB/HB/0 structure, while a significant portion (31%) falls into the attractor basin of HB/HB/2, i.e., they result in herringbone patterns of non-planar molecules. The other categories are significantly less populated as the remaining (26%) starting structures spread across the other four motifs. These results imply that the herringbone-arrangement is particularly robust with respect to the starting geometry guess, whereas the outcome whether the molecules assume a planar or twisted geometry is more sensitive.

The low-energy members of each category differ typically only regarding the orientation within the unit cell, i.e., with respect to **α**. Here, we postpone the question of whether this leads to different local minima or whether the orientation with respect to the surface is a comparably weak degree of freedom which takes particularly long to optimize. Rather, we focus on the conceptually different packing motifs, as they serve as ideal test structures for analyzing different contributions to the

SAM bonding. Therefore, we selected the energetically lowest lying pre-optimized geometry of each motif and performed a full relaxation until the remaining forces were smaller than 10^{-2} eV/Å. Finally, a vibrational analysis is performed in order to ascertain that all final geometries correspond to local minima. Whether and to which extent vibrational spectroscopy could be used as a tool to determine the motif experimentally is discussed in the supplementary material. We note that the vibrational zero-point energies between the different categories do not differ notably (less than 50 meV, see Table I) and are, therefore, not considered further. (Although inclusion of the zero-point energy changes the relative ordering of HB/CP/1 and CP/CP/0, the difference is small and this effect is not relevant for the further discussion.) The geometries of the obtained minima of each of the six categories are shown in Fig. 3.

As a general observation, the obtained geometries of the motifs are either almost perfectly planar or strongly twisted with $\gamma \approx 70°$-$80°$. Notably, the latter twist angle is much larger than the equilibrium γ found in the gas-phase.[62–64] Furthermore, we find that motifs with planar molecules are much more tilted ($\beta \approx 30°$) than the twisted ones ($\beta \approx 15°$), for reasons that will become evident later in this work. As expected, HB/HB/0 is the most stable category. All other structures are 0.5-1.0 eV higher in energy. In thermodynamic equilibrium they would, therefore, be hardly occupied. Nevertheless, it is useful to analyze the different local minimum structures in more detail, as they allow generating fundamental insight into the interactions that are responsible for the bonding within SAMs and that stabilize certain configurations compared to others.

Ranking the six categories according to the total energies of the obtained minima, we find the following order (from most to least stable): HB/HB/0 > HB/HB/2 > HB/CP/1 > CP/CP/0 > CP/CP/2 > CP/HB/1 (see Table I). This suggests that the relative arrangement of the upper phenyl rings is the most crucial parameter. It also implies that a T-shaped arrangement of neighboring rings resulting in a herringbone pattern is preferred over a co-planar situation. Another aspect is the twist of the two biphenyls in the unit cell: For a given motif of the upper ring, both molecules being planar (0) is more stable than both twisted (2), and either is significantly more stable than having one molecule twisted and one planar (1). Importantly, what we do not observe is that the planar structures are generally more stable than the twisted ones.

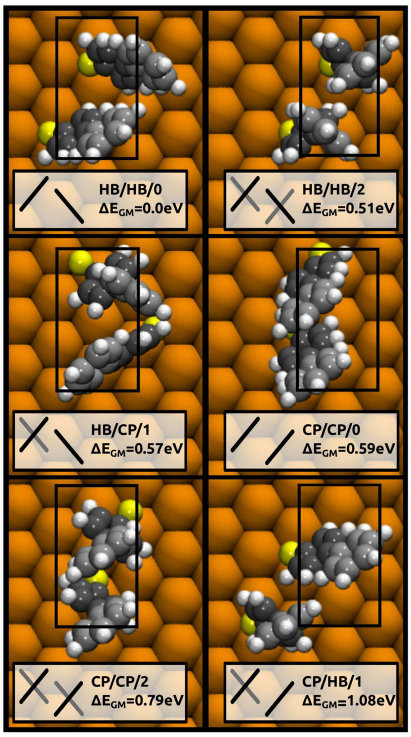

FIG. 3. Top view of the obtained minimum geometries for each category. The insets contain the naming convention (*HB* = herringbone, *CP* = co-planar, 0/1/2 = number of inter-ring twists per motif), the energy, ΔE_{GM}, relative to the lowest energy found in this study (*HB*/*HB*/0) and a schematic illustration of each motif. For the sake of clarity, only the two molecules that constitute the unit cell (black rectangle) are shown and neighboring molecules are omitted.

Analyzing the interactions in the various configurations

An obvious question at this point is what causes the notable energy differences between the various polymorphs, in particular, whether they originate from the geometric distortion of the molecules, the intermolecular interactions in the organic layer, or the adsorption of the organic material onto the metallic substrate. In order to investigate the physical aspects that drive the SAMs into specific structures, we designed a Gedankenexperiment splitting the SAM formation into three fundamental steps:

Starting from the isolated, fully optimized biphenylthiole molecule in the gas-phase, we calculate (i) the energy

TABLE I. Tilt, inter-ring twist, and azimuthal angles α, β, and γ of the lowest energy structures of the six main structural motifs in order of increasing total energies. The zero-point corrected energy, ΔE_{GM}, and the zero-point energy, ΔZPE_{GM}, are given relative to the energy of the global minimum system *HB*/*HB*/0.

Category	Azimuth, α (deg)	Tilt, β (deg)	Inter-ring twist, γ (deg)	Relative energy, ΔE_{GM} (meV)	Relative zero-point energy, ΔZPE_{GM} (meV)
HB/HB/0	0	28	0	0	0
HB/HB/2	1	13	80	512	−45
HB/CP/1	5	13/32	75/0	566	−17
CP/CP/0	72	25	0	585	−37
CP/CP/2	71	21	70	787	−34
CP/HB/1	25	23/38	80/0	1080	2

related to the deformation of the free molecules into the geometry they exhibit in the SAM, i.e., the "deformation energy," ΔE^{deform}, (ii) the energy required to assemble the deformed but isolated molecules into the periodic monolayer, i.e., the assembly energy, $\Delta E^{assembly}$, and (iii) the energy associated with the reaction of the free-standing monolayer with the surface, i.e., the adsorption energy, ΔE^{ads}. By definition, positive values indicate an endothermic and negative values indicate an exothermic process. For this analysis, we omit the HB/CP/1 and CP/HB/1 polymorphs that contain two qualitatively different molecules, which would complicate the following analysis without providing notable additional insight.

Step 1: Molecular deformation

To illustrate the energetic cost of deforming the molecule from its gas-phase geometry to the monolayer-induced geometry, ΔE^{deform}, we calculate the energy difference

$$\Delta E^{deform} = E_{mol,mon} - E_{mol,gp}, \quad (1)$$

where $E_{mol,gp}$ is the energy of an optimized molecule in its gas-phase conformation ($\gamma = 40°$); $E_{mol,mon}$ denotes the energy of a molecule forced into the geometry it adopts in the monolayer. The difference was calculated for both molecules in the unit cell separately. The final ΔE^{deform} represents the average value for the two molecules of the unit cell (the individual values can be found in the supplementary material, Table S2).

As shown in Fig. 4, the motifs formed by planar molecules, HB/HB/0 and CP/CP/0, show smaller deformation energies compared to the twisted HB/HB/2 and CP/CP/2 (ca. 20 meV and 60 meV, respectively), indicating that it is slightly *less* costly to planarize the single molecule than to enlarge its inter-ring twist. This seems to contradict the literature where it has been suggested that planarizing biphenyl is energetically more costly than twisting the rings by 90°.[52,62] As the same energetic order prevails when substituting the SH group by H [while keeping the geometry otherwise constant (see Table S3 in the supplementary material)], it is clear that this discrepancy is not related to the presence of the electron donating thiol group favoring a more planar conformation. Rather, we find that the origin for the "easier planarization" is a consequence of an interplay with other molecular degrees of freedom. When we allow the molecules to relax while fixing the monolayer-induced twist angle between the phenyl rings, we restore the expected situation that twisting the rings is energetically less costly than planarizing them. The corresponding calculations can be found in the supplementary material, Table S4.

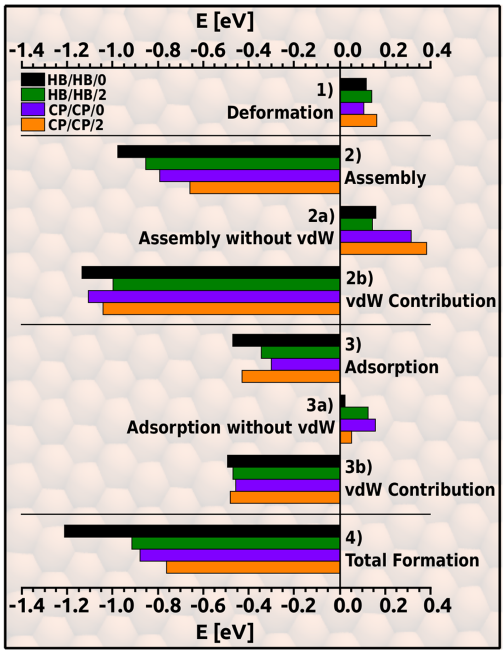

FIG. 4. SAM-formation process split into separate contributions: (1) deformation energy, ΔE^{deform}; (2) assembly energy, $\Delta E^{assembly}$; (2a) assembly energy without *vdW* correction; (2b) *vdW* contribution to the assembly process, ΔE^{vdW}; (3) adsorption energy, ΔE^{ads}; (3a) adsorption energy without vdW correction; (3b) *vdW* contribution to ΔE^{ads}; and (4) the sum of all contributions, ΔE^{total}, for the different local minimum structures *HB*/*HB*/0 (black), *HB*/*HB*/2 (green), *CP*/*CP*/0 (purple), and *CP*/*CP*/2 (orange).

This implies that the differences in deformation energy between different conformations are mostly due to geometry changes of the molecule other than twisting the rings. Such deformations are triggered by effects such as the tilting and close packing of the molecules. An even more important observation is that the energetic difference between planarization and twisting is overall rather small, which means that molecular deformations *per se* are *not* a major driving force favoring a specific polymorph. This also means that finding polymorphs with strongly twisted molecules is indeed a possibility that ought to be considered seriously in particular for molecules or unit cells somewhat differing from the present one. Indeed, in a recent study, some of us observed that for the structurally related molecule phenyl-piperidine-dithiocarbamate [assembled on Au(111) in the same unit cell as chosen here], the planar and twisted conformations are energetically almost degenerate.[65]

Step 2: Molecular assembly

Step 2 of our notational SAM-formation describes the assembly of isolated molecules, $E_{mol,mon}$ (already in the final structure), into an extended, free-standing monolayer with an energy E_{mon}. The corresponding energy, $\Delta E^{assembly}$, is given by

$$\Delta E^{assembly} = 0.5 \cdot (E_{mon} - 2E_{mol,mon}). \quad (2)$$

In analogy to ΔE^{deform}, $\Delta E^{assembly}$ is first assessed for each of the two molecules in the unit cell separately, with the average value presented in Fig. 4 (the individual values can be found in the supplementary material, Table S5). We find that the energies range from −660 meV to −980 meV, i.e., interestingly, the differences (up to 320 meV) are much more pronounced for this step than for any other in our gedankenexperiment. Indeed, the variation in the assembly step is so large that the hierarchy observed here is preserved in the overall energy tally (step 4). This indicates that the intermolecular interaction within the layer is the most important contribution determining which structure the molecular adsorbate will eventually adopt.

This raises the question, to what extent the SAM structure is determined by van der Waals (vdW) interactions. To address that, we first discuss $\Delta E^{assembly}$ omitting vdW interactions [step (2a) in Fig. 4] and then evaluate the vdW contribution to $\Delta E^{assembly}$ [step (2b) in Fig. 4] separately. This facilitates the

analysis and allows us to demonstrate that both components have a fundamentally different impact on the energetics.

For the energy contributions *without* vdW forces, we find that all four systems are clearly repulsive [step (2a)] with the repulsion for SAMs with molecules in a herringbone arrangement being smaller by ~200 meV compared to the co-planar polymorphs. Within a given arrangement (HB or CP), only a minor difference in energy is observed (~50 meV). This indicates that the arrangement of the backbones crucially affects the assembly energies, while the twisting of the biphenyls is insignificant.

Besides vdW interactions, the interactions between the molecules can conceptually be broken down into electrostatic interactions and interaction arising from the wave-function overlap. For closed-shell molecules, the latter is always repulsive as a consequence of Pauli-repulsion. Its magnitude increases with increasing wave-function overlap. Although Pauli-repulsion is difficult to quantify from our calculations, qualitative insights into the differences between the polymorphs can be obtained via the band-structure of the free-standing monolayers (since also the band-dispersion directly depends on the wave-function overlap). The corresponding plots can be found in the supplementary material (Fig. S3). If Pauli-repulsion were the main factor influencing the assembly energy, we would expect a positive correlation between the band-dispersion and $\Delta E^{assembly}$ when disregarding vdW interactions. A comparison between Fig. 4 and Fig. S3 of the supplementary material, however, shows that such a correlation does not exist. In fact, the least repulsive structure, HB/HB/0, is the one that shows the largest band dispersion for both of its highest occupied bands (ca. 300 meV), while the bandwidth for the other structures tends to be smaller by about a factor of two. From these observations, we infer that the interaction between the molecules in the monolayer is strongly impacted by electrostatic effects.[33–37]

The electrostatic interaction between the biphenylthiole molecules originates from the interaction of the π-electron cloud above and below the molecular plane and the σ-framework (C–H bonds) at the rim of the molecule. In our SAM categories, we can identify three prototypical interaction motifs that are often discussed in the literature in the context of aromatic interactions.[36–40] These are, as schematically indicated in Fig. 5, T-shaped stacking, parallel-displaced stacking, and "side-by-side" stacking. All categories contain a combination of these stacking variations: The herringbone arranged structures exhibit both T-shaped and parallel-displaced stacking [see Fig. 5(a) for HB/HB/0 and Fig. 5(b) for HB/HB/2]. The co-planar arrangements mostly display parallel-displaced stacking along both the long and short axes of the unit cell, while there is a "side-by-side" stacking along the unit cell diagonal [see Fig. 5(c) for CP/CP/0 and 5d for CP/CP/2].

From other studies on benzene dimers, it is known that T-shaped (edge-on structure) stacking is the most favorable arrangement.[36–40,66,67] In this motif, the molecules are almost perpendicular to each other and the hydrogen atoms of one molecule point towards the π-cloud of the adjacent molecule. The parallel-displaced stacking is energetically only slightly worse.[36,37] It consists of molecules that are horizontally shifted by ca. half the width of a molecule, such that the π-clouds of

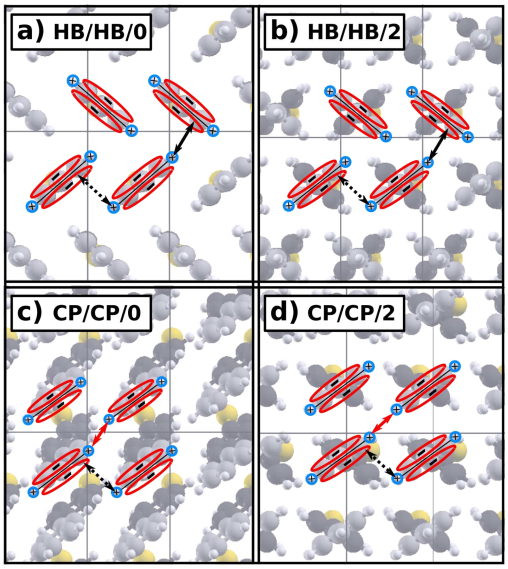

FIG. 5. Schematic sketch of the biphenyl stacking variations occurring in the discussed motifs. The overlay, which illustrates the electrostatic interactions, references only to the upper phenyl rings, while the bottom rings are darkened as a guide to the eye for illustrative purposes. T-shaped stacking is indicated with a black arrow, parallel-displaced stacking with a dashed arrow, and "side-by-side" stacking with a red arrow for the motifs (a) *HB*/*HB*/0, (b) *HB*/*HB*/2, (c) *CP*/*CP*/0, and (d) *CP*/*CP*/2.

adjacent molecules avoid each other and come as close as possible to the hydrogen atoms. In contrast, "side-by-side" stacking, where the molecules are aligned such that the hydrogen atoms repel each other, is energetically very unfavorable.

These considerations suggest that it is in particular the presence of the repulsive "side-by-side" stacking in the co-planar motifs that render them energetically less favorable than their herringbone stacked siblings.

Nevertheless, the vdW forces are responsible for the overall attractive interactions associated with the monolayer-assembly, as illustrated in step (2b), Fig. 4. These interactions contribute more than 1.0 eV to the binding energy for all investigated motifs, which makes them the largest of the individual contributions considered here and renders them a major driving force for SAM formation. Between the different categories, we find that vdW energies are larger for planar than for the twisted molecules. The motifs with planar molecules are also the ones with increased tilt angles (see Table I). This correlation is insofar reasonable, as the effective volume the molecules occupy decreases with increasing tilt. Consequently, SAMs consisting of more tilted molecules are more densely packed (assuming constant coverage), which results in a larger vdW attraction.

Step 3: Adsorption of the SAM

Adsorbing the hypothetical free-standing monolayer of biphenylthioles on the Au(111) surface, ΔE^{ads}, composes the third and last step in our Gedankenexperiment describing SAM-formation. The saturated monolayer binds to the gold slab by substituting the thiole S–H bond for a covalent thiolate S–Au bond. We are aware that the fate of the hydrogen atoms has been controversially discussed in the literature.[68] This, however, does not matter for the present discussion, since it

only constitutes an equal energy offset for all motifs. For simplicity, we thus assume that the hydrogen leaves the surface as molecular hydrogen, H_2. Hence, the adsorption energy of the SAM per molecule, ΔE^{ads}, was calculated as the energy difference between the complete system, E_{sys}, and its separate building blocks, where E_{mon} is the energy of the free-standing monolayer, E_{Au} is the energy of the gold slab, and E_{H2} is the energy of the hydrogen molecule,

$$\Delta E^{ads} = 0.5 \cdot \{E_{sys} - [E_{Au} + (E_{mon} - E_{H_2})]\}. \quad (3)$$

Here we stress that the process described in Eq. (3) does not describe the formation of the bond between the thiolate and the Au surface but rather quantifies the energy for replacing the covalent bond between S and H with a thiolate bond of the docking groups to the substrate (R–S–Au). In analogy to the SAM-formation (discussed in the section titled Step 2: molecular assembly), ΔE^{ads} yields solely positive values (step 3a) when omitting vdW contributions. Thus, without dispersion, no adsorption of the monolayer onto the surface would occur. The necessity of including vdW corrections even for covalently bonded SAMs has, in fact, already been reported previously.[32,69–72] Interestingly, the magnitude of the vdW attraction towards the surface is essentially equal for all conformations (within approximately 40 meV), i.e., it does not particularly prefer any packing motif over another (step 3b).

Although the variation in the adsorption energies without vdW interactions is significantly larger (differing by up to ca. 100 meV, see step 3a in Fig. 4), neither the intermolecular conformation (i.e., the planarity) nor the intramolecular arrangement (i.e., whether the molecules arrange HB or CP) seems to play a decisive role.

At this point, the question arises whether the strong variation can be traced to either steric interactions between the monolayers and the gold substrate or whether there is a notable difference in the chemical reactivity of thioles.

To answer that question, we calculated the energies (using Gaussian09, see above) associated with proton abstraction, i.e., the reaction,

$$\mathrm{Ph{-}Ph{-}SH} \rightarrow \mathrm{Ph{-}Ph{-}S^- + H^+}, \quad (4)$$

for each of the molecules in the unit cell separately fixing their geometries to the ones they adopted in the bonded SAMs (i.e., only the position of the H atom of PhPh–SH is relaxed). The reaction described in Eq. (4) does not contain any steric interaction with the gold substrate and would be expected to yield essentially equal results, if the molecules were also electronically equivalent. Interestingly, we find that they are not. Rather already for this reaction, we observe surprisingly large differences of up to 80 meV (see Table S6 in the supplementary material). This means that not only the reactivity between the different categories differs but even the two molecules in the unit cell can be chemically inequivalent. Indeed, this observation is also manifested in the band structure of the free-standing monolayers (see the supplementary material, Fig. S3), where the two highest occupied bands in all systems consist of states localized only on one of the molecules. Only in HB/HB/0, the shape of the two highest occupied bands is qualitatively equivalent, except for a small offset. For all other configurations, a strong asymmetry between the two bands can be found, corroborating the observed (electronic and chemical) asymmetry of the two molecules. We tentatively infer from these data that the different reactivity towards the substrate is mostly a consequence of the differing geometries of the monolayers, which are to a large part determined by the interaction energies in the assembly process (see above).

SUMMARY AND CONCLUSION

In the present paper, we analyze the relative importance of a variety of interactions for the stability of different polymorphs of biphenylthiolates on Au(111). This system serves as a prototypical example for a strongly bonded metal/organic interface consisting of building blocks that allow for some flexibility regarding their internal structure as well as relative arrangement. To generate diverse polymorphs as ideal test systems for analyzing the interactions, we extensively explore the potential energy surface (PES) for a structure with two molecules in a $c(3 \times \sqrt{3})$ unit cell to identify six packing motifs with fundamentally different conformations. These differ in the planarity of the molecules and in the relative arrangement of the rings in a co-planar or herringbone fashion.

To understand, which factors stabilize specific polymorphs over others, we discuss a hypothetical, albeit very insightful SAM-formation process consisting of the following: (i) molecular deformation, (ii) assembly of the molecules into a monolayer, and (iii) bonding of that monolayer to the substrate. Interestingly, although the conformations of the molecules massively differ in the different polymorphs, the energies necessary to distort the molecules are largely identical. Instead, the main factor that stabilizes certain motifs over others is the assembly of the single molecules into a free-standing monolayer, i.e., the intermolecular interaction energy. In particular, the most stable conformation with planar molecules arranged in a herringbone pattern benefits from the smallest intermolecular Coulomb repulsion combined with a high van der Waals attraction arising from an increased packing density. The most negative adsorption energy for the planar molecules arranged in a herringbone pattern further stabilizes that conformation. These results suggest that the most promising strategy for tuning the molecular conformation in self-assembled monolayer is to modify intra-molecular charge distributions, for example, through electron withdrawing/donating substituents or via the inclusion of heterocyclic rings. The latter strategy has the particular appeal that it would typically not result in detrimental steric effects, which more or less bulky substituents might cause.

SUPPLEMENTARY MATERIAL

See supplementary material for (i) a comparison between the energies for different slab thicknesses, (ii) a detailed explanation of the setup for the starting points, and (iii) computational details and analysis of the vibrational calculations. Moreover, it contains detailed information for the different bonding contributions applied to each of the two molecules in the unit cell separately and surface band structures for all polymorphs found in this study.

ACKNOWLEDGMENTS

The authors are grateful to Dr. Tomáš Bučko for implementing density-functional perturbation-theory (DF-PT) including vdW-corrections into our VASP version. Funding through the Austrian Science Fund (FWF): P27868-N36 and P24666-N20 is gratefully acknowledged. The computational results presented have been achieved using the Vienna Scientific Cluster (VSC).

[1] H. Chung and Y. Diao, J. Mater. Chem. C **4**, 3915 (2016).
[2] E. Margapoti, J. Li, Ö. Ceylan, M. Seifert, F. Nisic, T. L. Anh, F. Meggendorfer, C. Dragonetti, C.-A. Palma, J. V. Barth, and J. J. Finley, Adv. Mater. **27**, 1426 (2015).
[3] C.-H. Kim, H. Hlaing, J.-A. Hong, J.-H. Kim, Y. Park, M. M. Payne, J. E. Anthony, Y. Bonnassieux, G. Horowitz, and I. Kymissis, Adv. Mater. Interfaces **2**, 1400384 (2014).
[4] N. Crivillers, S. Osella, C. Van Dyck, G. M. Lazzerini, D. Cornil, A. Liscio, F. Di Stasio, S. Mian, O. Fenwick, F. Reinders, M. Neuburger, E. Treossi, M. Mayor, V. Palermo, F. Cacialli, J. Cornil, and P. Samorì, Adv. Mater. **25**, 432 (2013).
[5] L. Newton, T. Slater, N. Clark, and A. Vijayaraghavan, J. Mater. Chem. C **1**, 376 (2013).
[6] M. Halik and A. Hirsch, Adv. Mater. **23**, 2689 (2011).
[7] H. Ma, H.-L. Yip, F. Huang, and A. K.-Y. Jen, Adv. Funct. Mater. **20**, 1371 (2010).
[8] P. Marmont, N. Battaglini, P. Lang, G. Horowitz, J. Hwang, A. Kahn, C. Amato, and P. Calas, Org. Electron. **9**, 419 (2008).
[9] F. P. Zamborini and R. M. Crooks, Langmuir **14**, 3279 (1998).
[10] C. J. Ackerson, P. D. Jadzinsky, J. Z. Sexton, D. A. Bushnell, and R. D. Kornberg, Bioconjugate Chem. **21**, 214 (2010).
[11] T. Wink, S. J. van Zuilen, A. Bult, and W. P. van Bennekom, Analyst **122**, 43R (1997).
[12] A. M. Hiszpanski, R. M. Baur, B. Kim, N. J. Tremblay, C. Nuckolls, A. R. Woll, and Y.-L. Loo, J. Am. Chem. Soc. **136**, 15749 (2014).
[13] W. Azzam, B. I. Wehner, R. A. Fischer, A. Terfort, and C. Wöll, Langmuir **18**, 7766 (2002).
[14] N. Garg, E. Carrasquillo-Molina, and T. R. Lee, Langmuir **18**, 2717 (2002).
[15] E. G. Emberly and G. Kirczenow, Phys. Rev. B **64**, 235412 (2001).
[16] P. E. Kornilovitch and A. M. Bratkovsky, Phys. Rev. B **64**, 195413 (2001).
[17] T. Ishida, W. Mizutani, N. Choi, U. Akiba, M. Fujihira, and H. Tokumoto, J. Phys. Chem. B **104**, 11680 (2000).
[18] T. Y. B. Leung, P. Schwartz, G. Scoles, F. Schreiber, and A. Ulman, Surf. Sci. **458**, 34 (2000).
[19] R. Naaman, A. Haran, A. Nitzan, D. Evans, and M. Galperin, J. Phys. Chem. B **102**, 3658 (1998).
[20] Y.-T. Tao, C.-C. Wu, J.-Y. Eu, W.-L. Lin, K.-C. Wu, and C. Chen, Langmuir **13**, 4018 (1997).
[21] A. Bashir, E. Sauter, N. Al-Refaie, M. Rohwerder, M. Zharnikov, and W. Azzam, ChemPhysChem **18**, 702 (2017).
[22] A. Bashir, W. Azzam, M. Rohwerder, and A. Terfort, Langmuir **29**, 13449 (2013).
[23] N. N. Sirota, Cryst. Res. Technol. **17**, 661 (1982).
[24] P. Cyganik, M. Buck, W. Azzam, and C. Wöll, J. Phys. Chem. B **108**, 4989 (2004).
[25] E. Verwüster, O. T. Hofmann, D. A. Egger, and E. Zojer, J. Phys. Chem. C **119**, 7817 (2015).
[26] N. Meyerbroeker, P. Waske, and M. Zharnikov, J. Chem. Phys. **142**, 101919 (2015).
[27] Y. Carissan and W. Klopper, J. Mol. Struct.: THEOCHEM **940**, 115 (2010).
[28] G. Heimel, F. Rissner, and E. Zojer, Adv. Mater. **22**, 2494 (2010).
[29] L. Wang, G. M. Rangger, L. Romaner, G. Heimel, T. Bučko, Z. Ma, Q. Li, Z. Shuai, and E. Zojer, Adv. Funct. Mater. **19**, 3766 (2009).
[30] Q. Sun and A. Selloni, J. Phys. Chem. A **111**, 10170 (2007).
[31] G. Heimel, L. Romaner, J.-L. Brédas, and E. Zojer, Surf. Sci. **600**, 4548 (2006).
[32] Q. Sun, A. Selloni, and G. Scoles, J. Phys. Chem. B **110**, 3493 (2006).
[33] U. Kleineberg, A. Brechling, M. Sundermann, and U. Heinzmann, Adv. Funct. Mater. **11**, 208 (2001).
[34] J. F. Kang, S. Liao, R. Jordan, and A. Ulman, J. Am. Chem. Soc. **120**, 9662 (1998).
[35] M. O. Sinnokrot and C. D. Sherrill, J. Phys. Chem. A **110**, 10656 (2006).
[36] M. O. Sinnokrot, E. F. Valeev, and C. D. Sherrill, J. Am. Chem. Soc. **124**, 10887 (2002).
[37] T. Dahl, Acta Chem. Scand. **48**, 95 (1994).
[38] C. A. Hunter and J. K. M. Sanders, J. Am. Chem. Soc. **112**, 5525 (1990).
[39] C. A. Hunter, J. Singh, and J. M. Thornton, J. Mol. Biol. **218**, 837 (1991).
[40] G. Kresse and J. Furthmüller, Phys. Rev. B **54**, 11169 (1996).
[41] J. P. Perdew, K. Burke, and M. Ernzerhof, Phys. Rev. Lett. **77**, 3865 (1996).
[42] J. P. Perdew, K. Burke, and M. Ernzerhof, Phys. Rev. Lett. **78**, 1396 (1997).
[43] G. Kresse and D. Joubert, Phys. Rev. B **59**, 1758 (1999).
[44] P. Blöchl, Phys. Rev. B **50**, 17953 (1994).
[45] A. Tkatchenko and M. Scheffler, Phys. Rev. Lett. **102**, 073005 (2009).
[46] V. G. Ruiz, W. Liu, E. Zojer, M. Scheffler, and A. Tkatchenko, Phys. Rev. Lett. **108**, 146103 (2012).
[47] H. J. Monkhorst and J. D. Pack, Phys. Rev. B **13**, 5188 (1976).
[48] J. Neugebauer and M. Scheffler, Phys. Rev. B **46**, 16067 (1992).
[49] T. P. Hamilton and P. Pulay, J. Chem. Phys. **84**, 5728 (1986).
[50] T. Bučko, J. Hafner, and J. G. Ángyán, J. Chem. Phys. **122**, 124508 (2005).
[51] M. J. Frisch, G. W. Trucks, H. B. Schlegel, G. E. Scuseria, M. A. Robb, J. R. Cheeseman, G. Scalmani, V. Barone, B. Mennucci, G. A. Petersson, H. Nakatsuji, M. Caricato, X. Li, H. P. Hratchian, A. F. Izmaylov, J. Bloino, G. Zheng, J. L. Sonnenberg, M. Hada, M. Ehara, K. Toyota, R. Fukuda, J. Hasegawa, M. Ishida, T. Nakajima, Y. Honda, O. Kitao, H. Nakai, T. Vreven, J. A. Montgomery, Jr., J. E. Peralta, F. Ogliaro, M. Bearpark, J. J. Heyd, E. Brothers, K. N. Kudin, V. N. Staroverov, R. Kobayashi, J. Normand, K. Raghavachari, A. Rendell, J. C. Burant, S. S. Iyengar, J. Tomasi, M. Cossi, N. Rega, J. M. Millam, M. Klene, J. E. Knox, J. B. Cross, V. Bakken, C. Adamo, J. Jaramillo, R. Gomperts, R. E. Stratmann, O. Yazyev, A. J. Austin, R. Cammi, C. Pomelli, J. W. Ochterski, R. L. Martin, K. Morokuma, V. G. Zakrzewski, G. A. Voth, P. Salvador, J. J. Dannenberg, S. Dapprich, A. D. Daniels, Ö. Farkas, J. B. Foresman, J. V. Ortiz, J. Cioslowski, and D. J. Fox, GAUSSIAN 09, Revision D.01, Gaussian, Inc., Wallington, 2016.
[52] F. Grein, J. Phys. Chem. A **106**, 3823 (2002).
[53] P. Puschnig, K. Hummer, C. Ambrosch-Draxl, G. Heimel, M. Oehzelt, and R. Resel, Phys. Rev. B **67**, 235321 (2003).
[54] C. B. Pinheiro and A. M. Abakumov, IUCrJ **2**, 137 (2015).
[55] O. Potzel and G. Taubmann, Phys. Chem. Chem. Phys. **15**, 20288 (2013).
[56] A. T. H. Lenstra, C. Van Alsenoy, K. Verhulst, and H. J. Geise, Acta Crystallogr., Sect. B: Struct. Sci. **50**, 96 (1994).
[57] G.-P. Charbonneau and Y. Delugeard, Acta Crystallogr., Sect. B: Struct. Crystallogr. Cryst. Chem. **32**, 1420 (1976).
[58] W. Azzam, C. Fuxen, A. Birkner, H.-T. Rong, M. Buck, and C. Wöll, Langmuir **19**, 4958 (2003).
[59] A.-A. Dhirani, R. W. Zehner, R. P. Hsung, P. Guyot-Sionnest, and L. R. Sita, J. Am. Chem. Soc. **118**, 3319 (1996).
[60] S. Frey, V. Stadler, K. Heister, W. Eck, M. Zharnikov, M. Grunze, B. Zeysing, and A. Terfort, Langmuir **17**, 2408 (2001).
[61] J. Poater, M. Solà, and F. M. Bickelhaupt, Chem. - Eur. J. **12**, 2889 (2006).
[62] M. P. Johansson and J. Olsen, J. Chem. Theory Comput. **4**, 1460 (2008).
[63] A. Almenningen, O. Bastiansen, L. Fernholt, B. N. Cyvin, S. J. Cyvin, and S. Samdal, J. Mol. Struct. **128**, 59 (1985).
[64] J. Trotter, Acta Crystallogr. **14**, 1135 (1961).
[65] E. Sauter, G. Nascimbeni, D. Trefz, S. Ludwigs, E. Zojer, F. von Wrochem, and M. Zharnikov, "Structure and Electrostatic Effects in Self-Assembled Monolayers with Dithiocarbamate Anchoring Group" (unpublished).
[66] S. Tsuzuki, T. Uchimaru, K. Matsumura, M. Mikami, and K. Tanabe, Chem. Phys. Lett. **319**, 547 (2000).
[67] D. E. Williams and Y. Xiao, Acta Crystallogr., Sect. A: Found. Crystallogr. **49**, 1 (1993).
[68] L. Wang, G. M. Rangger, Z. Ma, Q. Li, Z. Shuai, E. Zojer, and G. Heimel, Phys. Chem. Chem. Phys. **12**, 4287 (2010).
[69] K. Tonigold and A. Groß, J. Chem. Phys. **132**, 224701 (2010).
[70] A. M. Track, F. Rissner, G. Heimel, L. Romaner, D. Käfer, A. Bashir, G. M. Rangger, O. T. Hofmann, T. Bučko, G. Witte, and E. Zojer, J. Phys. Chem. C **114**, 2677 (2010).
[71] J. Nara and S. Higai, J. Chem. Phys. **120**, 6705 (2004).
[72] S. Liao, Y. Shnidman, and A. Ulman, J. Am. Chem. Soc. **122**, 3688 (2000).

3.3 Supporting Information

Supporting Information to

Exploring the Driving Forces behind the Structural Assembly of Biphenylthiolates on Au(111)

*Elisabeth Verwüster, Elisabeth Wruss, Egbert Zojer, and Oliver T. Hofmann**

Institute of Solid State Physics, NAWI Graz, Graz University of Technology, Petersgasse 16, 8010 Graz, Austria

***Corresponding Author:** Oliver T. Hofmann, o.hofmann@tugraz.at

1. 5-layer slab vs. 3 layer slab:

While a systematically scan of the potential energy surface of biphenylthiole on Au(111) was done using a 3-layer slab to reduce computational cost, calculations for the notional SAM-formation process were done with a 5-layered slab to increase the accuracy. Test calculations show a difference of 15-60 meV in the total adsorption energy between the 3-layered and 5-layered slab, as shown in Table S1.

Table S1: *Comparison between the adsorption energies of various motifs when using a metal slab consisting of either three or five layers.*

ΔE^{ads} [eV]	**3-layer slab**	**5-layer slab**	**Diff [eV]**
HB/HB/0	-0.413	-0.451	0.040
HB/HB/2	-0.317	-0.328	0.011
CP/CP/0	-0.285	-0.282	0.003
CP/CP/2	-0.377	-0.412	0.035

2. Detailed system set up:

To generate a suitable set of starting geometries, three specific angles are modified; tilt- (**β**), inter-ring twist (**γ**) and azimuthal-angle (**α**). For each angle a set of four reasonable starting values are chosen. Specifically, as stated in the main paper;

- for the tilt angle β, we used 0°, 15°, 30° and 45°
- for the inter-ring twist γ, we used 0°, ±45° and ±90°
- for the azimuth α, we used 0, 30, 60 and 90°

A comprehensive list of all 95 starting configurations can be found as Supplementary Material PES.tar.

3. Vibrational Analysis: Computational Details:

To test whether an experimental distinction between the above-discussed polymorphs could be made and to ensure the true nature of the obtained local-minimum geometries, we calculate the vibrational modes for each motif. For doing the vibrational analysis, applying Density Functional Perturbation Theory (DF-PT) in VASP, the following settings are specified in the INCAR file:

- ➔ IBRION=7 sets the DF-PT method
- ➔ the tag LREAL, has to be set to .FALSE.; otherwise the results turned out to be meaningless
- ➔ NWRITE was set to 3 to print the SQRT(mass)-divided eigenvectors in the OUTCAR file
- ➔ LEPSILON is set to .TRUE. to calculate and print the BEC (born effective charge) tensor (refers to change of atoms' polarizabilities w.r.t. an external electric field).

- ➔ The dipole correction has to be switched off. Otherwise, a spurious imaginary mode describing a translational motion is encountered. This mode is displayed in Figure S1.
- ➔ NELM=120 and NELMIN=10 are set to obtain a sufficiently converged electron density.
- ➔ The symmetry tag is switched off: ISYM=0

These settings provide the necessary accuracy of the DF-PT calculations and ensure that the OUTCAR file contains all data needed for applying the post processing script by David Karhánek to calculate the intensity of each vibrational mode. (http://homepage.univie.ac.at/david.karhanek/downloads.html).

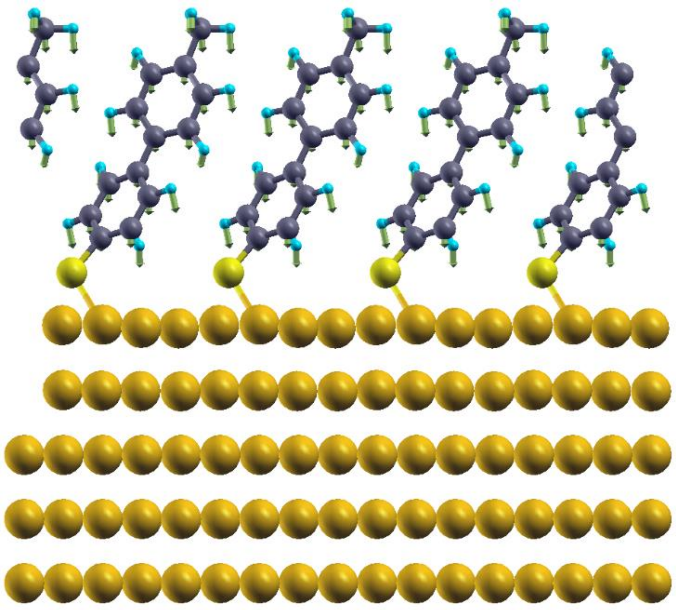

Figure S1: *Mode corresponding to the spurious imaginary frequency resulting from the dipole correction.*

4. Vibrational spectra of the different configurations:

In the biphenylthiolate system, the HB/HB/0 configuration is clearly the most stable motif mostly due to its electrostatic interactions. However, it appears likely that in related systems, where the electrostatic interactions are different (e.g., fluorinated molecules or pyrimidine-containing moieties) or where sterical constraints increase due to bulky substituents, other categories might be more stable and prevalent in experiment. Therefore, the question arises, how an experimental distinction between the above-discussed polymorphs could be made. A method that could be extremely useful for tackling this problem is vibrational spectroscopy, which is frequently applied for providing insight into the structure of SAMs.[1–10] A prerequisite for that would be the existence of "telltale modes", which are particular sensitive to the molecular conformation or the inter-molecular arrangement. Since we performed a vibrational analysis to ascertain that our motifs are true minima, in this appendix we explore whether in IR-spectroscopy such telltale modes do in fact exist.

To address that issue, we start by showing a survey over the spectral region up to 3500 cm^{-1} for all four categories in Figure S2. As expected, the overall shape of the spectra is very similar. Nonetheless, upon closer scrutiny, we can identify one set of vibrations that shift strongly (i.e., ~30 cm^{-1}) depending on the structural motif.

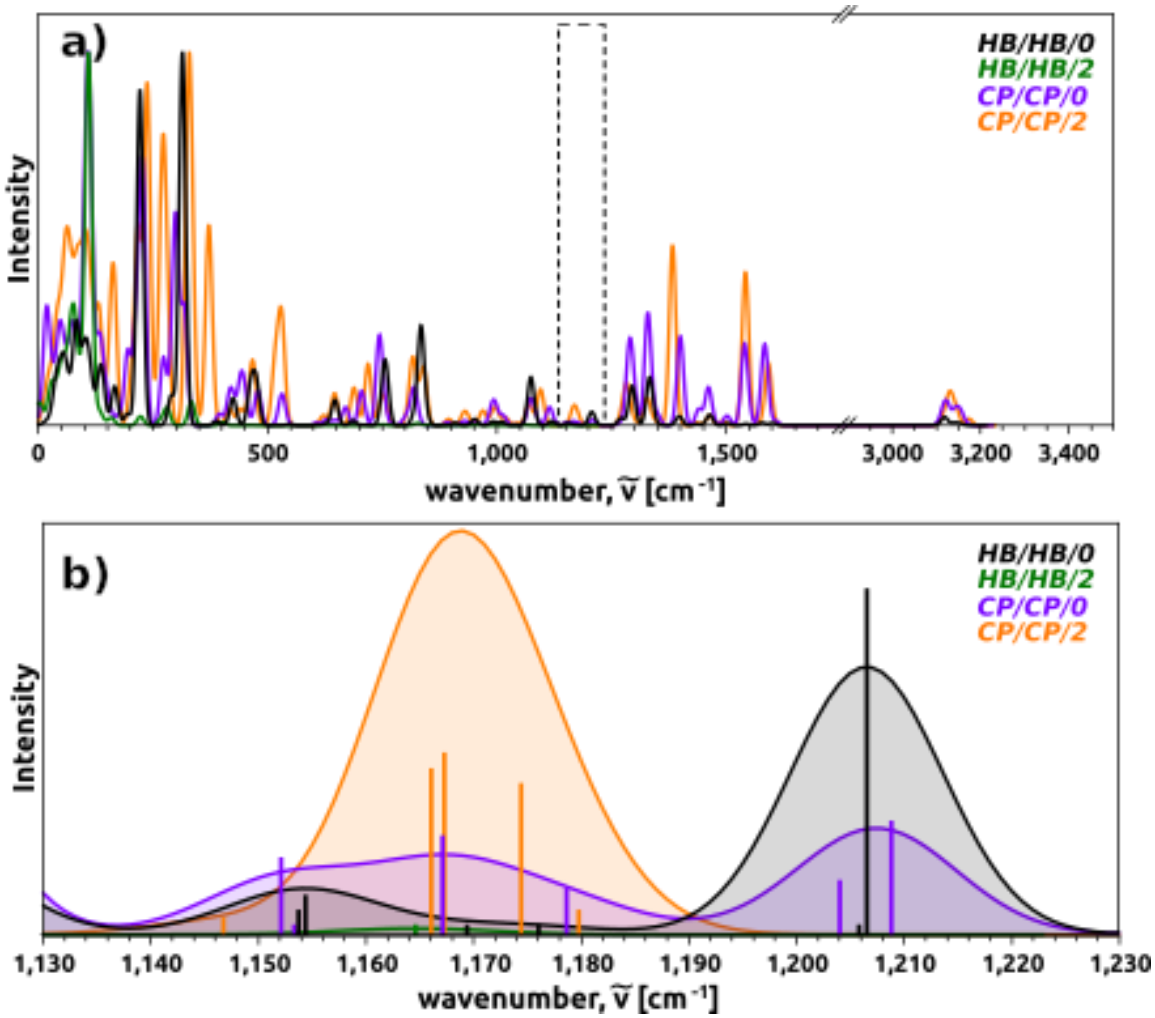

Figure S2: *a) IR-spectra for HB/HB/0 (black), HB/HB/2 (green), CP/CP/0 (purple) and CP/CP/2 (orange) normalized to the highest peak in every conformation. Zooms of the regions designated by dashed lines are separately plotted in panel b). b) Telltale mode indicating the planarity of the molecules. All modes are broadened by a Gaussian peak with* $\sigma = 5\ cm^{-1}$.

In principle, whether the conformation is arranged herringbone or planar could be indicated by the shift of an out-of-plane wagging mode that is located at ca. 390 cm^{-1} for HB and 420 cm^{-1} for CP. In practice, however, these modes coincide with several other, significantly IR-active modes at

similar energetic positions. These would likely obscure any shift in the wagging modes. Hence, IR-measurements are unlikely to yield authoritative information about the intermolecular arrangement. However, this information can experimentally be obtained from high-resolution STM measurements.[11–13]

Conversely, whether the molecular are planar or not is likely not evident from STM measurements, since tips cannot penetrate sufficiently deep in to the material. Fortunately, the vibrational spectra are more sensitive to this geometrical aspect. The planar HB/HB/0 motif shows peak at 1206 cm^{-1}. This peaks consists of two hydrogen scissoring mode vibrations (in-phase and out-of-phase). In the CP/CP/0 motif, a peak is found at a similar position, with a small shift between the out-of-phase and the in-phase modes, that are found at 1204 cm^{-1} and 1208 cm^{-1}, respectively.

If the molecules assume a twisted conformation, the hydrogen-wagging mode experiences less steric repulsion and therefore displays a bathochromic shifts to ca. 1165 cm^{-1}. Interestingly, for the twisted HB/HB/2 motif, the intensity of these modes vanish almost completely. Conversely, for the CP/CP/2 motif, the intensity is strongly increased. In any case, however, they now overlap with other modes (in plane CH) of various at a similar energetic position.

As a result, as shown in Figure S2 b), all four motifs show vibrations in the range between 1150 and 1170 cm^{-1} (although for HB/HB/0, the intensity of all peaks is negligible).

This leads to the situation that while the presence of a peak at ca. 1206 cm^{1} is clearly indicative of the presence of planar molecule, the converse conclusion, namely that the presence of a peak in the range of 1165 cm^{-1} indicated twisted molecules, cannot be made.

5. Deformation Energy, ΔE^{deform} :

Since the unit cell contains two non-equivalent molecules, the deformation energy is calculated for each molecule separately, as listed in Table S2. The averaged value of the two ΔE^{deform} is used to plot step 1 in Figure 4 in the main text. It is noteworthy that, similarly to the deprotonation discussed below, the values for the two molecules can differ notably by up to 142 meV.

Table S2: *Deformation energies, ΔE^{deform}, separately calculated for each molecule in the unit cell. The average value is plotted in step 1 of the SAM-formation in Figure 4 in the main text.*

ΔE^{deform} [eV]	**Molecule 1**	**Molecule 2**	**Average**
HB/HB/0	0.149	0.085	0.117
HB/HB/2	0.140	0.141	0.141
CP/CP/0	0.082	0.130	0.106
CP/CP/2	0.234	0.092	0.163

As mentioned in the main text, the observation that planar molecules show smaller deformation energies compared to twisted conformations appears to contradict literature. In order to test where this apparent discrepancy originates from, we performed a set of tests.

In Table S3, we report the deformation energies for the case where the thiole docking group, SH, is substituted by a single hydrogen atom H. The position of the H atom is optimized, while the rest of the geometry is kept fixed. Qualitatively, the order of the deformation energies remains the same. From this we conclude that the presence of the electron donating SH group does not notably favor a planar conformation of the biphenyl backbone.

Table S3: *Deformation energies, $\Delta E^{deform\text{-}Hsubst}$, calculated for each molecule in the unit cell separately and their average value, after substituting the thiole group S-H with a hydrogen H.*

ΔE^{deform} - Hsubst [eV]	**Molecule 1**	**Molecule 2**	**Average**
HB/HB/0	0.071	0.073	0.072
HB/HB/2	0.101	0.102	0.101
CP/CP/0	0.075	0.060	0.068
CP/CP/2	0.076	0.088	0.082

As a next step, we calculate the deformation energy of the molecules while keeping the monolayer-induced inter-ring twist angle fixed. As a result, the hierarchy of $\Delta E^{deform\text{-}fixed\text{-}gamma}$ changes. The expected situation, that twisting the rings is energetically less costly than planarizing, is recovered. The results are given in Table S4. This leads us to conclude that "secondary geometric distortions" due to tilting and close packing of the molecules define the hierarchy of ΔE^{deform}.

Table S4: *Deformation energies, $\Delta E^{deform\text{-}fixed\text{-}gamma}$, calculated for each molecule in the unit cell separately and their average value, after relaxing the molecules geometry while keeping the monolayer-induced inter-ring twist angel fixed.*

$\Delta E^{deform\text{ - }fixed\text{-}gamma}$ [eV]	**Molecule 1**	**Molecule 2**	**Average**
HB/HB/0	0.069	0.057	0.063
HB/HB/2	0.103	0.004	0.053
CP/CP/0	0.067	0.070	0.069
CP/CP/2	0.080	0.197	0.058

6. Assembly Energy, $\Delta E^{assembly}$

In step 2 of the notational SAM-formation we calculate the assembly of isolated molecules (already in the final structure) into an extended, free-standing monolayer. The corresponding assembly energy, $\Delta E^{assembly}$, is assessed for each of the two molecules in the unit cell separately, with the average value presented in Figure 4 in the main text.

Table S5: *Assembly energies, $\Delta E^{assembly}$, calculated for each molecule in the unit cell separately and their average value*

$\Delta E^{assembly}$ [eV]	**Molecule 1**	**Molecule 2**	**Average**
HB/HB/0	0.127	0.190	0.159
HB/HB/2	0.144	0.144	0.144
CP/CP/0	0.339	0.291	0.315
CP/CP/2	0.310	0.455	0.383

7. Band Structure:

In order to test whether there is a correlation between the assembly energy and the band dispersion of the monolayers, we calculated their band structures. Figure S3 shows the two highest occupied states (i.e., the valence band, VB, and the VB – 1), along the short axis of the unit cell (X-Γ) and the long axis of the unit cell (Y-Γ). Notably, the most stable structure, HB/HB/0, shows the highest band dispersion, thus refuting the initial hypothesis that band dispersion and assembly energy should correlate.

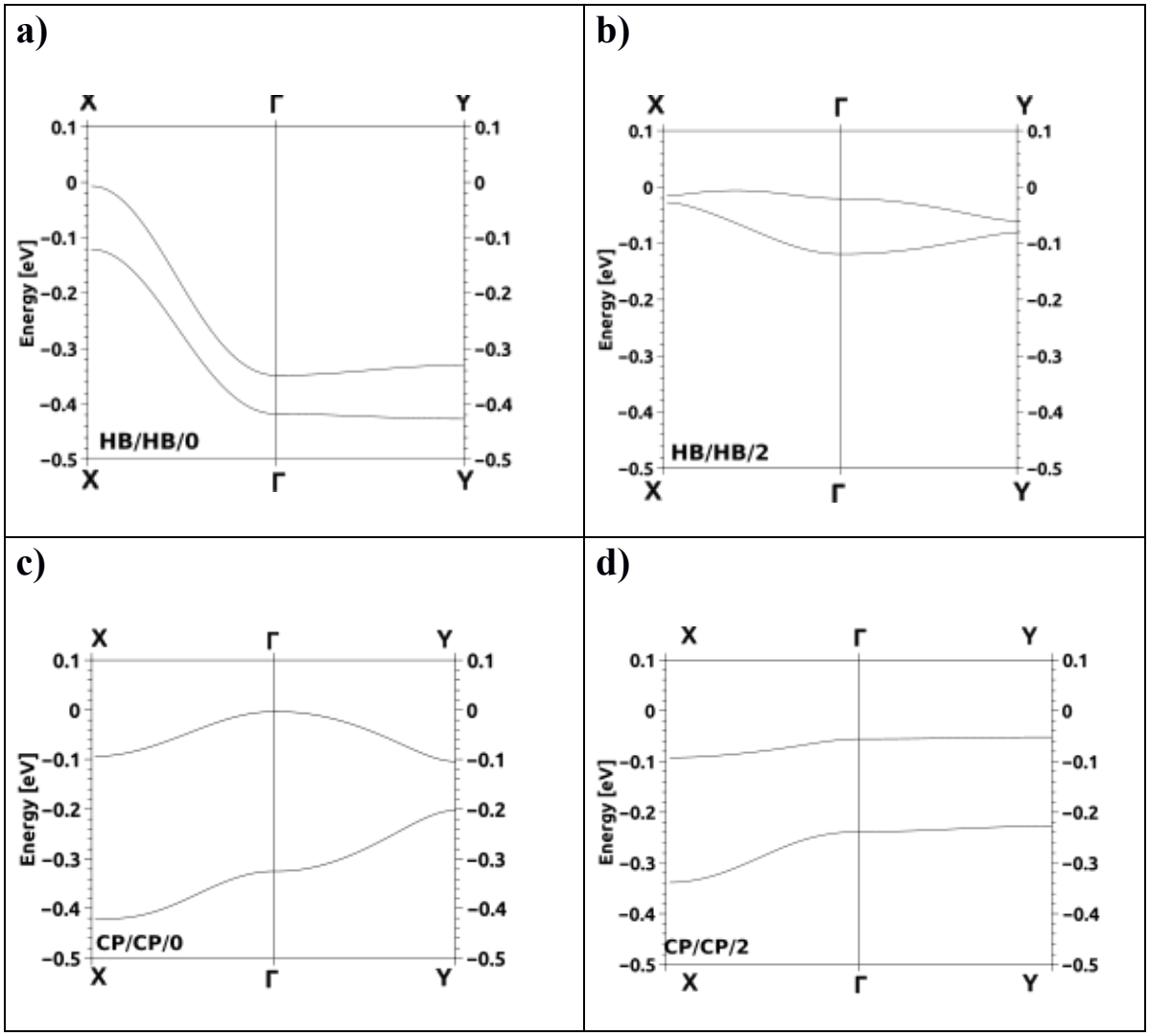

Figure S3: *Band structure from X along the x axis to Γ to Y along the y-axis (0.5 0.0 0.0 - 0.0 0.0 0.0 - 0.0 0.5 0.0) for motif a) HB/HB/0, b) HB/HB/2, c) CP/CP/0 and d) CP/CP/2.*

8. Proton Abstraction:

The calculations for the proton abstraction of the two molecules in the unit cell, i.e., the reaction

$$Ph\text{-}Ph\text{-}SH \rightarrow Ph\text{-}Ph\text{-}S^{-} + H^{+}$$

are performed using Gaussian09[14] using a 6-311* basis-set with the PBE[15] exchange-correlation functional. All molecules in this reaction are closed shell, i.e. all calculations are performed spin-restricted. We note that this reaction does not necessarily occur in reality, as the reaction mechanism for the adsorption is unknown, and the large values obtained here (that originate mostly from the high ionization potential of ~13.61 eV for H) indicate that indeed such a reaction would never occur (at least in the gas phase; in solution screening can change the situation qualitatively). Here, it merely serves to illustrate the chemical inequivalence of the molecules. The results for the two molecules in the unit cell are given in Table S6.

Table S6: *Abstraction energy from Ph-Ph-SH → Ph-Ph-S$^-$ + H$^+$. The deviation between the non-symmetric molecules in the unit cell of each motif amounts to a magnitude of ~100 meV. Calculations were done using the Gaussian09[14] code.*

	Abstraction Energy [eV]
cat1 molecule1	-14.083
cat1 molecule2	-14.163
Deviation	0.080
cat2 molecule1	-14.360
cat2 molecule2	-14.360
Deviation	0.000
cat5 molecule1	-14.118
cat5 molecule2	-14.177
Deviation	0.0593
cat6 molecule1	-14.276
cat6 molecule2	-14.288
Deviation	0.0126

References

[1] Y. Wang, A. Glenz, M. Muhler, and C. Wöll, Rev. Sci. Instrum. **80**, 113108 (2009).

[2] G. Krenn, I. Bako, and R. Schennach, J. Chem. Phys. **124**, 144703 (2006).

[3] K.K. Zhuravlev and M.D. McCluskey, J. Chem. Phys. **117**, 3748 (2002).

[4] W. Azzam, B.I. Wehner, R.A. Fischer, A. Terfort, and C. Wöll, Langmuir **18**, 7766 (2002).

[5] B.L. Frey and R.M. Corn, Anal. Chem. **68**, 3187 (1996).

[6] M.J. Hostetler, J.J. Stokes, and R.W. Murray, Langmuir **12**, 3604 (1996).

[7] J.M. Tour, L. Jones, D.L. Pearson, J.J.S. Lamba, T.P. Burgin, G.M. Whitesides, D.L. Allara, A.N. Parikh, and S.V. Atre, J. Am. Chem. Soc. **117**, 9529 (1995).

[8] P.N. Atul and D.L. Allara, J. Chem. Phys. **96**, 927 (1992).

[9] R. Superfine, P. Guyot-Sionnest, J.H. Hunt, C.T. Kao, and Y.R. Shen, Surf. Sci. **200**, L445 (1988).

[10] A.L. Harris, C.E.D. Chidsey, N.J. Levinos, and D.N. Loiacono, Chem. Phys. Lett. **141**, 350 (1987).

[11] W. Azzam, C. Fuxen, A. Birkner, H.-T. Rong, M. Buck, and C. Wöll, Langmuir **19**, 4958 (2003).

[12] Y.-T. Tao, C.-C. Wu, J.-Y. Eu, W.-L. Lin, K.-C. Wu, and C. Chen, Langmuir **13**, 4018 (1997).

[13] A.-A. Dhirani, R.W. Zehner, R.P. Hsung, P. Guyot-Sionnest, and L.R. Sita, J. Am. Chem. Soc. **118**, 3319 (1996).

[14] M.J. Frisch, G.W. Trucks, H.B. Schlegel, G.E. Scuseria, M.A. Robb, J.R. Cheeseman, G. Scalmani, V. Barone, B. Mennucci, G.A. Petersson, H. Nakatsuji, M. Caricato, X. Li, H.P. Hratchian, A.F. Izmaylov, J. Bloino, G. Zheng, J.L. Sonnenberg, M. Hada, M. Ehara, K. Toyota, R. Fukuda, J. Hasegawa, M. Ishida, T. Nakajima, Y. Honda, O. Kitao, H. Nakai, T. Vreven, J.A. Montgomery Jr., J.E. Peralta, F. Ogliaro, M. Bearpark, J.J. Heyd, E. Brothers, K.N. Kudin, V.N.

Staroverov, R. Kobayashi, J. Normand, K. Raghavachari, A. Rendell, J.C. Burant, S.S. Iyengar, J. Tomasi, M. Cossi, N. Rega, J.M. Millam, M. Klene, J.E. Knox, J.B. Cross, V. Bakken, C. Adamo, J. Jaramillo, R. Gomperts, R.E. Stratmann, O. Yazyev, A.J. Austin, R. Cammi, C. Pomelli, J.W. Ochterski, R.L. Martin, K. Morokuma, V.G. Zakrzewski, G.A. Voth, P. Salvador, J.J. Dannenberg, S. Dapprich, A.D. Daniels, Ö. Farkas, J.B. Foresman, J.V. Ortiz, J. Cioslowski, and D.J. Fox, *Gaussian09, Revision D.01* (n.d.).

[15] J.P. Perdew, M. Ernzerhof, and K. Burke, J. Chem. Phys. **105**, 9982 (1996).

III Summary

In the context of this thesis simulations based on density-functional theory (DFT) have been employed to explore electronic and structural properties of self-assembled monolayers. In particular biphenylthiole-based SAMs on Au(111), represented in Figure 20, were investigated towards the impact of structural imperfections. As the performance of organic electronic applications relies on a well defined structure of, e.g., densely-packed aromatic SAMs, investigating the effects of potential imperfections becomes of crucial importance.

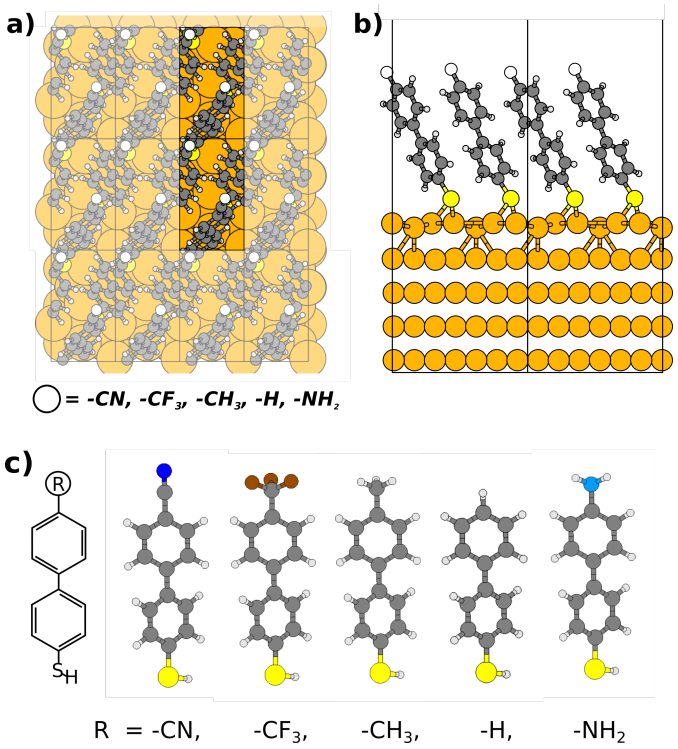

Figure 20: a) Top-view of a schematic biphenylthiole-SAM on Au(111) with the molecules arranged in herringbone-fashion. Two $3 \times \sqrt{3}$ unit-cells are highlighted, each occupied by two biphenylthioles. b) Side-view of two unit-cells. c) Sketch of the biphenyl-backbone, the cyano- (-CN) substituted-, trifluoro- ($-CF_3$) substituted-, methyl- (CH_3) substituted, unsubstituted- and amino- ($-NH_2$) terminated biphenylthiole

Biphenylthiole-based SAMs are frequently used as benchmark systems to explore the physical effects that occur in metal/organic interfaces. However, it is known that such organothiole-SAMs are prone to form films of low quality and exhibit polymorphism.[30,47,120,135–138] A reliable modeling of the structural and electronic properties thus demands the consideration of such imperfections.

The used modeling method employs the repeated slab approach, where one unit-cell is repeated in every spatial direction, creating an infinitely spread metal/organic interface. Introducing structural disorder, therefore, can only be done conceptionally as the (structural) perturbation in one unit cell is repeated in every other unit cell. Thus, the main focus of this work is not to realistically model disordered SAMs, but rather to understand the impact of specific structural imperfections on electronic and structural properties of the SAM. For a more flexible approach, large-scale molecular dynamic (MD) simulations would be a suitable choice. However, the employment of empirical force fields in MD simulations limits the reliability of the computed electronic properties. Nevertheless, despite the constraints imposed by the repeated slab approach regarding imperfections, valuable insight was collected on the physical effects within the monolayer and the metal/organic interface.
Investigating imperfections of metal/organic interfaces was motivated by the work of Maksymovych et.al.;[25,168] Leung et.al.,[47] Azzam et.al.;[149] and Cyganik et.al.,[151] exploring the impact of i) of adatoms,[25,168] ii) surface coverage modifications[47,149] and iii) polymorphism of the monolayer,[151] respectively.

The occurrence of adatoms in metal/organic interfaces is frequently reported for low density alkylthiole-SAMs on Au(111).[25,163,166–175] However, also reconstructed surfaces in densely packed arylthioles on Au(111) are discussed in literature.[27,167,176,177]

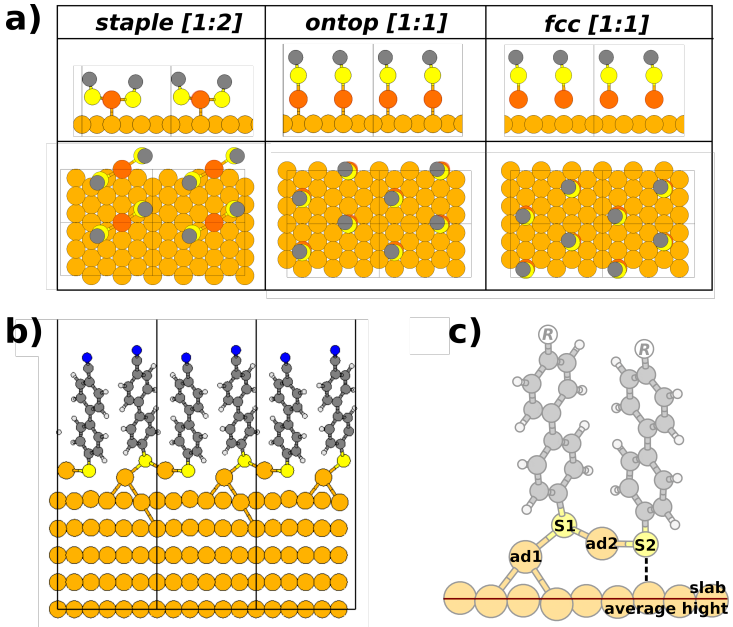

Figure 21: a) Top- and side-view of the starting geometries for the 1:2 ratio (adatom:molecule) staple-motif, the 1:1 ratio geometry with adatoms at fcc-hollow positions and the 1:1 ratio geometry with adatoms at ontop sites. Adatoms are colored in red, sulfur atoms in yellow and the first carbon atom of the backbone in gray; b) Three unit cells of the CN-substituted biphenylthiole-SAM in an adatom-polymer configuration, *CN-poly*$^{(f)}$ c) Close-up of the adatom-polymer configuration

To explore the possible impact of surface reconstructions on the properties of a densely packed biphenylthiole-based SAM, three different surface reconstructions were generated by introducing adatoms in a 1:1 and 1:2 (adatoms:molecule) ratio (schematic sketch in Figure 21 a), where the 1:2 systems forms the well known staple-motif.[163]
In the starting geometries of the 1:1 ratio systems the adatom, sulfur and first carbon atom of the backbone are arranged in an almost straight Au_{ad}-S-C line, see Figure 21 a. This initial-configuration avoids a geometric trajectory towards any specific local minimum structure. Such an arbitrary optimization approach enables the generation of versatile adatom-induced interfacial architectures, that are investigated on easily accessible observables such as the tilt angle, β, the work-function modification, $\Delta\Phi$, and the density of states (DOS).

Comparing the converged geometries displays a trend in the formation of a polymeric adatom-arrangement (Au_{ad}-SR-Au_{ad}-SR). While all -CN-substituted systems converge into a polymer-motif (represented in Figure 21 b and c), the -CH_3 analogues remain in a monomeric configuration (Au_{ad}-SR). The question to be answered is, whether a physical effect, e.g., originating from the electron-withdrawing (-CN), respectively -donating tail-groups (-CH_3), dictates this assumed trend, or whether the randomly generated interfacial configuration determines the structure of the monolayer.
However, due to collective electrostatic effects within the monolayer, diminishing the impact-reach of the tail-groups, their electronic impact may not have a primary effect on the resulting adatom-configuration. Further test calculations confirm this conclusion.

Investigating the energetics of the different adatom-motifs, we find the most favorable adsorption configuration of all structures, including the unreconstructed systems, to be the staple-motif. Polymeric structures in general display lower adsorption energies than monomeric motifs, resulting in a uniform hierarchy in adsorption energy valid for all tail-group substitutions: *staple* < *poly* < *unrec* < *mono*. This hierarchy in adsorption energy suggests a stabilizing impact of adatoms on metal/organic interfaces, given the formation of a staple- or polymeric-motif.

Exploring the electronic properties of the different adatom-induced systems, displays a strong dependence on the present adatom-motif. While the monomeric configurations originate strong changes in work-function modification, $\Delta\Phi$, up to 0.5 eV compared to the unreconstructed systems, the polymeric and staple-configurations display almost unchanged values for $\Delta\Phi$, with differences up to only 0.08 eV.

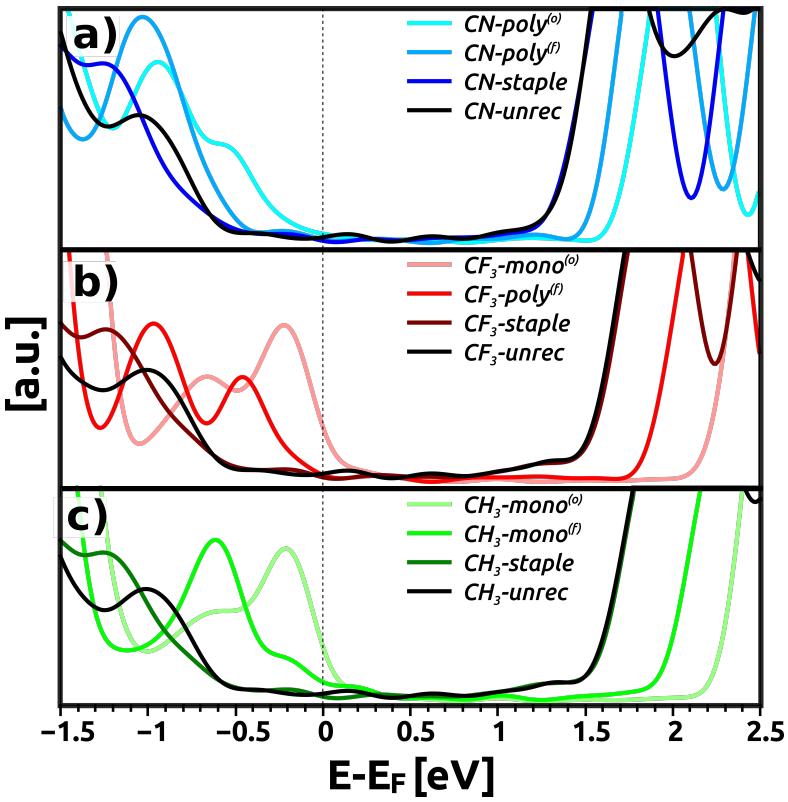

Figure 22: Density of states for the reconstructed and unreconstructed SAMs terminated by a) the -CN (blue), b) the -CF_3 (red) and c) the -CH_3 (green) tail-group. The DOS of the respective unreconstructed SAMs is displayed in black. The dashed line signifies E_F

Analogue to this deviation in impact depending on the adatom-configuration, simulating the density of states (DOS) for all calculated systems displays a similar trend. The monomeric-motifs show Fermi-level pinning[211] (see Figure 22) which may potentially serve as indicator for the presence of a certain adatom bonding-configuration. Furthermore insightful information for the research on single-molecule junctions could be obtained investigating such structures. The distribution of states for the staple- and polymeric-configurations however, almost perfectly resemble the unreconstructed derivatives.

Concluding these findings, motifs with highly coordinated adatoms (staple-, polymeric-motifs) show almost identical properties as the unreconstructed analogues. Since these motifs also have the lowest adsorption energies, the probability of their yet undetected existence in a multitude of high-density SAMs on a Au(111) substrates is reasonably high.

Imperfections in organothiole-based SAMs not only originate from “external” perturbations such as adatoms, but also arise due to the nature of the molecules that constitute the monolayer. The two published articles focus on such “intrinsic” perturbations regarding the arrangement of the molecules on the surface.

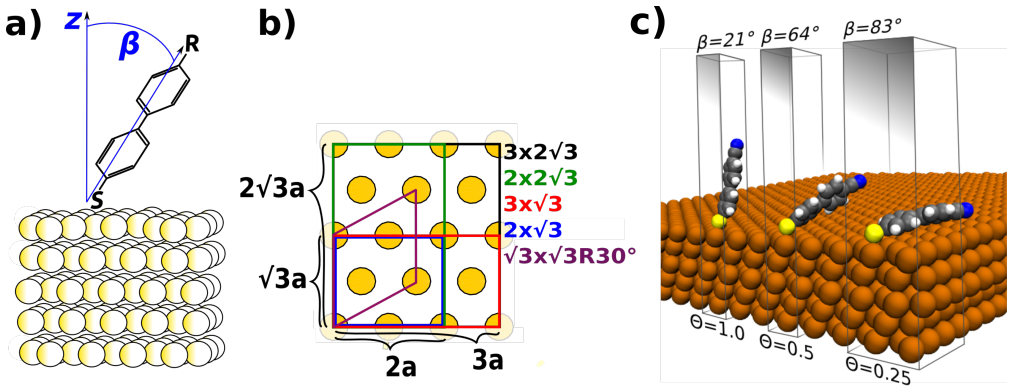

Figure 23: a) Schematic sketch of the studied substituted biphenylthiolate on a slab of five layers of gold. z denotes the axis perpendicular to the slab, β the tilt-angle between long-molecular axis and z, and R = CN, CF_3, NH_2. b) Surface unit cells used to simulate coverages of 1.0, 0.75, 0.5, 0.375, and 0.25; each unit cell contains one molecule. c) Schematic sketch of three differently sized unit cells, each containing one -CN substituted biphenylthiole on a Au(111) surface to visualize the dependency of the molecular tilt-angle, β, on the coverage, Θ. Surrounding molecules are omitted for the sake of clarity

Biphenylthioles tend to form films of rather bad quality. Upon close examination of the film-formation process, Azzam et.al.[30,149] and Leung et.al.[47] reported the formation of various monolayer motifs differing in their surface coverage during depositions. In the first steps of adsorbing biphenylthioles onto Au(111), a low coverage phase with the molecules arranged in a lying-down fashion is reported.[47,149] Upon further deposition of biphenylthioles the typically observed hexagonal standing-up phase forms in a $3 \times \sqrt{3}$ unit cell.[47] The coverage-dependent tilt-angle of the molecules is schematically represented in Figure 23 c.
Investigating the electronic properties of a biphenylthiole-based SAM upon varying the surface coverage revealed a non-trivial dependence between coverage and resulting work-function modification.

A varying surface coverage was achieved by using differently sized unit cells, schematically represented in Figure 23 b. The obtained coverages range from full (1.00) to 0.75, 0.50, 0.37 and 0.25. Upon decreasing the surface coverage, the tilt-angle, β (Figure 23 a) of the molecules increases up to the point where the molecules can be regarded as lying-down (β approximates 90°, see Figure 24 left panel a). As the molecules of the monolayer are substituted by electron-withdrawing (-CN), respectively donating tail-groups (-NH_2), the increasing tilt angle results in a strong change of the work-function modification, $\Delta\Phi$.

The correlation between β and $\Delta\Phi$ can be rationalized, as only the dipole-contribution in z-direction affects the work-function. Thus, upon the molecules "falling over" the z-component of the molecular dipoles diminish.

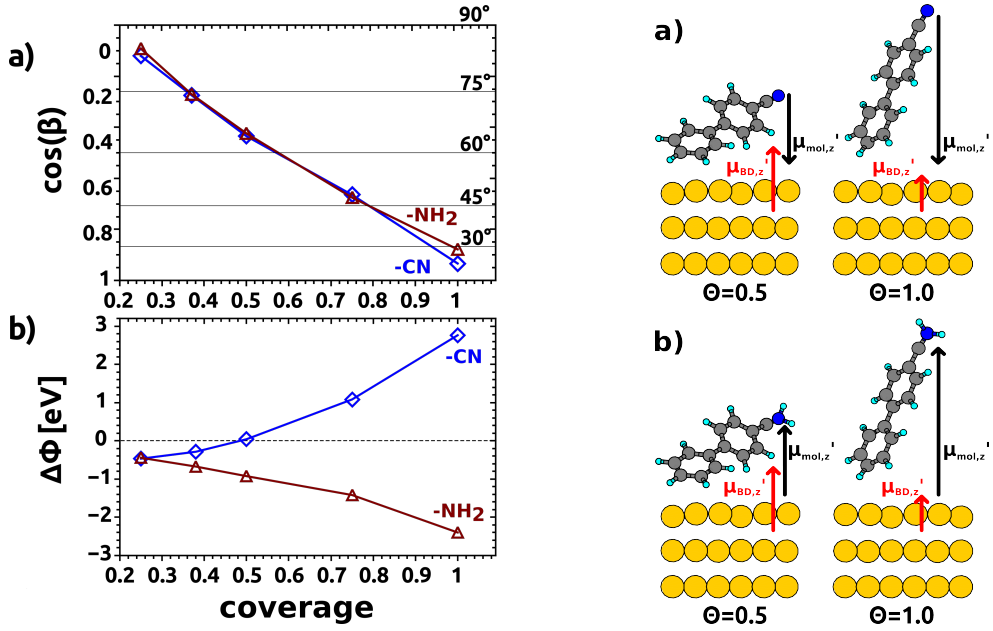

Figure 24: Left panel: coverage dependence of (a) the tilt angle, and cosine of the tilt angle ($cos(\beta)$) and (b) the work-function modification, $\Delta\Phi$. Results for the -CN substituted system are shown as blue diamonds and those for the -NH_2 substituted case as red triangles. Right panel: Schematic illustration of the resulting interplay of the molecular dipole $\mu_{mol,z'}$ and the interfacial dipole $\mu_{BD,z'}$ when going from full to half coverage for the hydrogen-substituted model system either bearing (a) an electron-accepting substituent (-CN) or (b) an electron-donating substituent (-NH_2)

One would, therefore, expect $\Delta\Phi$ to simply decrease with increasing tilt of the molecules. However, already at a surface coverage of 0.5 no modification of the work-function is observed. Further coverage reduction even leads to a change in sign for the electron-accepting tail-group (-CN) systems. $\Delta\Phi$ of the donor (-NH_2) substituted SAM, however, does not change its sign as a function of coverage. Here, $\Delta\Phi$ approaches the same value observed for the CN-substituted layer at the smallest surface coverage (see Figure 24 left panel b).

Conducting a Gedankenexperiment to elucidate this peculiar relation between β and $\Delta\Phi$, the thioles were substituted by single hydrogen atoms. Thereby the dipolar contribution of the docking-group was eliminated. This substitution revealed the responsible factor, besides the perpendicular component of the dipoles in the monolayer, to be the Pauli-Pushback effect. Upon the molecules falling over, Pauli-Pushback grows in magnitude, as the overlap between the π-system of the molecule and the electron-cloud tailing from the metal surface increases. The resulting interface dipole counteracts (enforces) the molecular dipole-contribution for the acceptor (donor-)substituted SAM s schematically represented in Figure 24 right panel. The "SAM-character" of such a densely packed SAM is increasingly lost with decreasing coverage. The resulting properties progressively resemble those of physisorbed monolayers.

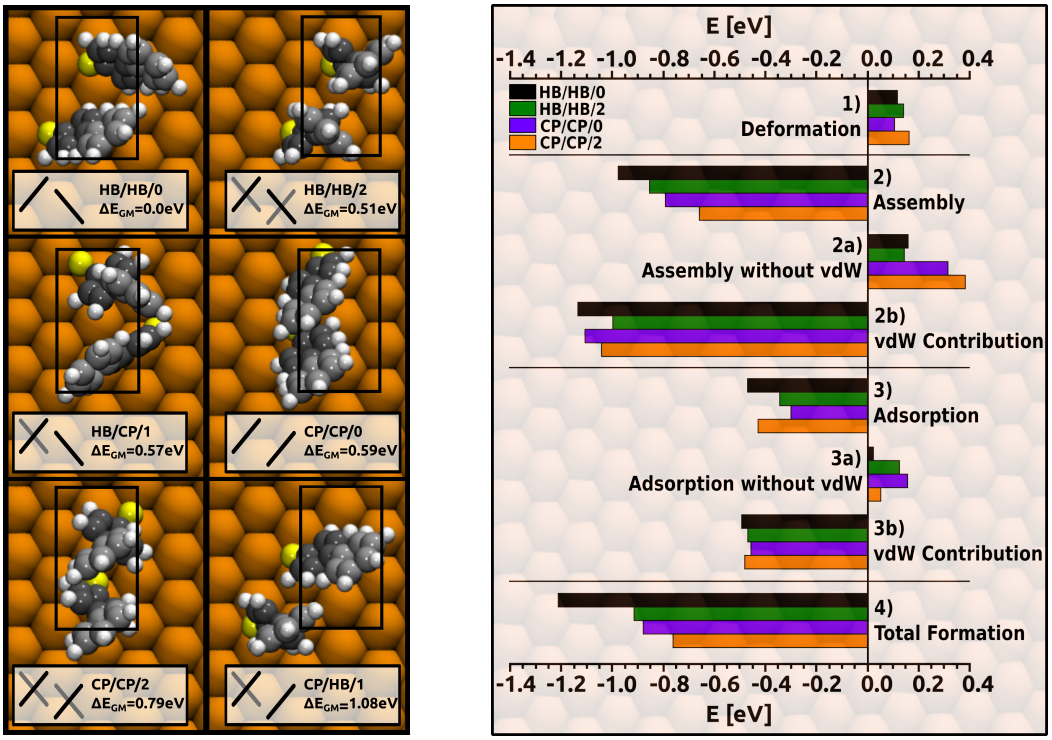

Figure 25: Left panel: Top view of the obtained minimum geometries for each category. The insets contain the naming convention (HB = herringbone, CP = co-planar, 0/1/2 = number of inter-ring twists per motif), the energy, ΔE_{GM}, relative to the lowest energy found in this study (HB/HB/0) and a schematic illustration of each motif. For the sake of clarity, only the two molecules that constitute the unit cell (black rectangle) are shown and neighboring molecules are omitted. Right panel: SAM-formation process split into separate contributions: (1) deformation energy, ΔE^{deform}; (2) assembly energy, $\Delta E^{assembly}$; (2a) assembly energy without vdW correction; (2b) vdW contribution to the assembly process, ΔE^{vdW}; (3) adsorption energy, ΔE^{ads}; (3a) adsorption energy without vdW correction; (3b) vdW contribution to ΔE^{ads}; and (4) the sum of all contributions, ΔE^{total}, for the different local minimum structures HB/HB/0 (black), HB/HB/2 (green), CP/CP/0 (purple), and CP/CP/2 (orange)

Going back to a full coverage densely packed monolayer of such arylthiole SAMs, the structural quality is limited, resulting in poor domain sizes, polymorphism and no features of an ordered structure when investigating the systems via GIXD, LEAD or STM).[30,62,67,137,138,152,153] The difficulty in obtaining high-quality monolayers for biphenylthioles originates from strong intermolecular interactions, creating additional energetic barriers impeding molecule-reorganization on the surface to form ordered films.[47,150,151]

Moreover, not only the strong intermolecular interactions perturb the assembly process, but also interactions of the monolayer with the substrate lattice of the Au(111). Stress and strain is generated in the SAM[136] due to a lattice mismatch between the adsorbate biphenylthiole-layer and the underlying metal substrate,

originating polymorphism.[135,136,151]

The "intrinsic" imperfection explored in the following refers to the biphenyl backbone, which can either adopt a planar or twisted conformation and the resulting motifs that can be formed on the surface. To understand the stability of the different polymorphs for a biphenylthiole-SAM on Au(111), inter- and intra-molecular interactions within a variety of motifs were investigated in detail. Exploring the potential energy surface (PES) for this prototypical system (two molecules in a $3 \times \sqrt{3}$ unit-cell) by systematically varying the starting configurations, resulted in six main packing motifs, schematically represented in Figure 25 in the left panel. These motifs differ in the planarity of the backbone and the relative arrangement of the molecules on the surface, which can be either a co-planar or herringbone fashion.

By modeling a hypothetical SAM-formation process consisting of (i) molecular deformation, (ii) assembly of the molecules into a monolayer, and (iii) bonding of that monolayer to the substrate (see the comprised results in Figure 25 right panel), we elucidated the factors that stabilize specific polymorphs over others.
The main factor that stabilizes certain motifs over others originates from the assembly of the single molecules into a free-standing monolayer. The combination of strong intermolecular electrostatic interactions and the smallest intermolecular Coulomb repulsion together with a high van der Waals attraction stabilizes the conformation with planar molecules arranged in a herringbone pattern. Tuning the molecular conformation in SAMs improving the quality of the formed monolayer can, thus, be achieved by modifying the intra-molecular charge distributions.

References

[1] E. Verwüster, O. T. Hofmann, D. A. Egger, and E. Zojer, "Electronic properties of biphenylthiolates on Au(111): the impact of coverage revisited," *The Journal of Physical Chemistry C*, vol. 119, no. 14, pp. 7817–7825, 2015.

[2] E. Verwüster, E. Wruss, E. Zojer, and O. T. Hofmann, "Exploring the driving forces behind the structural assembly of biphenylthiolates on Au(111)," *The Journal of Chemical Physics*, vol. 147, no. 2, p. 024706, 2017.

[3] C. J. Cramer, *Essentials of computational chemistry: theories and models*. John Wiley & Sons, 2013.

[4] K. Burke and L. O. Wagner, "Dft in a nutshell," *International Journal of Quantum Chemistry*, vol. 113, no. 2, pp. 96–101, 2013.

[5] W. Kohn and L. J. Sham, "Self-consistent equations including exchange and correlation effects," *Phys. Rev.*, vol. 140, pp. 1133–1138, Nov 1965.

[6] P. Hohenberg and W. Kohn, "Inhomogeneous electron gas," *Phys. Rev.*, vol. 136, pp. 864–871, Nov 1964.

[7] M. Born and R. Oppenheimer, "Zur quantentheorie der molekeln," *Annalen der Physik*, vol. 389, no. 20, pp. 457–484, 1927.

[8] J. P. Perdew, K. Burke, and M. Ernzerhof, "Generalized Gradient Approximation Made Simple," *Physical Review Letters*, vol. 77, pp. 3865–3868, Oct. 1996.

[9] J. P. Perdew, K. Burke, and M. Ernzerhof, "Generalized Gradient Approximation Made Simple [Phys. Rev. Lett. 77, 3865 (1996)]," *Physical Review Letters*, vol. 78, pp. 1396–1396, Feb. 1997.

[10] R. Peverati and D. G. Truhlar, "Quest for a universal density functional: the accuracy of density functionals across a broad spectrum of databases in chemistry and physics," *Philosophical Transactions of the Royal Society of London A: Mathematical, Physical and Engineering Sciences*, vol. 372, no. 2011, 2014.

[11] L. Kronik, T. Stein, S. Refaely-Abramson, and R. Baer, "Excitation gaps of finite-sized systems from optimally tuned range-separated hybrid functionals," *Journal of Chemical Theory and Computation*, vol. 8, no. 5, pp. 1515–1531, 2012. PMID: 26593646.

[12] V. G. Ruiz, W. Liu, E. Zojer, M. Scheffler, and A. Tkatchenko, "Density-Functional Theory with Screened vanÂ derÂ Waals Interactions for the Modeling of Hybrid Inorganic-Organic Systems," *Physical Review Letters*, vol. 108, p. 146103, Apr. 2012.

[13] W. Al Saidi, V. K. Voora, and K. D. Jordan, "An assessment of the vdw-ts method for extended systems," *Journal of chemical theory and computation*, vol. 8, no. 4, pp. 1503–1513, 2012.

[14] E. Zaremba and W. Kohn, "Van der waals interaction between an atom and a solid surface," *Physical Review B*, vol. 13, no. 6, p. 2270, 1976.

[15] E. Lifshitz, "Sov phys jetp," *Sov. Phys. JETP*, vol. 2, pp. 73–83, 1956.

[16] G. Kresse and J. Furthmüller, "Efficient iterative schemes for ab initio total-energy calculations using a plane-wave basis set," *Phys. Rev. B*, vol. 54, pp. 11169–11186, Oct 1996.

[17] G. Heimel, F. Rissner, and E. Zojer, "Modeling the Electronic Properties of Ï-Conjugated Self-Assembled Monolayers," *Advanced Materials*, vol. 22, pp. 2494–2513, June 2010.

[18] J. Neugebauer and M. Scheffler, "Adsorbate-substrate and adsorbate-adsorbate interactions of na and k adlayers on al(111)," *Phys. Rev. B*, vol. 46, pp. 16067–16080, Dec 1992.

[19] P. E. Blöchl, "Projector augmented-wave method," *Phys. Rev. B*, vol. 50, pp. 17953–17979, Dec 1994.

[20] H. J. Monkhorst and J. D. Pack, "Special points for Brillouin-zone integrations," *Physical Review B*, vol. 13, pp. 5188–5192, June 1976.

[21] T. Bučko, J. Hafner, and J. G. Ángyán, "Geometry optimization of periodic systems using internal coordinates," *The Journal of Chemical Physics*, vol. 122, p. 124508, Mar. 2005.

[22] M. Frisch, G. Trucks, H. Schlegel, G. Scuseria, M. Robb, J. Cheeseman, G. Scalmani, V. Barone, B. Mennucci, G. Petersson, *et al.*, "Gaussian 09, rev. a. 02," *Gaussian Inc., Wallingford, CT*, 2009.

[23] J. Baker and P. Pulay, "Geometry optimization of atomic microclusters using inverseâpower distance coordinates," *The Journal of Chemical Physics*, vol. 105, pp. 11100–11107, Dec. 1996.

[24] F. P. Cometto, P. Paredes-Olivera, V. A. Macagno, and E. M. Patrito, "Density Functional Theory Study of the Adsorption of Alkanethiols on Cu(111), Ag(111), and Au(111) in the Low and High Coverage Regimes," *The Journal of Physical Chemistry B*, vol. 109, pp. 21737–21748, Nov. 2005.

[25] P. Maksymovych, D. C. Sorescu, and J. T. Yates Jr, "Gold-adatom-mediated bonding in self-assembled short-chain alkanethiolate species on the au (111) surface," *Physical review letters*, vol. 97, no. 14, p. 146103, 2006.

[26] M. Yu, N. Bovet, C. J. Satterley, S. Bengiø', K. R. J. Lovelock, P. K. Milligan, R. G. Jones, D. P. Woodruff, and V. Dhanak, "True Nature of an Archetypal Self-Assembly System: Mobile Au-Thiolate Species on Au(111)," *Physical Review Letters*, vol. 97, p. 166102, Oct. 2006.

[27] P. Maksymovych and J. T. Yates, "Au adatoms in self-assembly of benzenethiol on the Au(111) surface," *Journal of the American Chemical Society*, vol. 130, pp. 7518–7519, June 2008.

[28] L. Wang, G. M. Rangger, L. Romaner, G. Heimel, T. Bučko, Z. Ma, Q. Li, Z. Shuai, and E. Zojer, "Electronic Structure of Self-Assembled Monolayers on Au(111) Surfaces: The Impact of Backbone Polarizability," *Advanced Functional Materials*, vol. 19, pp. 3766–3775, Dec. 2009.

[29] G. Krenn, I. Bako, and R. Schennach, "Co adsorption and co and o coadsorption on rh (111) studied by reflection absorption infrared spectroscopy and density functional theory," *The Journal of chemical physics*, vol. 124, no. 14, p. 144703, 2006.

[30] W. Azzam, B. I. Wehner, R. A. Fischer, A. Terfort, and C. Wöll, "Bonding and Orientation in Self-Assembled Monolayers of Oligophenyldithiols on Au Substrates," *Langmuir*, vol. 18, pp. 7766–7769, Oct. 2002.

[31] K. K. Zhuravlev and M. D. McCluskey, "Infrared spectroscopy of biphenyl under hydrostatic pressure," *The Journal of Chemical Physics*, vol. 117, pp. 3748–3752, Aug. 2002.

[32] J. M. Tour, L. Jones, D. L. Pearson, J. J. S. Lamba, T. P. Burgin, G. M. Whitesides, D. L. Allara, A. N. Parikh, and S. Atre, "Self-assembled monolayers and multilayers of conjugated thiols, .alpha.,.omega.-dithiols, and thioacetyl-containing adsorbates. understanding attachments between potential molecular wires and gold surfaces," *Journal of the American Chemical Society*, vol. 117, no. 37, pp. 9529–9534, 1995.

[33] B. L. Frey and R. M. Corn, "Covalent attachment and derivatization of poly (l-lysine) monolayers on gold surfaces as characterized by polarization- modulation ft-ir spectroscopy," *Analytical Chemistry*, vol. 68, no. 18, pp. 3187–3193, 1996.

[34] M. J. Hostetler, J. J. Stokes, and R. W. Murray, "Infrared spectroscopy of three-dimensional self-assembled monolayers: N-alkanethiolate monolayers on gold cluster compounds," *Langmuir*, vol. 12, no. 15, pp. 3604–3612, 1996.

[35] A. N. Parikh and D. L. Allara, "Quantitative determination of molecular structure in multilayered thin films of biaxial and lower symmetry from photon spectroscopies. i. reflection infrared vibrational spectroscopy," *The Journal of chemical physics*, vol. 96, no. 2, pp. 927–945, 1992.

[36] R. Superfine, P. Guyot-Sionnest, J. Hunt, C. Kao, and Y. Shen, "Surface vibrational spectroscopy of molecular adsorbates on metals and semiconductors by infrared-visible sum-frequency generation," *Surface science*, vol. 200, no. 1, pp. L445–L450, 1988.

[37] A. Harris, C. Chidsey, N. Levinos, and D. Loiacono, "Monolayer vibrational spectroscopy by infrared-visible sum generation at metal and semiconductor surfaces," *Chemical physics letters*, vol. 141, no. 4, pp. 350–356, 1987.

[38] P. Giannozzi and S. Baroni, "Density-functional perturbation theory," *Handbook of Materials Modeling*, pp. 195–214, 2005.

[39] S. Baroni, S. De Gironcoli, A. Dal Corso, and P. Giannozzi, "Phonons and related crystal properties from density-functional perturbation theory," *Reviews of Modern Physics*, vol. 73, no. 2, p. 515, 2001.

[40] X. Gonze, "Erratum: Adiabatic density-functional perturbation theory," *Physical Review A*, vol. 54, no. 5, p. 4591, 1996.

[41] N. Zein, "Density functional calculations of crystal elastic modula and phonon-spectra," *FIZIKA TVERDOGO TELA*, vol. 26, no. 10, pp. 3028–3034, 1984.

[42] X. Gonze and C. Lee, "Dynamical matrices, born effective charges, dielectric permittivity tensors, and interatomic force constants from density-functional perturbation theory," *Physical Review B*, vol. 55, no. 16, p. 10355, 1997.

[43] F. Tautz, "Structure and bonding of large aromatic molecules on noble metal surfaces: The example of ptcda," *Progress in Surface Science*, vol. 82, no. 9, pp. 479–520, 2007.

[44] G. Heimel, L. Romaner, E. Zojer, and J.-L. Bredas, "The Interface Energetics of Self-Assembled Monolayers on Metals," *Accounts of Chemical Research*, vol. 41, pp. 721–729, June 2008.

[45] J. C. Love, L. A. Estroff, J. K. Kriebel, R. G. Nuzzo, and G. M. Whitesides, "Self-Assembled Monolayers of Thiolates on Metals as a Form of Nanotechnology," *Chemical Reviews*, vol. 105, pp. 1103–1170, Apr. 2005.

[46] E. B. Troughton, C. D. Bain, G. M. Whitesides, R. G. Nuzzo, D. L. Allara, and M. D. Porter, "Monolayer films prepared by the spontaneous self-assembly of symmetrical and unsymmetrical dialkyl sulfides from solution onto gold substrates: structure, properties, and reactivity of constituent functional groups," *Langmuir*, vol. 4, no. 2, pp. 365–385, 1988.

[47] T. Y. B. Leung, P. Schwartz, G. Scoles, F. Schreiber, and A. Ulman, "Structure and growth of 4-methyl-4'-mercaptobiphenyl monolayers on Au(111): a surface diffraction study," *Surface Science*, vol. 458, pp. 34–52, June 2000.

[48] E. Sabatani, J. Cohen-Boulakia, M. Bruening, and I. Rubinstein, "Thioaromatic monolayers on gold: a new family of self-assembling monolayers," *Langmuir*, vol. 9, pp. 2974–2981, Nov. 1993.

[49] N. Koch, "Organic Electronic Devices and Their Functional Interfaces," *ChemPhysChem*, vol. 8, pp. 1438–1455, July 2007.

[50] A. J. Heeger, "Nobel lecture: Semiconducting and metallic polymers: The fourth generation of polymeric materials," *Rev. Mod. Phys.*, vol. 73, pp. 681–700, Sep 2001.

[51] P.-C. Chen, X.-J. Huang, and Z.-K. Xu, "Activation and deformation of immobilized lipase on self-assembled monolayers with tailored wettability," *Physical Chemistry Chemical Physics*, vol. 17, no. 20, pp. 13457–13465, 2015.

[52] F. P. Zamborini and R. M. Crooks, "Corrosion passivation of gold by n-alkanethiol self-assembled monolayers: effect of chain length and end group," *Langmuir*, vol. 14, no. 12, pp. 3279–3286, 1998.

[53] R. Gross and A. Marx, *Festkörperphysik*. Walter de Gruyter GmbH & Co KG, 2014.

[54] N. W. Ashcroft and N. D. Mermin, "Solid state physics (holt, rinehart and winston, new york, 1976)," *Google Scholar*, vol. 403, 2005.

[55] R. Hoffmann, "How chemistry and physics meet in the solid state," *Angewandte Chemie International Edition*, vol. 26, no. 9, pp. 846–878, 1987.

[56] A. M. Hiszpanski, R. M. Baur, B. Kim, N. J. Tremblay, C. Nuckolls, A. R. Woll, and Y.-L. Loo, "Tuning Polymorphism and Orientation in Organic Semiconductor Thin Films via Post-deposition Processing," *Journal of the American Chemical Society*, vol. 136, pp. 15749–15756, Nov. 2014.

[57] N. Garg, E. Carrasquillo-Molina, and T. R. Lee, "Self-Assembled Monolayers Composed of Aromatic Thiols on Gold:â Structural Characterization and Thermal Stability in Solution," *Langmuir*, vol. 18, pp. 2717–2726, Apr. 2002.

[58] E. G. Emberly and G. Kirczenow, "Models of electron transport through organic molecular monolayers self-assembled on nanoscale metallic contacts," *Physical Review B*, vol. 64, p. 235412, Nov. 2001.

[59] P. E. Kornilovitch and A. M. Bratkovsky, "Orientational dependence of current through molecular films," *Physical Review B*, vol. 64, p. 195413, Oct. 2001.

[60] T. Ishida, W. Mizutani, N. Choi, U. Akiba, M. Fujihira, and H. Tokumoto, "Structural Effects on Electrical Conduction of Conjugated Molecules Studied by Scanning Tunneling Microscopy," *The Journal of Physical Chemistry B*, vol. 104, pp. 11680–11688, Dec. 2000.

[61] R. Naaman, A. Haran, A. Nitzan, D. Evans, and M. Galperin, "Electron Transmission through Molecular Layers," *The Journal of Physical Chemistry B*, vol. 102, pp. 3658–3668, May 1998.

[62] Y.-T. Tao, C.-C. Wu, J.-Y. Eu, W.-L. Lin, K.-C. Wu, and C.-h. Chen, "Structure Evolution of Aromatic-Derivatized Thiol Monolayers on Evaporated Gold," *Langmuir*, vol. 13, pp. 4018–4023, July 1997.

[63] Q. Jin, J. Rodriguez, C. Li, Y. Darici, and N. Tao, "Self-assembly of aromatic thiols on au (111)," *Surface Science*, vol. 425, no. 1, pp. 101–111, 1999.

[64] M. T. Cygan, T. D. Dunbar, J. J. Arnold, L. A. Bumm, N. F. Shedlock, T. P. Burgin, L. Jones, D. L. Allara, J. M. Tour, and P. S. Weiss, "Insertion, conductivity, and structures of conjugated organic oligomers in self-assembled alkanethiol monolayers on au111," *Journal of the American Chemical Society*, vol. 120, no. 12, pp. 2721–2732, 1998.

[65] G. Poirier and E. Pylant, "The self-assembly mechanism of alkanethiols on au (111)," *Science*, vol. 272, no. 5265, p. 1145, 1996.

[66] R. G. Nuzzo and D. L. Allara, "Adsorption of bifunctional organic disulfides on gold surfaces," *Journal of the American Chemical Society*, vol. 105, no. 13, pp. 4481–4483, 1983.

[67] J. F. Kang, A. Ulman, S. Liao, and R. Jordan, "Mixed self-assembled monolayers of highly polar rigid biphenyl thiols," *Langmuir*, vol. 15, no. 6, pp. 2095–2098, 1999.

[68] A. Sandy, S. Mochrie, D. Zehner, K. Huang, and D. Gibbs, "Structure and phases of the au (111) surface: X-ray-scattering measurements," *Physical Review B*, vol. 43, no. 6, p. 4667, 1991.

[69] O. Dannenberger, M. Buck, and M. Grunze, "Self-assembly of n-alkanethiols: A kinetic study by second harmonic generation," *The Journal of Physical Chemistry B*, vol. 103, no. 12, pp. 2202–2213, 1999.

[70] S. Xu, S. J. Cruchon-Dupeyrat, J. C. Garno, G.-Y. Liu, G. Kane Jennings, T.-H. Yong, and P. E. Laibinis, "In situ studies of thiol self-assembly on gold from solution using atomic force microscopy," *The Journal of chemical physics*, vol. 108, no. 12, pp. 5002–5012, 1998.

[71] K. A. Peterlinz and R. Georgiadis, "In situ kinetics of self-assembly by surface plasmon resonance spectroscopy," *Langmuir*, vol. 12, no. 20, pp. 4731–4740, 1996.

[72] C. D. Bain, E. B. Troughton, Y. T. Tao, J. Evall, G. M. Whitesides, and R. G. Nuzzo, "Formation of monolayer films by the spontaneous assembly of organic thiols from solution onto gold," *Journal of the American Chemical Society*, vol. 111, no. 1, pp. 321–335, 1989.

[73] H. Wolf, H. Ringsdorf, E. Delamarche, T. Takami, H. Kang, B. Michel, C. Gerber, M. Jaschke, H.-J. Butt, and E. Bamberg, "End-Group-Dominated Molecular Order in Self-Assembled Monolayers," *The Journal of Physical Chemistry*, vol. 99, pp. 7102–7107, May 1995.

[74] C.-J. Zhong, N. T. Woods, G. B. Dawson, and M. D. Porter, "Formation of thiol-based monolayers on gold: implications from open circuit potential measurements," *Electrochemistry communications*, vol. 1, no. 1, pp. 17–21, 1999.

[75] H. Sellers, A. Ulman, Y. Shnidman, and J. E. Eilers, "Structure and binding of alkanethiolates on gold and silver surfaces: implications for self-assembled monolayers," *Journal of the American Chemical Society*, vol. 115, no. 21, pp. 9389–9401, 1993.

[76] L. Wang, G. M. Rangger, Z. Ma, Q. Li, Z. Shuai, E. Zojer, and G. Heimel, "Is there a au-s bond dipole in self-assembled monolayers on gold?," *Physical Chemistry Chemical Physics*, vol. 12, no. 17, p. 4287, 2010.

[77] M. Hasan, D. Bethell, and M. Brust, "The fate of sulfur-bound hydrogen on formation of self-assembled thiol monolayers on gold: 1h nmr spectroscopic evidence from solutions of gold clusters," *Journal of the American Chemical Society*, vol. 124, no. 7, pp. 1132–1133, 2002.

[78] G. E. Poirier, "Characterization of Organosulfur Molecular Monolayers on Au(111) using Scanning Tunneling Microscopy," *Chemical Reviews*, vol. 97, pp. 1117–1128, June 1997.

[79] A. Ulman, "Self-assembled monolayers of thiols (thin films)," 1998.

[80] H. Lüth, *Surfaces and interfaces of solid materials*. Springer Science & Business Media, 2013.

[81] L. H. Dubois, B. R. Zegarski, and R. G. Nuzzo, "Molecular ordering of organosulfur compounds on au (111) and au (100): Adsorption from solution and in ultrahigh vacuum," *The Journal of chemical physics*, vol. 98, no. 1, pp. 678–688, 1993.

[82] R. Feidenhans, "Surface structure determination by x-ray diffraction," *Surface Science Reports*, vol. 10, no. 3, pp. 105–188, 1989.

[83] H. Dosch, *Critical phenomena at surfaces and interfaces*. Springer, 1992.

[84] J. Pflaum, G. Bracco, F. Schreiber, R. Colorado, O. Shmakova, T. Lee, G. Scoles, and A. Kahn, "Structure and electronic properties of ch 3-and cf 3-terminated alkanethiol monolayers on au (111): a scanning tunneling microscopy, surface x-ray and helium scattering study," *Surface Science*, vol. 498, no. 1, pp. 89–104, 2002.

[85] M. Tolan, *X-ray scattering from soft-matter thin films: materials science and basic research*. Springer, 1999.

[86] I. Tidswell, B. Ocko, P. S. Pershan, S. Wasserman, G. Whitesides, and J. Axe, "X-ray specular reflection studies of silicon coated by organic monolayers (alkylsiloxanes)," *Physical Review B*, vol. 41, no. 2, p. 1111, 1990.

[87] R. G. Nuzzo, L. H. Dubois, and D. L. Allara, "Fundamental studies of microscopic wetting on organic surfaces. 1. formation and structural characterization of a self-consistent series of polyfunctional organic monolayers," *Journal of the American Chemical Society*, vol. 112, no. 2, pp. 558–569, 1990.

[88] A. Ulman, "An introduction to ultrathin organic films: From langmuir blodgett to self-assembly (academic, new york, 1991); g. cao, h.-g. hong, and te mallouk," *Acc. Chem. Res*, vol. 25, p. 420, 1992.

[89] J. Stohr, *NEXAFS spectroscopy*, vol. 25. Springer-Verlag Berlin, 1992.

[90] S. Hüfner, *Photoelectron spectroscopy: principles and applications*. Springer Science & Business Media, 2013.

[91] K. Seki, "Ionization energies of free molecules and molecular solids," *Molecular Crystals and Liquid Crystals*, vol. 171, no. 1, pp. 255–270, 1989.

[92] H. Meyer, T. Wagener, J. Weaver, M. Feyereisen, and J. Almlöf, "Photoemission, inverse photoemission, and ab initio scf investigations of the electronic structure of polyimide," *Chemical physics letters*, vol. 164, no. 5, pp. 527–532, 1989.

[93] W. R. Salaneck, S. Stafstrom, and J. L. Brédas, *Conjugated polymer surfaces and interfaces: electronic and chemical structure of interfaces for polymer light emitting devices*. Cambridge University Press, 2003.

[94] K. Seki, "Optical techniques to characterize polymer systems," *Elsevier Science Publishers, Amsterdam*, p. 115, 1989.

[95] D. Woodruff and T. Delchar, "Modern techniques of surface science cambridge univ," *Press Cambridge Translated under the title Sovremennye metody issledovaniya poverkhnosti, Moscow: Mir*, 1989.

[96] L. Apker, E. Taft, and J. Dickey, "Photoelectric emission and contact potentials of semiconductors," *Physical Review*, vol. 74, no. 10, p. 1462, 1948.

[97] D. Cahen and A. Kahn, "Electron energetics at surfaces and interfaces: concepts and experiments," *Advanced Materials*, vol. 15, no. 4, pp. 271–277, 2003.

[98] N. Lang and W. Kohn, "Theory of metal surfaces: work function," *Physical Review B*, vol. 3, no. 4, p. 1215, 1971.

[99] H. Ishii, K. Sugiyama, E. Ito, and K. Seki, "Energy Level Alignment and Interfacial Electronic Structures at Organic/Metal and Organic/Organic Interfaces," *Advanced Materials*, vol. 11, pp. 605–625, June 1999.

[100] B. deâBoer, A. Hadipour, M. M. Mandoc, T. vanâWoudenbergh, and P. W. M. Blom, "Tuning of Metal Work Functions with Self-Assembled Monolayers," *Advanced Materials*, vol. 17, pp. 621–625, Mar. 2005.

[101] A. Natan, L. Kronik, H. Haick, and R. T. Tung, "Electrostatic Properties of Ideal and Non-ideal Polar Organic Monolayers: Implications for Electronic Devices," *Advanced Materials*, vol. 19, no. 23, pp. 4103–4117, 2007.

[102] P. C. Rusu and G. Brocks, "Work functions of self-assembled monolayers on metal surfaces by first-principles calculations," *Physical Review B*, vol. 74, p. 073414, Aug. 2006.

[103] I. H. Campbell, S. Rubin, T. A. Zawodzinski, J. D. Kress, R. L. Martin, D. L. Smith, N. N. Barashkov, and J. P. Ferraris, "Controlling Schottky energy barriers in organic electronic devices using self-assembled monolayers," *Physical Review B*, vol. 54, pp. R14321–R14324, Nov. 1996.

[104] A. Terentjevs, M. P. Steele, M. L. Blumenfeld, N. Ilyas, L. L. Kelly, E. Fabiano, O. L. Monti, and F. Della Sala, "Interfacial Electronic Structure of the Dipolar Vanadyl Naphthalocyanine on Au(111): âPush-Backâ vs Dipolar Effects," *The Journal of Physical Chemistry C*, vol. 115, pp. 21128–21138, Nov. 2011.

[105] S. Braun, W. R. Salaneck, and M. Fahlman, "Energy-Level Alignment at Organic/Metal and Organic/Organic Interfaces," *Advanced Materials*, vol. 21, pp. 1450–1472, Apr. 2009.

[106] W. Osikowicz, M. P. d. Jong, S. Braun, C. Tengstedt, M. Fahlman, and W. R. Salaneck, "Energetics at Au top and bottom contacts on conjugated polymers," *Applied Physics Letters*, vol. 88, p. 193504, May 2006.

[107] G. Witte, S. Lukas, P. S. Bagus, and C. Wöll, "Vacuum level alignment at organic/metal junctions: âCushionâ effect and the interface dipole," *Applied Physics Letters*, vol. 87, p. 263502, Dec. 2005.

[108] P. S. Bagus, V. Staemmler, and C. Wöll, "Exchangelike Effects for Closed-Shell Adsorbates: Interface Dipole and Work Function," *Physical Review Letters*, vol. 89, p. 096104, Aug. 2002.

[109] Y. Kuzumoto and M. Kitamura, "Work function of gold surfaces modified using substituted benzenethiols: Reaction time dependence and thermal stability," *Applied Physics Express*, vol. 7, p. 035701, Mar. 2014.

[110] N. Crivillers, S. Osella, C. Van Dyck, G. M. Lazzerini, D. Cornil, A. Liscio, F. Di Stasio, S. Mian, O. Fenwick, F. Reinders, M. Neuburger, E. Treossi, M. Mayor, V. Palermo, F. Cacialli, J. Cornil, and P. Samorí, "Large Work Function Shift of Gold Induced by a Novel Perfluorinated Azobenzene-Based Self-Assembled Monolayer," *Advanced Materials*, vol. 25, pp. 432–436, Jan. 2013.

[111] O. T. Hofmann, D. A. Egger, and E. Zojer, "Work-Function Modification beyond Pinning: When Do Molecular Dipoles Count?," *Nano Letters*, vol. 10, pp. 4369–4374, Nov. 2010.

[112] D. A. Egger, F. Rissner, G. M. Rangger, O. T. Hofmann, L. Wittwer, G. Heimel, and E. Zojer, "Self-assembled monolayers of polar molecules on Au(111) surfaces: distributing the dipoles," *Physical Chemistry Chemical Physics*, vol. 12, pp. 4291–4294, Apr. 2010.

[113] F. Rissner, G. M. Rangger, O. T. Hofmann, A. M. Track, G. Heimel, and E. Zojer, "Understanding the Electronic Structure of Metal/SAM/OrganicâSemiconductor Heterojunctions," *ACS Nano*, vol. 3, pp. 3513–3520, Nov. 2009.

[114] G. Heimel, L. Romaner, J.-L. BrÃ©das, and E. Zojer, "Interface Energetics and Level Alignment at Covalent Metal-Molecule Junctions: Ï-Conjugated Thiols on Gold," *Physical Review Letters*, vol. 96, p. 196806, May 2006.

[115] E. Orgiu, N. Crivillers, J. Rotzler, M. Mayor, and P. Samorí, "Tuning the charge injection of P3ht-based organic thin-film transistors through electrode functionalization with oligophenylene SAMs," *Journal of Materials Chemistry*, vol. 20, no. 48, pp. 10798–10800, 2010.

[116] T. Moldt, D. Brete, D. Przyrembel, S. Das, J. R. Goldman, P. K. Kundu, C. Gahl, R. Klajn, and M. Weinelt, "Tailoring the Properties of Surface-Immobilized Azobenzenes by Monolayer Dilution and Surface Curvature," *Langmuir*, vol. 31, pp. 1048–1057, Jan. 2015.

[117] D. T. Valley, M. Onstott, S. Malyk, and A. V. Benderskii, "Steric Hindrance of Photoswitching in Self-Assembled Monolayers of Azobenzene and Alkane Thiols," *Langmuir*, vol. 29, pp. 11623–11631, Sept. 2013.

[118] L. Venkataraman, J. E. Klare, C. Nuckolls, M. S. Hybertsen, and M. L. Steigerwald, "Dependence of single-molecule junction conductance on molecular conformation," *Nature*, vol. 442, pp. 904–907, Aug. 2006.

[119] N. Cernetic, T. Weidner, J. E. Baio, H. Lu, H. Ma, and A. K.-Y. Jen, "Enhanced Performance of Self-Assembled Monolayer Field-Effect Transistors with Top-Contact Geometry through Molecular Tailoring, Heated Assembly, and Thermal Annealing," *Advanced Functional Materials*, vol. 25, pp. 5376–5383, Sept. 2015.

[120] A. Bashir, D. Iqbal, S. M. Jain, K. Barbe, T. Abu-Husein, M. Rohwerder, A. Terfort, and M. Zharnikov, "Promoting Effect of Protecting Group on the Structure and Morphology of Self-Assembled Monolayers: Terphenylylethanethioactate on Au(111)," *The Journal of Physical Chemistry C*, vol. 119, pp. 25352–25363, Nov. 2015.

[121] J. Ossowski, T. Wächter, L. Silies, M. Kind, A. Noworolska, F. Blobner, D. Gnatek, J. Rysz, M. Bolte, P. Feulner, A. Terfort, P. Cyganik, and M. Zharnikov, "Thiolate versus selenolate: Structure, stability, and charge transfer properties," *ACS Nano*, vol. 9, no. 4, pp. 4508–4526, 2015. PMID: 25857927.

[122] K. Szelagowska-Kunstman, P. Cyganik, B. Schupbach, and A. Terfort, "Relative stability of thiol and selenol based sams on au(111) - exchange experiments," *Phys. Chem. Chem. Phys.*, vol. 12, pp. 4400–4406, 2010.

[123] D. Käfer, A. Bashir, and G. Witte, "Interplay of anchoring and ordering in aromatic self-assembled monolayers," *The Journal of Physical Chemistry C*, vol. 111, no. 28, pp. 10546–10551, 2007.

[124] A. Shaporenko, P. Cyganik, M. Buck, A. Terfort, and M. Zharnikov, "Self-assembled monolayers of aromatic selenolates on noble metal substrates," *The Journal of Physical Chemistry B*, vol. 109, no. 28, pp. 13630–13638, 2005. PMID: 16852708.

[125] M. G. Samant, C. A. Brown, and J. G. Gordon, "Formation of an ordered self-assembled monolayer of docosaneselenol on gold(111). structure by surface x-ray diffraction," *Langmuir*, vol. 8, no. 6, pp. 1615–1618, 1992.

[126] C. J. Ackerson, P. D. Jadzinsky, J. Z. Sexton, D. A. Bushnell, and R. D. Kornberg, "Synthesis and bioconjugation of 2 and 3 nm-diameter gold nanoparticles," *Bioconjugate chemistry*, vol. 21, no. 2, p. 214, 2010.

[127] T. Wink, S. Van Zuilen, A. Bult, and W. Van Bennekom, "Self-assembled monolayers for biosensors," *Analyst*, vol. 122, no. 4, pp. 43R–50R, 1997.

[128] A. L. Briseno, J. Aizenberg, Y.-J. Han, R. A. Penkala, H. Moon, A. J. Lovinger, C. Kloc, and Z. Bao, "Patterned growth of large oriented organic semiconductor single crystals on self-assembled monolayer templates," *Journal of the American Chemical Society*, vol. 127, no. 35, pp. 12164–12165, 2005.

[129] R. Jordan, A. Ulman, J. F. Kang, M. H. Rafailovich, and J. Sokolov, "Surface-initiated anionic polymerization of styrene by means of self-assembled monolayers," *Journal of the American Chemical Society*, vol. 121, no. 5, pp. 1016–1022, 1999.

[130] A. Heise, H. Menzel, H. Yim, M. D. Foster, R. H. Wieringa, A. J. Schouten, V. Erb, and M. Stamm, "Grafting of polypeptides on solid substrates by initiation of n-carboxyanhydride polymerization by amino-terminated self-assembled monolayers," *Langmuir*, vol. 13, no. 4, pp. 723–728, 1997.

[131] B. Kretz, D. A. Egger, and E. Zojer, "A Toolbox for Controlling the Energetics and Localization of Electronic States in Self-Assembled Organic Monolayers," *Advanced Science*, vol. 2, pp. n/a–n/a, Mar. 2015.

[132] D. Fracasso, H. Valkenier, J. C. Hummelen, G. C. Solomon, and R. C. Chiechi, "Evidence for Quantum Interference in SAMs of Arylethynylene Thiolates in Tunneling Junctions with Eutectic GaâIn (EGaIn) Top-Contacts," *Journal of the American Chemical Society*, vol. 133, pp. 9556–9563, June 2011.

[133] M. McDowell, I. Hill, J. McDermott, S. Bernasek, and J. Schwartz, "Improved organic thin-film transistor performance using novel self-assembled monolayers," *Applied Physics Letters*, vol. 88, no. 7, p. 073505, 2006.

[134] S. Kobayashi, T. Nishikawa, T. Takenobu, S. Mori, T. Shimoda, T. Mitani, H. Shimotani, N. Yoshimoto, S. Ogawa, and Y. Iwasa, "Control of carrier density by self-assembled monolayers in organic field-effect transistors," *Nature materials*, vol. 3, no. 5, pp. 317–322, 2004.

[135] P. Cyganik, M. Buck, T. Strunskus, A. Shaporenko, J. D. E. T. Wilton-Ely, M. Zharnikov, and C. Wöll, "Competition as a Design Concept:â Polymorphism in Self-Assembled Monolayers of Biphenyl-Based Thiols," *Journal of the American Chemical Society*, vol. 128, pp. 13868–13878, Oct. 2006.

[136] P. Cyganik, M. Buck, J. D. E. T. Wilton-Ely, and C. Wöll, "Stress in Self-Assembled Monolayers:â Ï-Biphenyl Alkane Thiols on Au(111)," *The Journal of Physical Chemistry B*, vol. 109, pp. 10902–10908, June 2005.

[137] J. F. Kang, A. Ulman, S. Liao, R. Jordan, G. Yang, and G.-y. Liu, "Self-Assembled Rigid Monolayers of 4â-Substituted-4-mercaptobiphenyls on Gold and Silver Surfaces," *Langmuir*, vol. 17, pp. 95–106, Jan. 2001.

[138] K. Heister, M. Zharnikov, M. Grunze, and L. S. O. Johansson, "Adsorption of Alkanethiols and Biphenylthiols on Au and Ag Substrates:â A High-Resolution X-ray Photoelectron Spectroscopy Study," *The Journal of Physical Chemistry B*, vol. 105, pp. 4058–4061, May 2001.

[139] A. Kovalchuk, T. Abu-Husein, D. Fracasso, D. A.Â Egger, E. Zojer, M. Zharnikov, A. Terfort, and R. C.Â Chiechi, "Transition voltages respond to synthetic reorientation of embedded dipoles in self-assembled monolayers," *Chemical Science*, vol. 7, no. 1, pp. 781–787, 2016.

[140] T. Abu-Husein, S. Schuster, D. A. Egger, M. Kind, T. Santowski, A. Wiesner, R. Chiechi, E. Zojer, A. Terfort, and M. Zharnikov, "The effects of embedded dipoles in aromatic self-assembled monolayers," *Advanced Functional Materials*, vol. 25, no. 25, pp. 3943–3957, 2015.

[141] O. M. Cabarcos, A. Shaporenko, T. Weidner, S. Uppili, L. S. Dake, M. Zharnikov, and D. L. Allara, "Physical and Electronic Structure Effects of Embedded Dipoles in Self-Assembled Monolayers: Characterization of Mid-Chain Ester Functionalized Alkanethiols on Au{111}," *The Journal of Physical Chemistry C*, vol. 112, pp. 10842–10854, July 2008.

[142] N. Meyerbroeker, P. Waske, and M. Zharnikov, "Amino-terminated biphenylthiol self-assembled monolayers as highly reactive molecular templates," *The Journal of Chemical Physics*, vol. 142, p. 101919, Mar. 2015.

[143] Y. Carissan and W. Klopper, "Hydrogen abstraction from biphenyl, acenaphthylene, naphthalene and phenanthrene by atomic hydrogen and methyl radical: Dft and g3 (mp2)-rad data," *Journal of Molecular Structure: THEOCHEM*, vol. 940, no. 1, pp. 115–118, 2010.

[144] Q. Sun and A. Selloni, "Interface and Molecular Electronic Structure vs Tunneling Characteristics of CH3- and CF3-Terminated Thiol Monolayers on Au(111)," *The Journal of Physical Chemistry A*, vol. 111, no. 40, pp. 10170–10170, 2007.

[145] Q. Sun, A. Selloni, and G. Scoles, "Electronic Structure of Metal/Molecule//Metal Junctions:â A Density Functional Theory Study of the Influence of the Molecular Terminal Groupâ ," *The Journal of Physical Chemistry B*, vol. 110, pp. 3493–3498, Mar. 2006.

[146] U. Kleineberg, A. Brechling, M. Sundermann, and U. Heinzmann, "Stm lithography in an organic self-assembled monolayer," *Advanced Functional Materials*, vol. 11, no. 3, pp. 208–212, 2001.

[147] Y. Yourdshahyan, H. Zhang, and A. Rappe, "n-alkyl thiol head-group interactions with the au (111) surface," *Physical Review B*, vol. 63, no. 8, p. 081405, 2001.

[148] H. Grönbeck, A. Curioni, and W. Andreoni, "Thiols and disulfides on the au (111) surface: the headgroup- gold interaction," *Journal of the American Chemical Society*, vol. 122, no. 16, pp. 3839–3842, 2000.

[149] W. Azzam, C. Fuxen, A. Birkner, H.-T. Rong, M. Buck, and C. Wöll, "Coexistence of Different Structural Phases in Thioaromatic Monolayers on Au(111)," *Langmuir*, vol. 19, pp. 4958–4968, June 2003.

[150] A. Shaporenko, A. Terfort, M. Grunze, and M. Zharnikov, "A detailed analysis of the photoemission spectra of basic thioaromatic monolayers on noble metal substrates," *Journal of Electron Spectroscopy and Related Phenomena*, vol. 151, pp. 45–51, Mar. 2006.

[151] P. Cyganik and M. Buck, "Polymorphism in Biphenyl-Based Self-Assembled Monolayers of Thiols," *Journal of the American Chemical Society*, vol. 126, pp. 5960–5961, May 2004.

[152] H.-J. Himmel, A. Terfort, and C. Wöll, "Fabrication of a Carboxyl-Terminated Organic Surface with Self-Assembly of Functionalized Terphenylthiols:â The Importance of Hydrogen Bond Formation," *Journal of the American Chemical Society*, vol. 120, pp. 12069–12074, Nov. 1998.

[153] A.-A. Dhirani, R. W. Zehner, R. P. Hsung, P. Guyot-Sionnest, and L. R. Sita, "Self-Assembly of Conjugated Molecular Rods:â A High-Resolution STM Study," *Journal of the American Chemical Society*, vol. 118, pp. 3319–3320, Jan. 1996.

[154] F. Grein, "Twist Angles and Rotational Energy Barriers of Biphenyl and Substituted Biphenyls," *The Journal of Physical Chemistry A*, vol. 106, pp. 3823–3827, Apr. 2002.

[155] C. B. Pinheiro and A. M. Abakumov, "Superspace crystallography: a key to the chemistry and properties," *IUCrJ*, vol. 2, pp. 137–154, Jan. 2015.

[156] O. Potzel and G. Taubmann, "The pressure dependence of the solid state structure of biphenyl from DFT calculations," *Physical Chemistry Chemical Physics*, vol. 15, no. 46, pp. 20288–20293, 2013.

[157] A. T. H. Lenstra, C. Van Alsenoy, K. Verhulst, and H. J. Geise, "Solids modelled by crystal field ab initio methods. 5. The phase transitions in biphenyl from a molecular point of view," *Acta Crystallographica Section B: Structural Science*, vol. 50, pp. 96–106, Feb. 1994.

[158] G.-P. Charbonneau and Y. Delugeard, "Structural transition in polyphenyls. III. Crystal structure of biphenyl at 110 K," *Acta Crystallographica Section B: Structural Crystallography and Crystal Chemistry*, vol. 32, pp. 1420–1423, May 1976.

[159] S. Frey, V. Stadler, K. Heister, W. Eck, M. Zharnikov, M. Grunze, B. Zeysing, and A. Terfort, "Structure of Thioaromatic Self-Assembled Monolayers on Gold and Silver," *Langmuir*, vol. 17, pp. 2408–2415, Apr. 2001.

[160] A. Ulman, "Self-assembled monolayers of 4-mercaptobiphenyls," *Accounts of chemical research*, vol. 34, no. 11, pp. 855–863, 2001.

[161] M. Dendzik, A. Terfort, and P. Cyganik, "OddâEven Effect in the Polymorphism of Self-Assembled Monolayers of Biphenyl-Substituted Alkaneselenolates on Au(111)," *The Journal of Physical Chemistry C*, vol. 116, pp. 19535–19542, Sept. 2012.

[162] P. Cyganik, M. Buck, W. Azzam, and C. Wöll, "Self-Assembled Monolayers of Ï-Biphenylalkanethiols on Au(111):â Influence of Spacer Chain on Molecular Packing," *The Journal of Physical Chemistry B*, vol. 108, pp. 4989–4996, Apr. 2004.

[163] S. J. Stranick, A. N. Parikh, D. L. Allara, and P. S. Weiss, "A New Mechanism for Surface Diffusion: Motion of a Substrate-Adsorbate Complex," *The Journal of Physical Chemistry*, vol. 98, pp. 11136–11142, Oct. 1994.

[164] H. Häkkinen, "The gold-sulfur interface at the nanoscale," *Nature Chemistry*, vol. 4, pp. 443–455, June 2012.

[165] D. OtÃ¡lvaro, T. Veening, and G. Brocks, "Self-Assembled Monolayer Induced Au(111) and Ag(111) Reconstructions: Work Functions and Interface Dipole Formation," *The Journal of Physical Chemistry C*, vol. 116, pp. 7826–7837, Apr. 2012.

[166] J. Mielke, F. Hanke, M. V. Peters, S. Hecht, M. Persson, and L. Grill, "Adatoms underneath Single Porphyrin Molecules on Au(111)," *Journal of the American Chemical Society*, vol. 137, pp. 1844–1849, Feb. 2015.

[167] G. Rajaraman, A. Caneschi, D. Gatteschi, and F. Totti, "A periodic mixed gaussians–plane waves dft study on simple thiols on au (111): adsorbate species, surface reconstruction, and thiols functionalization," *Physical Chemistry Chemical Physics*, vol. 13, no. 9, pp. 3886–3895, 2011.

[168] P. Maksymovych, O. Voznyy, D. B. Dougherty, D. C. Sorescu, and J. T. Yates Jr., "Gold adatom as a key structural component in self-assembled monolayers of organosulfur molecules on Au(1Â 1Â 1)," *Progress in Surface Science*, vol. 85, pp. 206–240, May 2010.

[169] C. Vericat, M. E. Vela, G. Benitez, P. Carro, and R. C. Salvarezza, "Self-assembled monolayers of thiols and dithiols on gold: new challenges for a well-known system," *Chemical Society Reviews*, vol. 39, no. 5, p. 1805, 2010.

[170] O. Voznyy, J. J. Dubowski, J. T. Yates, and P. Maksymovych, "The Role of Gold Adatoms and Stereochemistry in Self-Assembly of Methylthiolate on Au(111)," *Journal of the American Chemical Society*, vol. 131, pp. 12989–12993, Sept. 2009.

[171] O. Voznyy and J. J. Dubowski, "c (4× 2) structures of alkanethiol monolayers on au (111) compatible with the constraint of dense packing," *Langmuir*, vol. 25, no. 13, pp. 7353–7358, 2009.

[172] N. A. Kautz and S. A. Kandel, "Alkanethiol Monolayers Contain Gold Adatoms, and Adatom Coverage Is Independent of Chain Length," *The Journal of Physical Chemistry C*, vol. 113, pp. 19286–19291, Nov. 2009.

[173] A. Cossaro, R. Mazzarello, R. Rousseau, L. Casalis, A. Verdini, A. Kohlmeyer, L. Floreano, S. Scandolo, A. Morgante, M. L. Klein, and G. Scoles, "X-ray Diffraction and Computation Yield the Structure of Alkanethiols on Gold(111)," *Science*, vol. 321, pp. 943–946, Aug. 2008.

[174] R. Mazzarello, A. Cossaro, A. Verdini, R. Rousseau, L. Casalis, M. F. Danisman, L. Floreano, S. Scandolo, A. Morgante, and G. Scoles, "Structure of a ${\mathrm{CH}}_{3}\mathrm{S}$ Monolayer on Au(111) Solved by the Interplay between Molecular Dynamics Calculations and Diffraction Measurements," *Physical Review Letters*, vol. 98, p. 016102, Jan. 2007.

[175] L. M. Molina and B. Hammer, "Theoretical study of thiol-induced reconstructions on the Au(1Â 1Â 1) surface," *Chemical Physics Letters*, vol. 360, pp. 264–271, July 2002.

[176] P. Maksymovych, D. C. Sorescu, O. Voznyy, and J. T. Yates Jr, "Hybridization of phenylthiolate-and methylthiolate-adatom species at low coverage on the au (111) surface," *Journal of the American Chemical Society*, vol. 135, no. 13, pp. 4922–4925, 2013.

[177] X. Fan, C. Zhang, Y. Liu, and W. M. Lau, "Effects of intrinsic surface defects on thiophenol self-assembly on au (111): surface structures and reaction mechanisms," *The Journal of Physical Chemistry C*, vol. 116, no. 37, pp. 19909–19917, 2012.

[178] M. Kind and C. Wöll, "Organic surfaces exposed by self-assembled organothiol monolayers: Preparation, characterization, and application," *Progress in Surface Science*, vol. 84, pp. 230–278, July 2009.

[179] F. Schreiber, "Structure and growth of self-assembling monolayers," *Progress in surface science*, vol. 65, no. 5, pp. 151–257, 2000.

[180] J.-M. Lehn, "Perspectives in supramolecular chemistryâfrom molecular recognition towards molecular information processing and self-organization," *Angewandte Chemie International Edition in English*, vol. 29, no. 11, pp. 1304–1319, 1990.

[181] J. Kestell, R. Abuflaha, J. A. Boscoboinik, M. Garvey, D. W. Bennett, and W. T. Tysoe, "Determination of adsorbate structures from 1, 4-phenylene diisocyanide on gold," *The journal of physical chemistry letters*, vol. 5, no. 20, pp. 3577–3581, 2014.

[182] G. Poirier, "Mechanism of formation of au vacancy islands in alkanethiol monolayers on au (111)," *Langmuir*, vol. 13, no. 7, pp. 2019–2026, 1997.

[183] D. P. Woodruff, "The interface structure of n-alkylthiolate self-assembled monolayers on coinage metal surfaces," *Physical Chemistry Chemical Physics*, vol. 10, no. 48, p. 7211, 2008.

[184] A. Laguna, *Modern supramolecular gold chemistry: gold-metal interactions and applications*. John Wiley & Sons, 2008.

[185] H. Schmidbaur, *Gold: progress in chemistry, biochemistry, and technology*. John Wiley & Sons Inc, 1999.

[186] R. J. Puddephatt, *The chemistry of gold*. Elsevier Scientific Pub. Co.; distributors for the US and Canada Elsevier/North-Holland, 1978.

[187] D. Paulius, D. Torres, F. Illas, and W. E. Archibald, "A study on adatom transport through (â3 Ã â3)âR30Â°âCH $_3$ S self-assembled monolayers on Au(111) using first principles calculations," *Phys. Chem. Chem. Phys.*, vol. 16, pp. 23067–23073, Sept. 2014.

[188] "Atop adsorption site of sulphur head groups in gold-thiolate self-assembled monolayers,"

[189] H. Kondoh, M. Iwasaki, T. Shimada, K. Amemiya, T. Yokoyama, T. Ohta, M. Shimomura, and S. Kono, "Adsorption of thiolates to singly coordinated sites on au(111) evidenced by photoelectron diffraction," *Phys. Rev. Lett.*, vol. 90, p. 066102, Feb 2003.

[190] H. Grönbeck and M. Odelius, "Photoemission core-level shifts reveal the thiolate-Au(111) interface," *Physical Review B*, vol. 82, p. 085416, Aug. 2010.

[191] H. Grönbeck and H. Häkkinen, "Polymerization at the Alkylthiolateâ Au(111) Interface," *The Journal of Physical Chemistry B*, vol. 111, pp. 3325–3327, Apr. 2007.

[192] A. Nagoya and Y. Morikawa, "Adsorption states of methylthiolate on the Au(111) surface," *Journal of Physics: Condensed Matter*, vol. 19, p. 365245, Sept. 2007.

[193] E. Pensa, A. A. Rubert, G. Benitez, P. Carro, A. G. Orive, A. H. Creus, R. C. Salvarezza, and C. Vericat, "Are 4-Mercaptobenzoic Acid Self Assembled Monolayers on Au(111) a Suitable System to Test Adatom Models?," *The Journal of Physical Chemistry C*, vol. 116, pp. 25765–25771, Dec. 2012.

[194] R. Ouyang, J. Yan, P. S. Jensen, E. Ascic, S. Gan, D. Tanner, B. Mao, L. Niu, J. Zhang, C. Tang, N. S. Hush, J. R. Reimers, and J. Ulstrup, "Intermixed Adatom and Surface-Bound Adsorbates in Regular Self-Assembled Monolayers of Racemic 2-Butanethiol on Au(111)," *ChemPhysChem*, vol. 16, pp. 928–932, Apr. 2015.

[195] J. Zhou, Y. Li, P. Zahl, P. Sutter, D. J. Stacchiola, and M. G. White, "Characterization of one-dimensional molecular chains of 4, 4'-biphenyl diisocyanide on au (111) by scanning tunneling microscopy," *The Journal of chemical physics*, vol. 142, no. 10, p. 101901, 2015.

[196] J. Kestell, J. Walker, Y. Bai, J. A. Boscoboinik, M. Garvey, and W. T. Tysoe, "Adsorption and oligomerization of 1, 3-phenylene diisocyanide on au (111)," *The Journal of Physical Chemistry C*, vol. 120, no. 17, pp. 9270–9275, 2016.

[197] G. Heimel, L. Romaner, J.-L. BrÃ©das, and E. Zojer, "Organic/metal interfaces in self-assembled monolayers of conjugated thiols: A first-principles benchmark study," *Surface Science*, vol. 600, pp. 4548–4562, Oct. 2006.

[198] J. F. Kang, S. Liao, R. Jordan, and A. Ulman, "Mixed Self-assembled Monolayers of Rigid Biphenyl Thiols:â Impact of Solvent and Dipole Moment," *Journal of the American Chemical Society*, vol. 120, pp. 9662–9667, Sept. 1998.

[199] G. Kresse and J. Furthmüller, "Efficient iterative schemes for ab initio total-energy calculations using a plane-wave basis set," *Physical Review B*, vol. 54, pp. 11169–11186, Oct. 1996.

[200] G. Kresse and D. Joubert, "From ultrasoft pseudopotentials to the projector augmented-wave method," *Physical Review B*, vol. 59, pp. 1758–1775, Jan. 1999.

[201] P. Blöchl, "Projector augmented-wave method," *Physical Review B*, vol. 50, pp. 17953–17979, Dec. 1994.

[202] A. Tkatchenko and M. Scheffler, "Accurate Molecular Van Der Waals Interactions from Ground-State Electron Density and Free-Atom Reference Data," *Physical Review Letters*, vol. 102, p. 073005, Feb. 2009.

[203] T. P. Hamilton and P. Pulay, "Direct inversion in the iterative subspace (DIIS) optimization of openâshell, excitedâstate, and small multiconfiguration SCF wave functions," *The Journal of Chemical Physics*, vol. 84, pp. 5728–5734, May 1986.

[204] J. Neugebauer and M. Scheffler, "Adsorbate-substrate and adsorbate-adsorbate interactions of Na and K adlayers on Al(111)," *Physical Review B*, vol. 46, pp. 16067–16080, Dec. 1992.

[205] M. Tachibana, K. Yoshizawa, A. Ogawa, H. Fujimoto, and R. Hoffmann, "SulfurâGold Orbital Interactions which Determine the Structure of Alkanethiolate/Au(111) Self-Assembled Monolayer Systems," *The Journal of Physical Chemistry B*, vol. 106, pp. 12727–12736, Dec. 2002.

[206] A. Ulman, J. F. Kang, Y. Shnidman, S. Liao, R. Jordan, G.-Y. Choi, J. Zaccaro, A. S. Myerson, M. Rafailovich, J. Sokolov, and C. Fleischer, "Self-assembled monolayers of rigid thiols," *Reviews in Molecular Biotechnology*, vol. 74, pp. 175–188, Sept. 2000.

[207] V. Obersteiner, D. A. Egger, G. Heimel, and E. Zojer, "Impact of collective electrostatic effects on charge transport through molecular monolayers," *The Journal of Physical Chemistry C*, vol. 118, no. 38, pp. 22395–22401, 2014.

[208] N. Ballav, B. Schüpbach, O. Dethloff, P. Feulner, A. Terfort, and M. Zharnikov, "Direct Probing Molecular Twist and Tilt in Aromatic Self-Assembled Monolayers," *Journal of the American Chemical Society*, vol. 129, pp. 15416–15417, Dec. 2007.

[209] S. Liao, Y. Shnidman, and A. Ulman, "Adsorption Kinetics of Rigid 4-Mercaptobiphenyls on Gold," *Journal of the American Chemical Society*, vol. 122, pp. 3688–3694, Apr. 2000.

[210] L. F. Peiretti, P. M. Quaino, and F. Tielens, "The competition between two high density assemblies of poly phenyl thiols on au (111)," *The Journal of Physical Chemistry C*, 2016.

[211] J. Bardeen, "Surface states and rectification at a metal semi-conductor contact," *Phys. Rev.*, vol. 71, pp. 717–727, May 1947.

List of Figures

List of Tables